Micropaleontological (Foraminifera, Testate Amoeba) and μXRF Analysis of the Upper Cretaceous (Turonian) Notom Delta, Ferron Sandstone Member, Mancos Shale Formation, Centeral Utah, USA

Micropaleontological (Foraminifera, Testate Amoeba) and μXRF Analysis of the Upper Cretaceous (Turonian) Notom Delta, Ferron Sandstone Member, Mancos Shale Formation, Central Utah, USA

By Majed N.Turkistani, BSc., MSc.

A Thesis Submitted to the School of Graduate Studies in the Partial Fulfillment of the Requirements for the Degree Doctor of Philosophy

McMaster University
Doctor of Philosophy (2020)
Hamilton, Ontario (School of Earth, Environment and Society)

TITLE: Micropaleontological (Foraminifera, Testate Amoeba) and μXRF Analysis of the Upper Cretaceous (Turonian) Notom Delta, Ferron Sandstone Member, Mancos Shale Formation, Central Utah, USA
AUTHOR: Majed N.Turkistani (McMaster University)
SUPERVISOR: Dr. Eduard G.Reinhardt
NUMBER OF PAGES: xiii, 109

Abstract

In this thesis, the results of microfossil, biofacies, and geochemical analyses (μXRF) of the Upper Cretaceous (Turonian) Ferron – Notom delta, Utah, USA are reported and discussed. The Notom delta is the oldest of three clastic deltas in the Ferron Sandstone Member, Mancos Shale Formation. Foraminifera and testate amoebae were recovered from ninety-eight mudstone samples among five well-exposed outcrops (Caineville North, Steamboat, Blue Hills, Neilson Wash, and Coalmine Wash). Detailed observations showed foraminifera, and testate amoebae tests have undergone post-burial compression (flattening), dissolution, and transport/reworking; therefore, identification of these assemblages to their species level is difficult.

The micropaleontological analysis of the Ferron-Notom delta consists of three studies. Morphogroup analysis was applied on foraminifera and testate amoebae, where a relationship between the test morphology and habitat was established. Morphogroup analysis resulted in four main morphogroups and eleven morphotypes and were assigned to life mode, environment, and feeding strategies. Three foraminifera morphogroups and one testate amoebae morphogroup were established indicating a range of environments, from shallow shelf to shallow shelf to lagoon/estuary environments. Biofacies analysis using the morphotypes was applied on three outcrops (Caineville North, Steamboat, and Blue Hills). We use the morphotypes to define the four main biofacies using cluster analysis, and biodiversity indices. Four biofacies showed marine and fluvial (freshwater) influences. Salinity and OM indices were derived from the relationship of foraminifera morphotypes (BiS, TrS, TS) and testate amoebae morphotypes (Ta-F, Ta-D, Ta-S) that follows lithofacies trends. Because of the under-representation of calcareous foraminifera (due to taphonomic and/or diagenetic factors), the biodiversity indices are treated herein as relative measures. Despite this taphonomic bias, the agglutinated foraminifera and testate amoebae morphogroups show trends with salinity both among the outcrops and stratigraphically within the outcrops. The Blue Hills outcrop represents the most landward and lowest salinity environment (tidally-influenced backwater), Steamboat is more coast proximal with a higher salinity of the delta front and fluvial estuarine environments, and the Caineville North outcrop represents the most coast proximal (fluvial/estuarine to deltaic/prodeltaic) with salinities ranging from low to medium. It appears that the landward transport and coastward of tests was a significant source of taphonomic bias. Nonetheless, the assemblages provide useful depositional information that correlates with previously documented lithofacies data. A salinity index based on a ratio of trochospiral taxa versus testate amoebae was found to provide a useful measure of coastal proximity that matches lithofacies trends.

The μXRF analysis was conducted on twenty-nine mudstone samples from the Caineville North outcrop to examine elemental proxies for paleo-salinity (Sr/Ba), organic matter (K/S), redox (V/Ni), and sediment sources (Zr/Rb, Ti/Fe, Ti/Ca). Twenty-nine surface mudstone samples collected from four lithofacies representing prodelta, delta front, fluvial valley fill and shelf environments. Fourteen elements (Ti, Fe, Ca, Sr, Ba, Ni, Rb, Zr, S, V, Cu, Mn, Si, and K) were used to calculate proxy ratios to detect variations in terrigenous sediments, carbonate production, salinity, grain size, and fluvial inputs in the Caineville North outcrop. Elemental data showed good correspondence between the elemental data and the lithofacies and microfossil indices. Sr/Ba and Ca/Fe showed relationships with carbonate content and proximity to the shoreline. The paleo-salinity proxy (Sr/Ba) did not respond to salinity, but was more responsive to lithological change of carbonate content. The microfossil salinity index seems to be a more accurate paleo-salinity indicator. The proxy for fluvial input of sediment (Zr/Rb and Ti/Fe) agree well with the lithofacies trends, and Zr/Rb and Ti/Fe showed highest values within the fluvial valley fill facies, with higher variability of Ti/Fe compared to the other lithofacies (prodelta, delta front, and shelf), corresponding to response to the proximity of the depositional sites to a fluvial sediment source. The redox proxy V/Ni matched the previously derived microfossil OM index ("bolivind-type" taxa) showing a strong relationship between eutrophication and redox trends. The study aims to establish important baseline geochemical compositions of sediment sources to establish patterns and trends with sediment succession in the deeper basin (offshore; i.e. Mancos Shale). Potentially, these nearshore to fluvial trends will provide important geochemical data to assess changes in paleoclimate, and sea-level in offshore sediment successions.

Acknowledgements

First and foremost, I raise my gratitude to **Allah (God)** for helping me through my higher educations for the last nine years.

My sincere gratitude to **Dr. Eduard Reinhardt** for his insightful comments, guidance through my Ph.D. work. **Dr. Reinhardt** is like a father and an older brother to me. I like to thank him for having and honoring me as one of his students and allowing me to work with his team.

It is a privilege to work with **Dr. Janok P. Bhattacharya**, who honors me to work in his project and become one of his team. Thank you for your support, comments, guidance, and kindness. I want to thank **Dr. Joseph Boyce** for his insightful comments and support.

My special gratitude to my family, and my parent, for supporting me all these years and being patient for leaving them alone. My family, thank you for the support you provided to me in the past eight years.

My special thanks to my lovely wife **Abeer**, and my kids, **Meral** and **Malek**. I could not survive these years without you and your love and companion. There are no words I can say/write that give you enough credits for what you have done for me.

My friends and lab mates, I thank you very much for making me feel at home. My special thanks to **Nick Riddick** and **Jeremy Gabriel** for your edits and comments that help me publishing my papers as well as the endless discussions we had. My thanks to **Winnie-May Chan, Chelsi McNeil, Douglas Bloomfield, Tynan Pringles, Jorgen Pitt, and Anya Janzen**, my friends and make me feel welcome. I will never forget the things we discussed, the games we have played. I will remember you till the last breath.

Special thanks to **Dr. David Kynaston** helped me collect samples and work on the Ferron project and thanking him for his insightful comments, suggestions, and guidance. I would thank my friends back home **Ryan Thiga, and Zied Mowalad**, for their endless overseas assistance, and to my two doctors to be friends **Dr. Anas Rabie** and **Dr. Hassan Mastor**.

I want to thank **McMaster University** for the great opportunity they gave me to be one of their students and working on my Ph.D. project. I would also like to thank **Canadian Centre for Electron Microscopy (CCEM)** for allowing me to use their SEM. Finally, I want to thank the government of the **Kingdom of Saudi Arabia**, **Education Ministry**, and the **Saudi Arabia Embassy** for their assistance during my study in Canada in the last nine years. ...

Contents

List of Figures

List of Tables

Declaration of Authorship

I, Majed N.Turkistani, declare that this thesis titled, "Micropaleontological (Foraminifera, Testate Amoeba) and μXRF Analysis of the Upper Cretaceous (Turonian) Notom Delta, Ferron Sandstone Member, Mancos Shale Formation, Central Utah, USA" and the work presented in it are my own. I confirm that:

- FORAMINIFERA AND TESTATE AMOEBAE MORPHOGROUP ANALYSIS OF THE UPPER CRETACEOUS (TURONIAN) FERRON-NOTOM DELTA, CENTRAL UTAH, USA.
- FORAMINIFERA AND TESTATE AMOEBAE MORPHOGROUPS AND BIOFACIES OF THE UPPER CRETACEOUS (TURONIAN) OF THE FERRON-NOTOM DELTA, CENTRAL UTAH, USA.
- μXRF AND MICROFOSSIL ANALYSES OF THE UPPER CRETACEOUS (TURONIAN) Caineville NORTH, FERRON-NOTOM DELTA, CENTRAL UTAH, USA.

الحمدلله يؤتى الفضل من يشاء... والحمدلله الذى يُسبغُ نعمه على من يشاء... وصلى الله وسلم على خاتم الانبياء الذى قال: ((لايشكر الله منلا يشكر الناس)).

وبعد:

فعرفانًا بجميل من كانوا لى سندا وعونًا فى دراستى خلال مرحلة ابتعاثى أهدى هذه الرسالة. إلى من شجعنى ودعا لى ورعانى طوال العشر سنوات الماضية. إلى أبى و أمى وزوجتى وأبنائى واهلى وعزوتى وخاصتى من أصدقائى لكم منى خالص الشكر و التقدير.

Praise be to Allah, who brings blessings to whomever He pleases... And Peace be Upon the final Messenger "Mohammad", who said, "Allah does not thank the person who does not thank people".

My gratitude to those who have been supportive and helpful in my studies during my scholarship phase, I present my Ph.D. dissertation. To those who encouraged me, prayed for me, and looked after me for the past ten years. To my father, my mother, my wife, my children, my family, my dear friends. You have my sincere thanks and appreciation.

Chapter 1

Introduction

Our understanding of deltaic sequence stratigraphy and their facies associations have been extensively researched (Elliott, 1989). Deltas may contain several sub-environments (i.e. rivers, estuaries, marshes, lagoons) that maybe represented in ancient successions. Also, deltas are economically significant because of their rich organic shales and coal deposits, which are important hydrocarbon reserves (Elliott, 1989). The study of ancient delta stratigraphy is largely limited to physical lithologic criteria. For example, the Upper Cretaceous Ferron-Notom delta, which is the present focus, has been stratigraphically well-investigated (Zhu, 2010; Zhu et al., 2012; Wu et al., 2012; Wu, 2013; Bhattacharyya et al., 2015b; Wu and Bhattacharya, 2015; Wu et al., 2016a; Wu et al., 2016b; Kynaston and Bhattacharya, 2019). Modern deltaic environments can be characterized by physiochemical criteria, such as salinity, temperature, and sea-level (Smart et al., 1994; Hintz et al., 2004; Scott et al., 2005; Marins et al., 2016). In many ancient deltaic systems these physiochemical criteria cannot be measured directly but must be inferred from paleobiologic or geochemical proxies (Scott et al., 2005). However, microfossil proxies, such as foraminifera, and testate amoebae have only been applied in a limited capacity in geologic settings, because they are often low in abundance or are poorly preserved in deltaic sediments. To overcome this bias, we apply morphogroup analysis to these microfossil assemblages for paleoenvironmental analysis. For decades, micropaleontology has been an important tool in paleoenvironmental studies of Holocene coastal environments. Microfossils are sensitive to a wide range of ecological variables, but there is often a strong salinity control, which is useful for reconstructing coastal paleoenvironments (Lipps, 1981; Vernal and Pedersen, 1997; Scott et al., 2005; Gorbarenko et al., 2010). Foraminifera are unicellular organisms widely distributed from the ocean to brackish water settings (e.g. foraminifera), and testate amoebae are found in freshwater environments (Scott et al., 2005; Armstrong and Brasier, 2013). Together, these two groups

of micro-organisms are useful for determining paleo-salinity in estuarine environments, because they have either autogenous secreted carbonate or xenogenous (agglutinated) tests, which readily preserve as fossils (Scott et al., 2005; Armstrong and Brasier, 2013).

Foraminifera and testate amoebae have not evolved extensively through the geologic record, whereas foraminifera are well documented, testate amoebae are rare with only twenty-five fossil species that have been reported (Scott et al., 2005). There are a few studies that document ancient systems using foraminifera and testate amoebae (e.g. Medioli et al., 1990b; Porter and Knoll, 2000; Foissner and Schiller, 2001; van Hengstum et al., 2007; Bassi et al., 2008; Babalola, 2009; Riveiros and Patterson, 2009; Farooqui et al., 2010; Singh et al., 2015), with only a few studies from the Neoproterozoic to Early Miocene in various depositional environments. The oldest record of well preserved testate amoebae is in the Neoproterozoic Era from marine sediment of the Chuar Group, Grand Canyon, Arizona, where testate amoebae are described as vase-shaped microfossils (Porter and Knoll, 2000). Testate amoebae were found in marine sediments of the Early-Permian Manjir Formation northwest of Himalaya in India (Kumar et al., 2011), and in the Permian-Triassic Boundary in the Guryul Ravine Section, India (Singh et al., 2015). Testate amoebae in these studies show exceptionally well-preserved morphological characteristics (e.g. spines and test shape) that are also found in extant genera, such as *Centropyxids* and *Difflugids* (Porter and Knoll, 2000; Kumar et al., 2011; Singh et al., 2015). The presence of testate amoebae in marine sediments in the Paleozoic deposits shows a later evolution of testate amoebae from marine (Paleozoic) to terrestrial habitats (Mesozoic to Holocene; Porter and Knoll, 2000; Kumar et al., 2011; Singh et al., 2015). However, as suggested in this dissertation, some of these examples from marine sediments maybe misinterpreted because of testate amoebae maybe transported into marine environments, which maybe a taphonomic bias. In van Hengstum et al. (2007), thousands of well-preserved testate amoebae were recovered from Cretaceous (Late Albian) river floodplain deposits near Lincoln, Nebraska. Their study showed that testate amoebae tests had not evolved very much, and that most of the testate amoebae maintain their original test characteristics as modern taxa. However, most species showed post-depositional compression and flattening affecting the final appearance of the tests (Medioli et al., 1990b; van Hengstum et al., 2007). Overall, their study shows that the strain concept applies to testate amoebae from different ages, and it is possible to make comparisons between new and old tests (Reinhardt et al., 1998). Within the context of the present study, Nagy (2016) provided an example of using foraminifera morphogroups in recognizing and characterizing components of sequence architecture such as flooding events and systems tracts in Triassic and Jurassic deposits. In geologically recent (e.g. Quaternary), foraminifera or testate

amoebae assemblages retain their test's original morphology and ornamentation, which makes them easy to identify to the species level. However, in geologically older contexts, samples have been affected by dissolution and compression, so it is often difficult to identify foraminifera and testate amoebae to the species level due to the loss of characteristics, such as ornamentation, spines, coiling and even the overall shape of the chambers (Scott et al., 2005; Saraswati and Srinivasan, 2015). Morphogroup analysis combines similar test morphologies, and builds relationships between form and function with preferred microhabitats (Murray, 1973; Murray, 2006; Alperin et al., 2011). Previously, morphogroup analysis had only been applied to agglutinated tests, but recent studies show this analysis can also be applied to calcareous taxa (Rebolledo et al., 2008). The concept of morphogroups was first proposed by Heron-Allen and Earland (1930b), who noticed that the test shape of some selected agglutinated taxa were adapted to particular environments. Jones and Charnock (1985) used the term "morphogroups" to describe four morphological groups that have preferred trophic habitats, and these divisions were refined by others, such as Gooday (1993) and Nagy et al. (1995), who identified additional trophic divisions. Morphogroup analysis has two main advantages: 1) it enables reliable comparisons between assemblages from different ages, and limits divergence caused by biological evolution, and 2) it reduces the amount of data in comparison to formal identification methods using a large number of species, but still remains an effective paleoenvironmental proxy (Severin, 1983; Nagy, 1992; Nigam et al., 1992; Matyszkiewicz and Felisiak, 1992; Rebolledo et al., 2008; Colpaert et al., 2017).

1.0.1 Elemental Analysis and Application

The newly developed μXRF core scanning instrument is capable of high-resolution analysis of sediment cores (100-200μm). It is automated, non-destructive and can analyze long stratigraphy sequences with great efficiency (e.g. Turner et al., 2010; Gregory et al., 2015; Profe et al., 2016; Peros et al., 2017; Gregory et al., 2019). It has been widely applied to soft sediment cores but less so to rock cores. Individual samples as well as split sediment cores can be analyzed by this method (Gregory et al., 2019). Several studies have used elemental proxies to indicate environmental changes, such as weathering, and climate over geological time scales (Croudace and Rothwell, 2015). Studies have highlighted common elements, such as iron (Fe), titanium (Ti), potassium (K), silicon (Si), sulfur (S), calcium (Ca), zircon (Zr), strontium (Sr), rubidium (Rb), manganese (Mn), copper (Cu), and barium (Ba) as being useful in the detection of dry/wet seasons, and as indicators of weathering processes and biological productivity (Croudace and Rothwell, 2015). In the present research, we use elemental data obtained with an ITRAX-μXRF core scanner from mudstone samples of the Upper Cretaceous (Turonian)

Ferron-Notom delta and compare it with palynologic (Akyuz et al., 2015), and micropaleontological (foraminifera and testate amoebae) data (Chapter 2), along with lithofacies and sequence stratigraphic records (e.g. Zhu et al., 2012; Bhattacharyya et al., 2015b; Bhattacharyya et al., 2015a). The mudstone samples collected from the Caineville North outcrop represent complete sequences, with various lithofacies, such as prodelta, delta front, fluvial channels (Zhu et al., 2012; Wu et al., 2012). The μXRF elemental and micropaleontological data combined (Chapter 3) provide insights on the paleoenvironmental conditions of the Ferron-Notom delta, and will serve as a foundation for future studies. μXRF analysis has been widely used in studies of lake and marine sediment cores in order to detect flood events, grain-size variations, and sediment provenance. However, there are few applications to coastal and shallow shelf sediments, such as deltaic facies. Applying μXRF analysis to coastal and shallow shelf depositional systems could potentially be important for understanding long-shale sequences further offshore in the basin (e.g. Mancos Shale) because it provides data on the geochemical make-up of riverine and shallow marine source sediments, and may aid in the interpretation of sea-level and climate forcing in the Cretaceous Western Interior Seaway (Croudace and Rothwell, 2015).

1.0.2 Ferron Sandstone Member, Notom Delta

The Ferron Sandstone was deposited in a foreland basin during the Upper Cretaceous (Turonian) in the Western Interior Seaway (KWIS), which split the North American continent into two sub-continents, Laramidia (west) and Appalachia (east). The KWIS extended North from the Gulf of Mexico and connected to the Boreal Seaway connected to the Arctic, which was 3500 miles in length; the depth of the KWIS was a few hundred meters wide (Akyuz et al., 2015). The eastern part of the KWIS was a stable craton, and sediment accumulation, subsidence, uplift, and erosion were much less than on the western part (Franks et al., 1959; Oliver, 1971; Karl, 1976; Siemers, 1976; Retallack and Dilcher, 1981; Witzke et al., 1983). During the Cenomanian, the shoreline migrated rapidly westward during a transgressive stage. The main features of the eastern side of the KWIS are backstepping, and tide-dominated deltas, and peat that accumulated in marginal to interdistributary or lagoonal settings (Franks et al., 1959; Oliver, 1971; Karl, 1976; Siemers, 1976; Retallack and Dilcher, 1981; Witzke et al., 1983). The Janssen Clay Member of the Dakota Formation was deposited in Kansas, and it contained thin coal formed in a coastal plain with both marine influence and freshwater environments. In addition, the Woodbury Member of the Dakota Formation was deposited in eastern Nebraska and western Iowa, and it also contains thin coal beds (Franks et al., 1959; Oliver, 1971; Karl, 1976; Siemers, 1976; Retallack and Dilcher, 1981; Witzke et al., 1983). Rivers on the eastern side of the KWIS flowed westward, and

in Iowa and Kansas, and they flowed south to southwest based on paleocurrent data (Franks et al., 1959; Oliver, 1971; Karl, 1976; Siemers, 1976; Retallack and Dilcher, 1981; Witzke et al., 1983).

The oxygen isotope records during the Turonian show the warmest climate in the Cretaceous period, and the highest sea level in the Mesozoic and Cenozoic (Peterson and Ryder, 1975; Cobban et al., 2006; Akyuz et al., 2015). The Ferron Sandstone is a member of the Mancos Shale Formation located in central Utah, USA. The Ferron Sandstone Member has three primary progradational deltaic wedges (Notom, Vernal, and Last Chance) overlying the Tununk shale disconformity (Wu, 2013; Akyuz et al., 2015) that formed during the Turonian period (Upper Cretaceous). On the western part of KWIS, the Ferron Sandstone Member is overlaid by the Blue Gate Shale Formation with a sharp contact. The three deltas range in age from oldest to youngest: Notom, Vernal, and Last Chance. The Notom delta is comprised of six sequences, eighteen parasequence sets, and forty-three parasequences (Li et al., 2010; Zhu et al., 2012). Based on radioisotopic dating of bentonite beds, the six sequences represent a 100,000-year cycle (Milankovitch-frequency). Sequence 1 and 2 are non-marine sediments (interpreted as incised valley and floodplain deposits), sequence 3 and 4 are fluvial-deltaic deposits, and sequence 5 and 6 are shoreline trajectory (LST) and fluvial-storm dominated facies (HST), respectively (Zhu et al., 2012; Wu and Bhattacharya, 2015; Akyuz et al., 2015; Famubode and Bhattacharya, 2016). Many studies have investigated and modeled the sequence stratigraphy of the Ferron Sandstone Member. However, the only micropaleontological study attempting to reconstruct the paleoecology of the Ferron Sandstone Member was based on palynology data defining the broad depositional environment and climatic setting (Akyuz et al., 2015). In their study, terrestrial palynomorphs dominated the hydromorphic floodplain paleosols, which had a subtropical to tropical climate. In addition, four intervals of marine/tidal influenced sediments showed the occurrence of dinoflagellates (marine cysts), but they were rare (Akyuz et al., 2015).

1.1 Research Objectives

This study explores foraminifera and testate amoebae trends in the stratigraphic succession of the Upper Cretaceous (Turonian) Ferron-Notom delta. Foraminifera and testate amoebae, morphogroup, biofacies, and geochemical analysis (μXRF) are utilized to determine paleoenvironmental change in the Ferron-Notom Delta outcrops. This study provides a new application of testate amoebae and foraminifera morphogroup analysis to geologically old deltaic sequences. This study applies geochemical proxies, to evaluate aspects, such as rainfall, runoff, carbonate production, and salinity within the Caineville North outcrop using μ

XRF core scanning that will be useful for future study of long-shale sequences (e.g. Mancos Shale).

This study aims at achieving the following research objectives:

- Identify different environments represented within the Ferron-Notom Delta using microfossil morphogroup analysis with comparison to modern case studies.
- Undertake biofacies analysis of the studied succession using morphotypes trends to determine salinity and OM indices in the different lithofacies.
- Geochemical analysis of mudstones to identify sediment sources, organic matter (OM), redox, and paleo-salinity trends within the Ferron-Notom Delta.

1.2 Thesis Structure

In the first chapter (Chapter 2), we propose a systematic taxonomy of foraminifera and testate amoebae using Cainenville North, Steamboat, Blue Hills, Neilson Wash and Coalmine Wash outcrops of the Ferron-Notom Delta. We have applied the concept of morphogroup analysis (Jones and Charnock, 1985; Nagy, 1992; Reolid et al., 2008), where foraminifera and thecmoebians were identified based on their test shape. Based on the outcome of Chapter 2, we conducted a biofacies analysis (Chapter 3) of the three outcrops (Caineville North, Steamboat, and Blue Hills) developing microfossil indices for salinity and organic matter (OM). The third chapter (Chapter 4) uses the μXRF elemental data and microfossil indices in Chapter 3 to examine the deltaic succession of the Caineville North outcrop.

Chapter 2

Foraminifera and Testate Amoebae Morphogroups analysis of the Upper Cretaceous (Turonian) Ferron-Notom Delta, Utah, USA

Majed N. Turkistani*, Eduard G. Reinhardt*, David Kynaston* and Janok P. Bhattacharya*

*School of Earth, Environment and Society, McMaster University, 1280 Main Street West, Hamilton, ON L8S 4K1 Canada

This paper was submitted to *Journal of Foraminiferal Research* and will included in its published form once accepted.

Abstract

This study focuses on the microfossil content (foraminifera and testate amoebae) of the Upper Cretaceous (Turonian) Ferron-Notom delta, Utah, USA. Moderately preserved foraminifera and testate amoebae assemblages were recovered from samples obtained from muddy strata in five outcrops, namely, Caineville North, Steamboat, Blue Hills, Neilson Wash, and Coalmine Wash. A previous palynological analysis showed that the Ferron-Notom delta had a subtropical to tropical climate. The current study aims to further investigate the Ferron-Notom delta using micropaleontological analysis of foraminifera and testate amoebae to determine paleosalinity using morphogroup analysis. A total of ninety-eight samples were used in the morphogroup analysis. Tests have undergone some degree of destruction, including flattening (compaction), and dissolution, which hindered identification to the species level, and the assemblages have been biased towards agglutinated taxa. Four morphogroups were established based on the relationship between the overall test morphology, feeding strategy, and life mode. Nine foraminiferal genera, namely *Gavelinella, Ammobaculites, Trochammina, Miliammina, Bathysiphon, Reophax, Neobulimina, and Textularia* were identified, of which two are extinct (*Gavelinella and Neobulimina*). Two testate amoebae genera, namely *Difflugia, and Centropyxis* were identified that belong to extant species. These taxa are subdivided into eleven morphotypes based on overall test morphology and were assigned to an environmental range and salinity based on modern and Cretaceous examples.

Keywords: Ferron Sandstone, Upper Cretaceous, Morphogroup analysis, Taxonomy Foraminifera, Testate amoebae, marginal marine settings, paleoenvironments

2.1 Introduction

Foraminifera and testate amoebae are diverse organisms that live in modern oceans and freshwater environments, respectively, and because of their wide geographical range and sensitivity to environmental changes, they are useful proxies for paleoenvironmental studies (Scott et al., 2005; van Hengstum et al., 2007). Their ecological diversity is dependent on physiochemical criteria, such as *pH*, temperature, oxygenation, and salinity, so lakes and other freshwater environments can be differentiated using testate amoebae assemblages, while benthic foraminifera can be used in brackish marshes, estuaries, the shallow shelf and deep ocean (Scott et al., 2005). Testate amoebae and foraminifera both maintain simple autogenous or xenogenous tests (van Hengstum et al., 2007). Foraminifera have either a multilocular or unilocular test can be calcareous, or organic walled, or made-up

of agglutinated particles and the tests can vary in shape, chamber number, and ornamentation. In contrast, testate amoebae have a unilocular test with a simple morphology, and only have an agglutinated or organic wall (sack, donut or vase shaped; Scott et al., 2005; van Hengstum et al., 2007). In the geological record, foraminifera are more abundant and diverse than testate amoebae, with ≈ 6705 species identified to date, while only twenty-five species of fossil testate amoebae have been documented (Scott et al., 2005). Many Holocene-based studies have documented the application of foraminifera and testate amoebae as paleoenvironmental proxies. Scott et al. (2005) cites many applications in sea-level, estuarine, and marsh studies. These studies provide a basis for paleoenvironment reconstruction using fossil foraminifera and testate amoebae in older geological contexts (Culver, 2019).

Studies have investigated foraminifera and testate amoebae in ancient systems. Porter and Knoll (2000) indirectly linked testate amoebae to a marine origin in their study of Neoproterozoic marine strata, even though they currently inhabit freshwater environments. However, testate amoebae seem to show minimal ecological and morphological evolution throughout the Phanerozoic, which is supported by the first documented testate amoebae in freshwater deposits from the Early Permian of the Siul River, Manjir Formation, India (Farooqui et al., 2010). The migration of testate amoebae from marine to freshwater likely occurred in the early-Paleozoic (Porter and Knoll, 2000). However, testate amoebae were also found in marine sediments of the Early Permian Manjir Formation northwest of Himalaya in India (Kumar et al., 2011), and in the Permian-Triassic Boundary in the Guryul Ravine Section, India (Singh et al., 2015), so there is uncertainty on the timing or frequency of marine to freshwater transitions. Testate amoebae in these studies show exceptionally well preserved morphological characteristics (e.g. spines and test shape) also observed in extant species, such as *Centropyxids* and *Difflugids* (Porter and Knoll, 2000; Kumar et al., 2011; Singh et al., 2015). Well-preserved testate amoebae were found in the Early Cretaceous deposits of Ruby Creek, Alberta, Canada, and in Late Albian deposits, of Nebraska (Medioli et al., 1990a; van Hengstum et al., 2007). Generally, fossilized testate amoebae can only be identified to genus level, because of flattening during compaction and fossilization (Nagy, 1992; Scott et al., 2005; van Hengstum et al., 2007; Reolid et al., 2008). In contrast, there is extensive research using foraminiferal assemblages as proxies for paleoenvironments in ancient coastal systems (Wightman, 1990; Tibert and Scott, 1999; Lloyd, 2000; Nielsen et al., 2008; Nagy et al., 2011; Jain and Farouk, 2017). Benthic foraminifera are known from the pre-Cambrian inhabiting brackish to marine environments (Armstrong and Brasier, 2013). However, there is not extensive research combining testate amoebae and foraminifera for paleoenvironmental analysis of ancient coastal systems, even though they have

been widely applied in the Holocene (Scott and Medioli, 1980a; Scott et al., 2005).

Morphogroup analysis is an approach used to assess paleoenvironmental conditions (Nagy, 1992; Reolid et al., 2008) first introduced by Jones and Jones and Charnock (1985) based on modern faunas. Modern and ancient studies have demonstrated a direct relationship between foraminiferal shell type, life mode and feeding strategy (Corliss, 1985; Jones and Charnock, 1985; Corliss, 1991; Tyszka, 1994; Reolid et al., 2008; Murray et al., 2011). The benefit of applying morphogroup analysis is threefold: 1) it allows comparison of differently aged assemblages by eliminating the effect of biological evolution, which leads to taxonomic divergence; 2) it does not require identifying microfossils to the species level; and 3) it reduces data variables simplifying analysis (Nagy, 1992; Nagy et al., 1995; Bąk, 2004; Szydo, 2004; Lemaska, 2005). Morphogroup analysis has been applied in studies from the shelf to deltaic environments, wherein these morphogroups have helped to differentiate biofacies and environments. Morphogroup analysis is also applicable using both calcareous and agglutinated foraminiferal assemblages (Reolid et al., 2008). The overall trends of the morphogroup criteria (e.g. life position, micro-habitat, and feeding strategy) can be used to establish different environments, such as those reported from paleoenvironmental studies on the Jurassic - Cretaceous strata in Nepal and Spain (Nagy, 1992; Nagy et al., 1995). Furthermore, morphogroup analysis allows relative comparisons within the same stratigraphic succession.

The present study uses morphogroups on moderately preserved foraminifera and testate amoebae recovered from five outcrops of the Upper Cretaceous (Turonian) Ferron-Notom delta, the oldest of three deltas within the Ferron Sandstone Member, Utah, USA. The specimens were identified to either the genus or species level, depending on their preservation (e.g. sediment load "flattened," dissolution), and assigned to morphotypes based on reliability of identification and ecological tolerances. This study establishes the taxonomic and morphogroup basis for future biofacies of the Ferron-Notom delta (Chapter 3).

2.1.1 Ferron "Notom Delta" Geological Setting

In the Late Cretaceous, at the peak of thrust faulting during the Sevier Orogeny in Utah foredeep basin in response to thin skinned crustal shortening (Decelles et al., 1995; Willis, 1999; Coogan and Decelles, 2007). The Mancos Shale was deposited in the Western Interior Basin as it filled in response to high rates of syn-orogenic sedimentation and, subsidence during a period of globally high sea level (Fig. 2.1). Three clastic deltaic wedges comprise the Turonian Ferron Sandstone Member of the Mancos Shale: The Last Chance, Vernal, and Notom Deltas (Uresk, 1979; Hill, 1982; Bhattacharya and Tye, 2004; Corbeanu et al., 2004; Fielding, 2011).

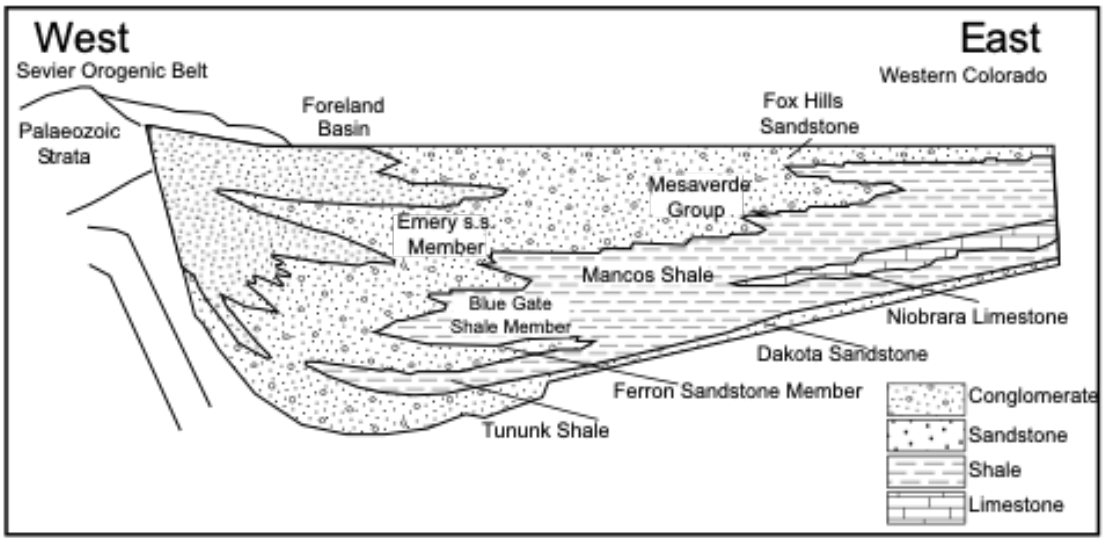

Figure 2.1: Regional stratigraphic cross section of the Mancos Shale showing the relative location of the Ferron Sandstone Member, the overlying Blue gate Shale Member, and the underlying Tununk Shale (modified from: Li and Zhu, 2014)

The Ferron-Notom delta overlies the Tununk Shale Member of the Mancos Shale Formation and shows a gradational contact. Above the Ferron-Notom delta is a sharp contact with the overlying Bluegate Shale Member. The Ferron-Notom delta is composed of six sequences, which are further divided into eighteen parasequence sets and forty-two parasequences (Li et al., 2011a; Zhu et al., 2012) . The lower four sequences are composed of shoreface and heterolithic deltaic facies, while the upper two sequences show incision of lowstand compound incised valleys truncating underlying deltaic and shoreface deposits (Li et al., 2010; Li and Bhattacharya, 2013; Famubode and Bhattacharya, 2016).

Recent studies (Li et al., 2010; Fielding, 2011; Zhu et al., 2012; Richards and Bhattacharya, 2018), have mapped the extent of the Ferron Notom Delta outcrop (Fig. 2.2) across regional strike and dip cross-sections (Figs. 2.3 and 2.4). The study areas lie along these correlations in strata whose lithology and paleoenvironment have been previously documented using traditional facies analysis (Li et al., 2011a; Zhu et al., 2012; Li and Bhattacharya, 2013; Ullah et al., 2015; Richards and Bhattacharya, 2018), within a regional sequence stratigraphic framework.

A palynological study helped reconstruct and refine the broader depositional environments and evaluate the climatic settings within the floodplain paleosol deposits (Akyuz et al., 2015). Terrestrial palynomorphs indicate a subtropical to tropical ever-wet climate (Akyuz et al., 2015). In addition, four horizons of

marine/tidal influence sequences are marked by dinoflagellates (marine cysts) and confirm that marine influence can be correlated with flooding surfaces (Akyuz et al., 2015).

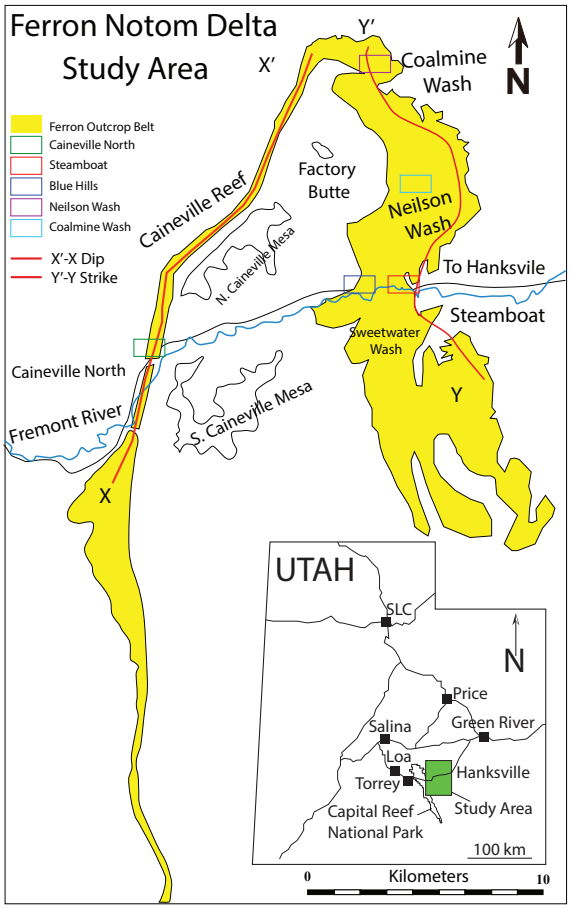

Figure 2.2: The regional study area within Utah (modified from: Zhu et al., 2012). Cross section locations (Figs. 2.3 and 2.4) are indicated by red lines. The colored boxes indicate sample locations, which are also represented; the strike and dip cross-sections (Figs. 2.4 and 2.3).

2.2 Methodology

Ninety-eight hand-sized mudstone samples were collected from muddy facies of the Ferron-Notom delta, representing six sequences in differing depositional environments, including marine, pro-delta, delta front, transitional (e.g. marsh, estuarine) and fluvial facies. The samples were collected for detailed micropaleontological analysis to reconstruct paleoenvironmental criteria, including salinity, organic matter, oxygen, and sea-level changes. A subsample (2.5-10 cm^3) was soaked in distilled water to disaggregate the sediments over a week. The sediments were then wet sieved using a 63 μm screen and dried for examination using a binocular microscope (100x). Each sample was weighed, and then dry-split into 1/8th for a count of $\approx$ 300 specimens per sample (Fishbein and Patterson, 1993). Exceptionally preserved tests that maintained some, or all test morphology and ornamentation were selected for analysis and imaging with a scanning electron microscope (SEM). The samples were mounted, gold sputter-coated to increase electrical conductivity and analyzed using a JEOL 6610LV SEM equipped with a tungsten filament at the Canadian Center for Electron Microscopy at McMaster University (CCEM). Most of the foraminifera and testate amoebae tests have undergone some post-depositional alteration (such as flattening cf.), making it difficult to identify the tests to species level using a binocular microscope.

2.2.1 Morphogroup Analysis

Morphogroup analysis categorizes foraminiferal species into groups based on their overall test morphology (Jones and Charnock, 1985) and relationships with life position and feeding habits. Foraminifera and testate amoebae are divided into morphogroups and subgroups, each designated by abbreviations following Nagy (1992) and Nagy et al. (1995) and Reolid et al. (2008). The current study follows the morphogroup principle and employs morphotype as a lower rank using a descriptive term. The foraminifera recovered from the Ferron-Notom delta are benthic, and belong to nine families: *Gavelinellidae, Lituolidae, Haplophragmoididae, Ammomarginulininae, Trochamminidae, Astorhizidae, Miliammina, Turriknidae* and *Textularia*. In addition, we newly identify and apply two testate amoebae genera (*Difflugia*- like and *Cenropyxis*- like). A number was assigned to each morphogroup, and an abbreviation was assigned to each morphotype (Table 2.1) based on general test morphology, mode of coiling, and the number of chambers (if apparent). Four morphogroups and eleven morphotypes were established following Nagy (1992) and Nagy et al. (1995) and Reolid et al. (2008).

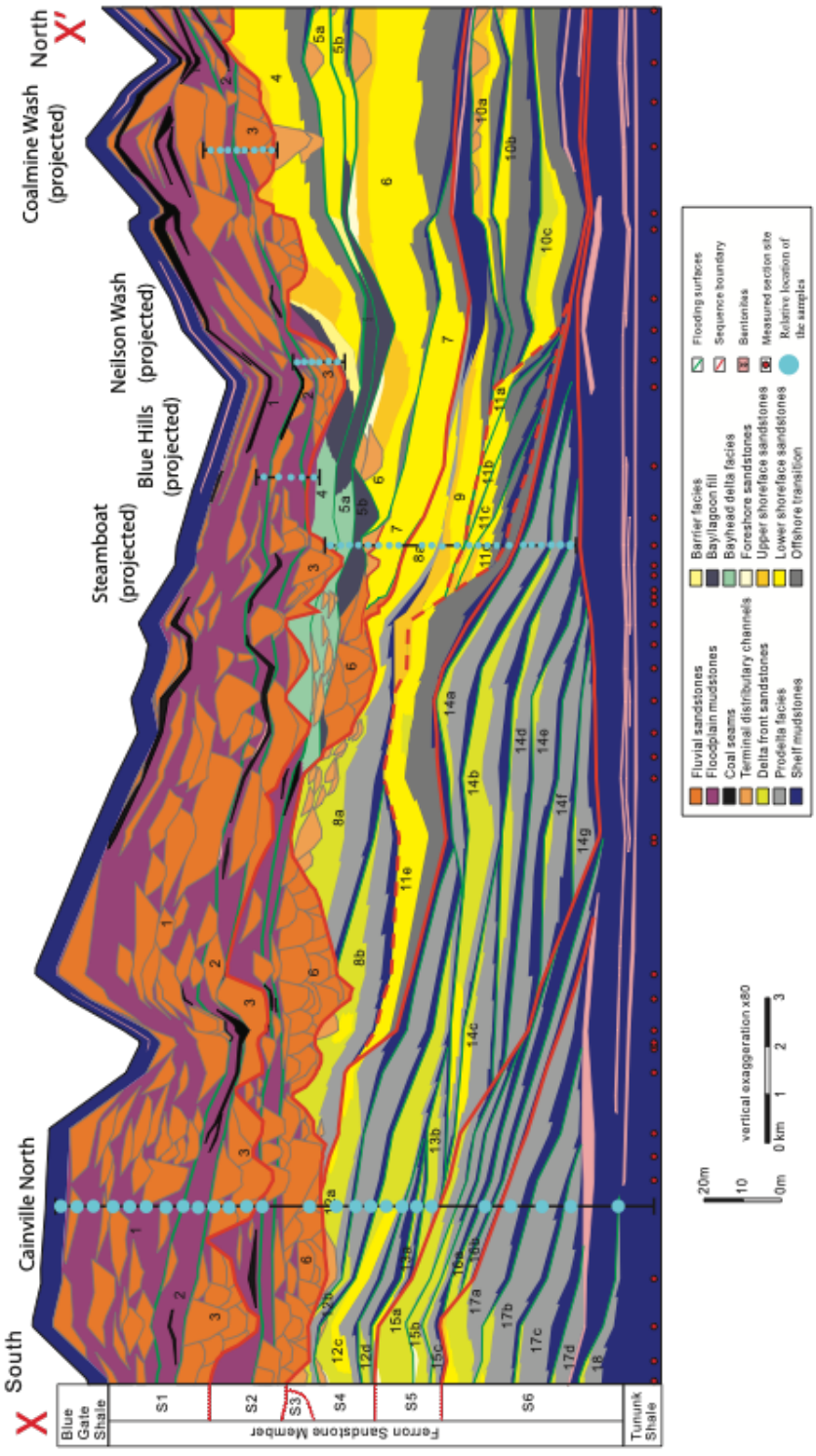

FIGURE 2.3: Strike cross-section Y-Y' (Fig. 2.2), showing the approximate sample intervals. Approximate locations of outcrops directly north of Caineville are also shown projected on this section (modified from Li et al., 2011b).

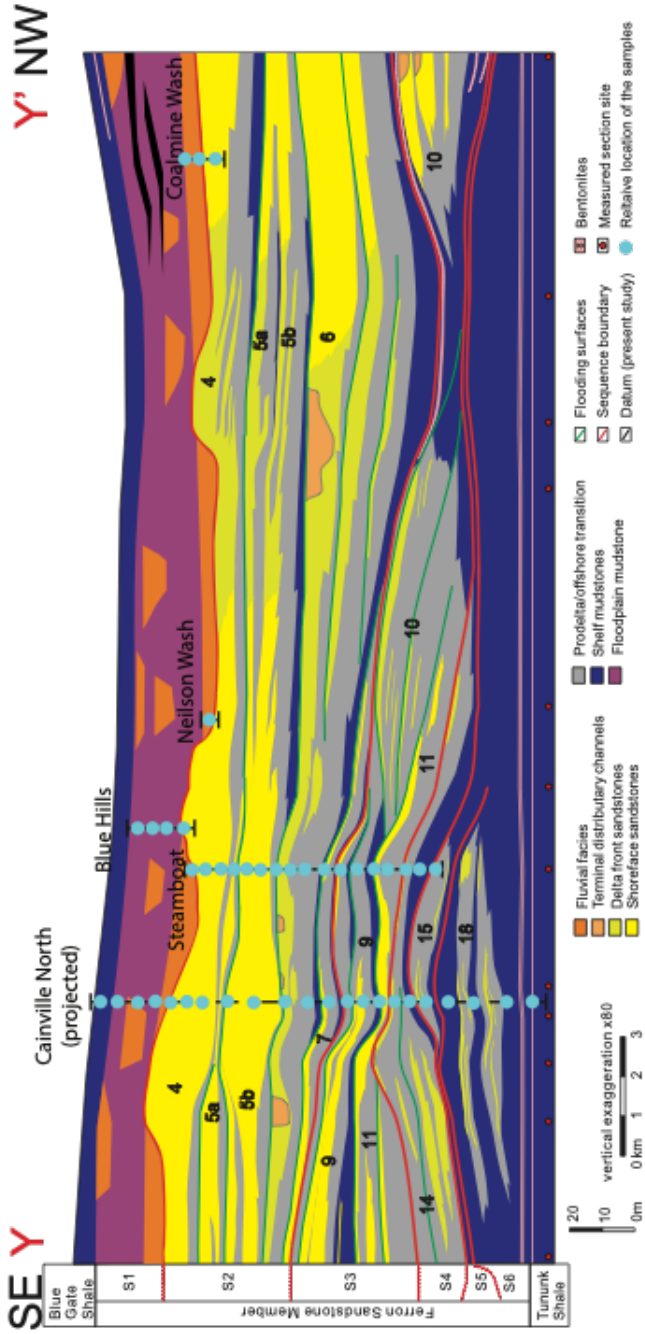

FIGURE 2.4: Dip oriented cross-section X-X' (Fig. 2.2), showing the sampled intervals north of Caineville and the projected sampled intervals (modified from (Zhu et al., 2012; Richards and Bhattacharya, 2018)

TABLE 2.1: Foraminiferal and testate amoebae morphogroups from the Ferron-Notom delta, with inferred microhabitats and feeding strategies (Severin, 1983; Jones and Charnock, 1985; Bernhard, 1986; Koutsoukos et al., 1990; Nagy, 1992; Rebolledo et al., 2008).

	MORPHOGROUP	MORPHOTYPE	TEST FORM	LIFE POSITION	FEEDING STRATEGY	CHAMBERS/ TEST TYPE		ENVIRONMENT	TAXA
Foraminifera	1 PS		Flattened trochospiral nearly planispiral	Epifauanal	Active to passive herbivore detritivore.		Agglutinated & Calcareous	High energy lagoon & estuary - Inner shelf to upper bathyal	*Gavelinella ammoniodes Gavelinella loreniana Haplophragmoides spp.*
	1 Ps/UnS		Planispiral to Uniserial	Infauna	Active to passive detritivore	Multilocular	Agglutinated	Inner shelf to upper bathyal with increased OC	*Ammobaculites subcretaceus*
	1 TS		Flattened Trochospiral	Surficial epifauna	Active herbivore deteritivore			Marsh	*Trochammina sp.*
	2 Mi		Miliolid	Epifauna	Active herbivore deteritivore		Agglutinated	Estuary to coastline	*Miliammina sp.*
	3 UnLT		Elongated Tubular	Erect epifauna	Suspension feeders	Unilocular	Agglutinated	Tranquil bathyal & abyssal with low OC	*Bathysiphon sp.*
	3 UnSE		Elongated Uniserial	Infaunal		Multilocular		Pro-delta mid - outer shelf deep lagoon shallow brackish lagoon	*Rephax sp.*
	3 TrS		Triserial	Infaunal	Active to passive detritivore	Multilocular	Agglutinated & Calcareous	outer shelf shallow deep lagoon high energy shallow water	*Neobulimina albertensis*
	3 BiS		Biserial	Infaunal			Agglutinated		*Textularia sp.*

	MORPHOGROUP	MORPHOTYPE	TEST FORM	LIFE POSITION	FEEDING STRATEGY	CHAMBERS/ TEST TYPE		ENVIRONMENT	TAXA
Testate Amoebae	4 Ta-F		Flask-shape	Epifauna	Active to passive herbivore detritivore.	Unilocular	Agglutinated	Freshwater	*Difflugia oblonga, Difflugia proteiformis Difflugia corona, Difflugia urceolata Lagenodifflugia vas.*
	4 Ta-D		Donut-shape					Fresh to slightley brackish	*Centropyix constricta*
	4 Ta-S		Sack-shape						*Centropyix aculeata*

Agglutinated Benthic Foraminifera Morphogroup

Morphogroup 1. This group is subdivided into three morphotypes (Table 2.1), namely, trochospiral (TS), planispiral (PS), and initially planispiral to uniserial PS/UnS). The tests are multilocular, and are adapted to an epifaunal or infaunal habitat and are herbivores to omnivores. In the stratigraphic succession, this group is represented by *Gavellenila, and Haplophragmoides* (Table 2.1, PS; Plate 1, Figs. 1-4, and 5), *Ammobaculites* (Table 2.1, PS/UnS; Plate 1, Figs. 7-9) and *Trochammina* (Table 2.1, TS; Plate 1, Fig. 6). All three morphotypes are equivalent to 2-b and 3-a in Nagy (1992) and C2 and D in Rebolledo et al. (2008).

Morphogroup 2. This group includes foraminifera with multilocular, and Miliolid (Mi) tests, which are adapted to epifaunal to shallow infaunal habitats. This group is represented by *Miliammina spp.* (Table 2.1-Mi; Plate 2, Figs. 1-4) in the stratigraphic successions.

Morphogroup 3. The foraminifera in this group are divided into four morphotypes. Two morphotypes (Table 2.1, UnLT, and UnSE) comprises UniLocular (tubular), elongated, UniSerial tests, which are adapted to a shallow infaunal/erect epifaunal mode of life with a suspension feeding strategy. This group is equivalent to 1-a in Nagy (1992), and A, C1, and C3 in Rebolledo et al. (2008). They are represented by *Bathysiphon spp.*, and *Reophax spp.* in the stratigraphic succession. The other two morphotypes (Table 2.1, TrS, and BiS) are multilocular, with Bi- or Tri-Serial tests, and they are adapted to shallow - deep infaunal habitats with a bacterial scavenging feeding strategy (detritivores). These two morphotypes are equivalent to 3-b in Nagy (1992), A8 in Tyszka (1994) and C3 in Rebolledo et al. (2008). TrS and BiS morphotypes are represented by *Neobulimina albertensis* and *Textularia spp.* in the stratigraphic succession.

Agglutinated Testate Amoebae Morphogroup

Morphogroup 4. The Testate amoebae (Ta) in this group are divided into three morphotypes (Ta-F, Ta-D and Ta-S). Species in these groups are unilocular, and they are adapted to an epifaunal habitat and herbivorous feeding strategy (Ogden and Hedley, 1980; Medioli et al., 1987) . The first sub-group consists of Flask-shaped tests (Table 2.1, Ta-F), and is represented by *Difflugia oblonga*, *Difflugia proteiformis*, *Difflugia urceolata* and *Lagenodifflugia cf. vas.* The second sub-group consists of Donut-shaped tests (Table 2.1, Ta-D), and it is represented by *Centropyxis constricta* (Scott et al., 2005), and the third morphogroup includes the Sack-shaped tests (Table 2.1, Ta-S) and it is represented by *Centropyxis aculeata.*

2.3 Result and Discussion

Samples were collected from five outcrops scattered within the Ferron-Notom delta; each sample was taken from muddy sections within these stratigraphic exposures. We applied morphogroup analysis that divided the foraminifera and testate amoebae into morphotypes based on their overall test morphology, their function, and life modes (Jones and Charnock, 1985; Nagy, 1992). This analysis allows us to reduce the data by identifying microfossils to their genus level instead of species following Nagy (1992) and Nagy et al. (1995), and Reolid et al. (2008). Case studies from Holocene/Quaternary and Mesozoic strata have made contributions to understanding controlling factors that have a direct or indirect impact on the distributions of both assemblages. Scott et al. (2005) included many case studies as examples, where foraminifera and testate amoebae were used as paleoenvironmental proxies. These studies include using marsh foraminifera for sea-level fluctuations (1m; Scott and Medioli, 1980a), and seismically induced coastal changes (Atwater, 1987; Atwater, 1992; Gayes et al., 1992; Scott et al., 1995a; Scott et al., 1995b; Scott et al., 2005). In addition, one of the more important and relevant studies is the estuarine classification by Scott and Medioli (1980a) from five localities in Canada. In the present study, our goal is to establish a foundation for biofacies analysis based on morphogroups. Currently, there is no morphogroups analysis using testate amoebae, but on geologically old successions may they prove useful for environments and sea-level changes in Cretaceous coastal successions.

Taphonomy. Taphonomic processes, including compaction, dissolution, transport, and diagenesis, can greatly impact the fossil record of foraminifera and testate amoebae (Berger, 1971; Berkeley et al., 2007; Scott et al., 2005; Berkeley et al., 2009). Foraminifera and testate amoebae studied herein have undergone some degree of compaction that caused deformation and flattening of tests similar to van Hengstum et al. (2007). Only two samples out of 98 samples were found to contain calcareous tests, and of these, calcareous tests were uncommon (e.g. 8/2). The calcareous tests belong to two genera, namely, *Gavelinella* (4 specimens), and *Neobulimina* (4 specimens), and were found within samples from the Blue Gate and Tununk shale members. The lack of calcareous tests can be explained as a result of dissolution and/or diagenesis, but calcareous taxa may not have been part of the original biocenosis. Because calcareous tests are largely absent, agglutinated taxa are used in our environment interpretations.

Morphogroup 1. This group includes three morphotypes (Table 2.1. PS, PS/UnS, and TS). There are three life positions and feeding strategies for these morphotypes (Table 2.1, PS, PS/UnS, and TS). In general, this morphogroup seems to be sensitive to currents, sea-level change (e.g. tide cycles) and organic content based on their life position and feeding strategies, and their range from

the shelf to high energy lagoons/estuaries (Nagy, 1992; Nagy et al., 1995).

Morphotype-PS comprises a flattened trochospiral nearly planispiral, and *Gavelinella and Haplophragmoides* represent this morphotype. Two *Gavelinella* species have been observed within the Ferron-Notom delta's samples, namely *G.ammonoides* and *G. lorneiana* (Plate 1, Figs. 1-4). The former is the early ancestor of *G. lorneiana* in the Upper Turonian, and its complete stratigraphic range is unknown (Dubicka and Peryt, 2014). *G. lorneiana* has a large and low trochospiral test reported from Cretaceous strata in several European countries, such as northern France, Germany, United Kingdom, and in the Western Interior Seaway (Texas; Dubicka and Peryt, 2014). Both *Gavelinella* and *Neobulimina* are described as a transitional fauna that can tolerate low oxygen environments (Leckie, 1985; Ashckenazi-Polivoda et al., 2010). *Haplophragmoides spp.* dominates the samples with *Trochammina spp.*, and *Haplophragmoides spp.* is reported in brackish to tidal marshes in The Minho River northern Portugal (Fatela et al., 2009).

Morphotype-PS/UnS contains elongated uniserial initially coiled tests. This morphotype includes *Ammobaculites*, and this genus typically has a range in Holocene environments, from low marsh to shallow upper estuarine environments, where the salinity is less than 20 ppt (Scott et al., 2005; Chen et al., 2020). In our samples, all the *Ammobaculites* specimens belong to *A. subcretaceus* (Cushman and Alexander, 1930) with varying lengths.

Morphotype-TS includes flattened trochospiral tests. This morphotype is represented by *Trochammina spp.*, which is a high marsh type species (Scott et al., 2005). It has been reported in Holocene salt marsh environments (i.e., New Zealand) that are affected by tides (Hayward et al., 1999), and typically inhabit salinity ranges from 5 ppt to 40 ppt (Teal, 2001). This species was identified based on the test shape of modern extant species (Hudackova et al., 2018) and a study from the Canadian Western Interior Seaway (McNeil and Caldwell, 1981). *Trochammina spp.* are a common proxy for sea-level reconstructions in Holocene sediments along with *M.fusca*, which is a low marsh species (Hayward et al., 1999; Leorri et al., 2010).

Morphogroup 2. This morphogroup includes multilocular, miliolid morphotypes (Mi), and it is represented by *Miliammina spp.* (e.g. *Miliammina fusca*; Plate 2, Fig. 1-4) taxa.

Morphotype-Mi. The specimens lacked most of the defining characteristics of *M. fusca*, but the location of the aperture and faint lines defining the chambers helped identify the specimens as *M. fusca*. This morphotype was found in only a few sections and samples. In modern settings, the distribution of *Miliammina*

spp. is found in environments with low salinity (≈6 ppt) indicating low marshes to upper estuaries (Scott and Medioli, 1980c; Chen et al., 2020). Similar to *Trochammina spp.* and *Ammobaculites spp.*, *M.fusca* is a good proxy for sea-level as there distribution is zoned with tidal range (Hayward et al., 1999; Leorri et al., 2010).

Morphogroup 3. Four morphotypes are included in this group, and their tests are elongated with different chamber arrangements.

Morphotype-UnLT. This morphotype includes uniocular-tubular (Table 2.1) specimens, namely, *Bathysiphon spp.* (Plate 2, Fig. 7). The *Bathysiphon spp.* (UnLT) is equivalent to morphogroup 1-a in Nagy (1992) and Reolid et al. (2008). Like *Rhizammina spp.* this species stands erect with its aperture elevated above the sediment (Nagy, 1992), so its position in the sediment is an adaptation to suspension feeding as suggested by Jones and Charnock (1985), Mullineaux (1987) and Altenbach (1988). This morphotype (UnLT) is found in both in the deep sea and in shallow water, thus, they are highly affected by the water current velocity and turbidity events as suggested by Nagy (1992).

Morphotype-UnSE. This morphotype includes the elongated uniserial (Table 2.1) specimens. This morphotype was assigned to *Reophax spp.* (Plate 2, Fig. 5-6). This species is described as an opportunistic infaunal taxon in Mesozoic strata (Jenkins, 2000), and change their habitat according to nutrient abundance. It has been recorded in Jurassic pro-deltaic facies (Nagy and Johansen, 1989), the mid to outer shelf (Reolid and Nagy, 2005), deep lagoon (Hughes, 2004) and shallow brackish lagoonal facies (Bhalla and Talib, 1991; Reolid et al., 2008).*Reophax spp.* are found to be tolerant of low oxygen conditions (Kaminski et al., 1995; Reolid et al., 2008), and is commonly used as an indicator for high organic contents (Scott et al., 2005).

Morphotype-BiS. Elongated biserial specimens (Table 2.1) were assigned to morphotype-BiS, which is represented by *Textularia spp.*, and are adapted to an infaunal life position and are detritivores (Reolid et al., 2008). In ancient examples, they are abundant in outer shelf environments (Bernier, 1984) and shallow to deep lagoons (Hughes, 2004). *Textularia spp.* were found to be tolerant of high-energy shallow water conditions within carbonate buildups (Oxfordian strata, Cracow area, Southern Poland; Bernier, 1984; Matyszkiewicz and Felisiak, 1992). However, in Holocene sediment *Textularia spp.* are commonly found in a wide range of coastal environments (Scott et al., 2005).

Morphotype-TrS. The elongated triserial morphotype is represented by (Table 2.1) *Neobulimina albertensis*, which is an extinct species, but this morphotype likely had a similar life mode and feeding strategy as *Textularia spp. Neobulimina albertensis* has been associated with an environmental range from the outer shelf

to deep lagoons. This species is also likely tolerant of low-oxygen levels (Leckie, 1985; Ashckenazi-Polivoda et al., 2010).

Morphogroup 4. This morphogroup consists of three subgroups with three morphotypes (Tabel.2.1, Ta-F, Ta-D, and Ta-S), and it includes only agglutinated testate amoebae (testate amoebae). All species belonging to these morphotypes are epifauna and adapted to herbivore and detritivore feeding.

Morphotype-Ta-F comprises five testate amoebae species with unilocular, flask-shaped tests namely, *Difflugia oblonga, Difflugia proteiformis, Difflugia corona, Difflugia urceolata* and *Lagenodifflugia vas,* which are all extant species. Three of these taxa have been recorded in the Cretaceous Dakota Formation near Lincoln, Nebraska, USA (*D. oblonga, D. proteiformis and L. vas*; van Hengstum et al., 2007). All species belonging to this morphotype (Ta-F) inhabit freshwater environments (Scott et al., 2005). *D. oblonga* is mainly found in water with *pH* <6.2 (Ellison, 1995) and is often found in organic-rich sediments and warmer climates (Kliza, 1994; McCarthy et al., 1995; Asioli et al., 1996). *D. proteiformis* is resistant to high amounts of ammonia, nitrogen, and nitric nitrogen, and it is common in organic rich sediments with sulfides, sulfites and low oxygen (Asioli et al., 1996). These taxa are often used to indicate sea-level changes in Holocene sediments (Mutti et al., 1988; Medioli and Barbara, 1995), and freshwater influence in estuarine environments (Bartlett, 1966; Ellison and Nichols, 1976; Scott et al., 1977; Scott and Medioli, 1980c).

Morphotypes Ta-D and Ta-S. These two morphotypes have donut-shaped and sack-shaped tests, respectively, and are represented by *Centropyxis aculeata* and *Centropyxis constricta.* Both can tolerate extreme environmental conditions (Scott et al., 2005). *C. aculeata* and *C. constricta* in modern studies are found in brackish ponds in coastal areas affected by salt spray (Scott and Medioli, 1983). Both species are also used as an indicator for estuarine environments, where they form the transition from marine to fresher water (low salinity < 5 *ppt*; Scott and Medioli, 1980c).

Systematics

Foraminifera species were identified using McNeil and Caldwell (1981), Corliss and Chen (1988), Eduardo et al. (1990), Nagy (1992), Nagy et al. (2009), and Cetean et al. (2011) and (Murray et al., 2011). Nine genera of foraminifera *Gavelinella* (Brotzen, 1942), *Haplophragmides*, *Ammobaculites* (Cushmann, 1917), *Trochammina* (Parker and Jones, 1859), *Reophax, Bathysiphon* (Sars, 1872), *Milimmina* (Heron-Allen and Earland, 1930a), *Neobulimina* (Cushman and Cole, 1930), and *Textularia* (Defrance,1824). Three testate amoebae genera were documented,

which Medioli et al. (1990a) described as "*Difflugid*," "*Lagenodifflugia*" and "*Centropyxid*-like." Species belonging to these genera are *Difflugia oblonga*, *Difflugia urceolata*, *Difflugia corona*, *Difflugia proteiformis* and *Lagenodifflugia* which are freshwater indicators. *Centropyxis aculeata* and *Centropyxis constricta* are also found in freshwater environments, but can also tolerate low salinity (<5‰) environments, such as upper estuaries. They are also an opportunistic species that can tolerate harsh conditions (Scott and Medioli, 1980a; Medioli et al., 1990a).

Foraminifera Taxonomic Descriptions

Family GAVELINELLIDAE Hofker, 1956

Genus *Gavelinella* Brotzen,1942

Gavelinella ammonoides (Reuss, 1845) Fig. 4.1-4.2

Plate 1. Fig. 1-2.; Table 2.1-morphogroup 1-PS

Discussion. This species is calcareous and found in two samples, but it was difficult to identify under a binocular microscope (20x).The test features can be observed with the SEM. In general, the test is flattened trochoid, consisting of three whorls, with low spiral height and low to moderate convex in the umbilical side. In some specimens, chamber sutures can be seen and are partially perforated. Most of the tests are flattened due to sediment loading and compaction.

Gavelinella lorneiana (d'Orbigny, 1840)

Rosalina lorneiana d'Orbigny, 1840, p. 36, Plate 3, Fig. 20-22.

Gavelinella kelleri (Vasilenko and Mjatliuk). Kaptarenko-Chernousova et al., 1979, p. 127, Plate 48, Fig. 8.

Gavelinella lorneiana (d'Orbigny). Edwards, 1981, p. 396, 397, Plate 56, Fig. 1–5; Hradecká, 1996, p. 90, Plate 4, Fig. 1–6; Revets, 2001, p. 14, Plate 3, Fig. 10–12.

Plate 1, Fig. 3-4; Table 2.1-morphogroup 1-PS

Discussion. Similar to *G.ammonoides*, *G.lorneiana* calcareous and found in two samples, and were easily identified using binocular microscope (20x) based on their low trochospiral test. *G. lorneiana* consists of several whorls, and its spire height is moderate and biconvex. The chambers are difficult to observe, but with the SEM, the chambers and sutures can be identified. The umbilical side is slightly concave. This species might have evolved from *G. ammonoides* (Dubicka and Peryt, 2014).

Superfamily LITUOLOIDEA

Family LITUOLIDAE de Blainville, 1825

Family HAPLOPHRAGMOIDIDAE Mayne 1952

Genus *Haplophragmoides* Cushman 1910

Haplophragmoides porrectus Maslakova 1955

1955. *Haplophragmoides porrectus* Maslakova: p. 47, Plate 3, Fig. 5, 6.

Haplophragmoides spp.. Plate 1, Fig. 5; Table 2.1-morphogroup 1-TS

Discussion. This species is agglutinated and abundant in all samples, and showing large involute planispiral coiling flattened agglutinated wall, and consisting of two to three whorls (McNeil and Caldwell, 1981).

Subfamily AMMOMARGINULININAE Podobina, 1978

Genus *Ammobaculites* Cushman, 1910

Ammobaculites subcretaceus Cushman & Alexander 1930.

Plate 1, Fig. 7-9; Table 2.1-morphogroup 1-PS/UnS

Discussion. Ammobaculites spp. species in the samples were identified from agglutinated test morphology. Tests are flattened planispiral (coiled) to an uncoiled portion (uniserial-elongated arrangement), and the uncoiled part is short. The test wall is agglutinated, and poorly to moderately preserved. No chamber can be observed (McNeil and Caldwell, 1981).

Family TROCHAMMINIDAE Schwager, 1877

Genus *Trochammina* Parker and Jones, 1859

Trochammina spp.

Plate 1 Fig. 6; Table 2.1-morphogroup 1-TS

Discussion. Trochammina spp. has agglutinated test, and was identified based on the outline morphology of the tests, and in SEM. It is possible to see faint lines (septum) that defined chambers. Most of the specimens have undergone deformation and are poorly preserved.

Family ASTORHIZIDAE Brady, 1881

Genus *Bathysiphon* Sars, 1872

Bathysiphon spp.

Plate 2, Fig. 5-7; Table 2.1-morphogroup 3-UnLT

Discussion. This species is agglutinated and abundant in all samples. No other characters can be observed, except the location of the aperture and overall test morphology.

Family RZEHAKINIDAE Cushman, 1933

Genus MILIAMMINA Heron-Allen and Earland, 1930

Miliammina spp.

Plate 2, Fig. 1-4; Table 2.1-morphogroup 2-Mi

Discussion. Miliammina spp. is agglutinated and rare in most of the samples likely due to poor preservation. In lateral view, the test is sub-rectangular in shape, and it is moderate in size. Chambers are not visible, but from the overall test morphology, chambers appear to be tubular arranged in a quinqueloculine plan. The test wall is agglutinated and fine-grained. Aperture is obscure, and is an opening at the end of the tubular chamber (McNeil and Caldwell, 1981).

Family TURRILNIDAE Cushman, 1927

Genus *Neobulimina* Cushman and Wichenden,

1928 *Neobulimina albertensis* (Stelck and Wall), 1954 Plate 3, Fig. 1-6; Table 2.1-morphogroup 3-TrS

1954. *Guembelitria cretacea* Cushman *var. albertensis* Stelck and Wall, p. 23, Plate 2, Fig. 19. 11. 2-4.

1954. *Bulimina wyomingensis* Fox, p. 118-119, Plate 26, Fig. 8-11.

1955. *Guembelitria cretacea* Cushman *var. spiritensis* Stelck and Wall, p.44, Plate 2, Fig. 5

1962. *Neobulimina albertensis* (Stelck and Wall); Tappan, p.184, Plate 48, Fig. 3-6.

1965. *Praebulimina wyomingensis* (Fox); Eicher, p. 903, Plate 106, Fig. 4.

1966. *Neobulimina albertensis* (Stelck and Wall); Eicher, p. 26, Plate 5, Fig. 5-8.

1967a. *Praebulimina wyomingensis* (Fox); Eicher, p. 185, Plate 18, Fig. 7.

1970b. *Neobulimina albertensis* (Stelck and Wall); Eicher and Worstell, p.290, Plate 4, Fig. 8

1976. *Neobulimina albertensis* (Stelck and Wall); Evetts, Plate 3, Fig. 8-10.

Discussion. Neobulimina albertensis is abundant and flattened. Overall, tests were small, stout, with sharp tapered to near parallel shaped and rounded towards the distal end. The greatest width was midway between proximal and distal ends. The chambers were inflated, sub-globular to sub-rectangular in lateral view, and arranged triserially or trochospire (with 3 chambers per whorl) and later bi-serial arrangement (McNeil and Caldwell, 1981).

Family TEXTULARIIDAE Ehrenberg, 1838

Genus *Textularia* Defrance,1824,

Textularia spp., Plate 3 Fig. 7-9.; Table 2.1-morphogroup 3-BiS

Discussion. This genus was identified based on the general morphology that characterizes *Textularia spp.*: bi-serial and elongated, and in all samples shows flattened tests, with no clear distinction between chambers and aperture.

Testate amoebae Taxonomic Description

Phylum PROTOZOA Goldfuss, 1818

Subphylum SARCODINA Schmarda, 1871

Class RHIZOPODA von Siebold, 1845

Subclass LOBOSA Carpenter, 1861

Order ARCELLINIDA Kent, 1880

Superfamily ARCELLACEA Ehrenberg, 1830

Family DIFFLUGIDAE Stein, 1859

Genus *Difflugia* Leclerc in Lamarck, 1816

Difflugia oblonga Ehrenberg, 1832, p.90.

Difflugia oblonga Ehrenberg in Medioli and Scott, 1983, Plate 2, Fig. 1-27.

Plate 4, Fig. 1-4; Table 2.1-morphogroup 4-Ta-F

Discussion. This taxa shows high variation, and was widespread in the samples. *Difflugia oblonga* were laterally compressed (Plate 5, Fig. 1-4), and rarely they retained their original shape. However, they show remarkable similarity with Holocene examples (Patterson and Kumar, 2002; van Hengstum et al., 2007).

Difflugia proteiformis Lamarck 1816

Difflugia proteiformis Lamarck, 1816, p.95 (with reference to the material by LeClerc).

Difflugia proteiformis Lamarck in Medioli and Scott, 1983, Plate 1, Fig. 15-20.

Plate 5, Fig. 1; Table 2.1-morphogroup 4-Ta-F

Discussion. Representative specimens are few. The aperture was wide in comparison to some of Holocene examples and the neck was absent. No specimens retained their original test shape and were flattened and could potentially be mistaken for *Difflugia oblonga.*

Difflugia corona Walich

Difflugia proteiformis (sic) (Ehernberg)

subspecies *D. globularis* (Dujardin) *var. D. corona* Walich, 1864, p.244, Plate 15, Fig. 4b, Plate 16, Fig. 19, 20.

Difflugia corona Walich. Archer, 1866, p.186; Medioli and Scott, 1983, p.22, Plate 1, Fig.

6-14; Scott and Medioli, 1983, p.818, Fig. 9P; Patterson et al., 1985, p.134, Fig. 1-6.

Plate 5, Fig. 2; Table 2.1-morphogroup 4-Ta-F

Discussion. Tests are subspherical in shape and compressed and missing their mouth collar.

Difflugia urceolata Carter

Difflugia urceolata Carter, 1864, p.27, Plate 1, Fig. 7; Scott et al., 1977, p.1578, Plate 1, Fig. 3, 4; Scott et al., 1980, p. 224, Plate 1, Fig. 10-12; Medioli and Scott, 1983, p.31, Plate 3, Fig. 1-23, Plate 4, Fig. 1-4; Scott and Medioli, 1983, p.818, Fig. 9F, G; Patterson et al., 1985, p.134, Plate 2, Fig. 11, 12.

Lagunculina vadescens Cushman and Brönnimann, 1948a, p.15, Plate 3, Fig. 1, 2; Parker, 1952a, p.451, Fig. 8.

Plate 5, Fig. 3-5; Table 2.1-morphogroup 4-Ta-F

Discussion. This species as other *Difflugids* was identified based on its flask-shaped test, which is similar to *D. oblonga.* However, this species has a very wide test and large aperture.

Genus *Lagenodifflugia* Medioli and Scott, 1983

Lagenodiffuliga cf. vas (Leidy, 1874)

Difflugia vas Leidy, 1874, p. 155.

Lagenodifflugia vas (Leidy, 1874) Medioli and Scott, 1983.

Plate 5, Fig. 6; Table 2.1-morphogroup 4-Ta-F

Discussion. Tests are agglutinated, flask-shaped, and laterally compressed. Circular restriction in the neck around the circumference was apparent.

Genus *Centropyxis* Stein, 1859

Centropyxis aculeate Ehrenberg

Arcella aculeate Ehrenberg, 1832 (ab Ehrenberg, 1830, p.60, nomen nudum), p.91.

Centropyxis excentricus (Cushman and Brönnimann).

Scott, 1976b, p.320, Plate 1, Fig. 1,2; Scott et al, 1977, p.1578, Plate 1, Fig. 1,2; Scott et al, 1980, p. 224, Plate 1, Fig. 1-3.

Centropyxis aculeata (Ehrenberg). Stein, 1859, p. 43;

Medioli and Scott, 1983, p.39, Plate 7, Fig. 10-19; Scott and Medioli, 1983, p.819, Fig. 91; Patterson et al., 1985, p.134, Plate 4, Fig. 1-7; Scott et al., 1991, p.384, Plate 1, Fig. 7-9.

Plate 5, Fig. 7-8; Table 2.1-morphogroup 4-Ta-S

Discussion. *C. aculeata* species was identified by its overall test morphology, which is sack-shape, and it shows deformation due to the compression and poor preservation. In SEM, the aperture appears angled and broken.

Centropyix constricta (Ehrenberg)

Arcella constricta Ehrenberg, 1843, p. 410, Plate 4, Fig. 35, Plate 5, Fig. 1.

Difflugia constricta (Ehrenberg). Leidy, 1879, p. 120, Plate 18, Fig. 8-55.

Urnulina compressa Cushman, 1930a, p. 15, Plate 1, Fig. 2; Parker, 1952, p. 460, Plate 1, Fig.

9; Scott et al., 1977, p. 1578, Plate , Fig. 7, 8; Scott et al., 1980, p. 224, Plate 1, Fig. 13–15.

Centropyxis constricta (Ehrenberg). Deflandre, 1929, p. 340, text-Fig. 6-67; Medioli and Scott, 1983, p. 41, Plate 7, Fig. 1-9; Scott and Medioli, 1983, p. 819, Fig. 9K; Patterson et al., 1985,

p. 134, Plate 4, Fig. 8–14; Scott et al., 1991, p. 384, Plate 1, Fig. 4.

Plate 5, Fig. 9; Table 2.1-morphogroup 4-Ta-D

Discussion. This species was identified by its overall test morphology, which is donut-shape, and as in *Difflugia oblonga*, this species shows lateral compression. We could not observe the aperture because of the poor preservation, and lateral compression. However, it can be identified by its more/less circular shape and a slight central depression from the aperture.

2.4 Conclusions

This research establishes a taxonomic framework for the Ferron-Notom delta using morphogroup analysis of foraminifera and testate amoebae. The morphogroup analysis identifyied nine foraminiferal morphotypes, which included genera of *Gavelinella, Ammobaculites, Trochammina, Miliammina, Bathysiphon, Reophax, Neobulimina, and Textularia*, and two morphotypes of testate amoebae, which included two genera: *Difflugia and Centropyxis*. All morphotypes are agglutinated walled-tests, and calcareous walled-test are largely absent, with only ten specimens documented in two samples. Taphonomic processes, including compaction, and dissolution, have had a significant impact on foraminifera and testate amoebae preservation in the study area. All specimens were flattened due sediment compaction which led to test deformation and the calcareous tests are absent. However, despite these taphonomic biases, morphogroup analysis will provide useful information on salinity trends with the inclusion of the testate amoebae morphogroup in estuarine settings.

2.5 Acknowledgements

This work was made possible through Natural Sciences and Engineering Research Council (NSERC) Discovery Grants (EGR — 2015-057250) and the Canada Foundation for Innovation John R. Evans Leaders Fund (CFI-JELF grant 105-04523). CRD to Dr. Bhattacharya, as well as BP Canada, and the Susan Cunningham Research Chair in Geology. King Abdulaziz University funded a scholarship through the Kingdom of Saudi Arabia Embassy, and the Kingdom of Saudi Arabia Cultural Bureau, Ottawa, ON, Canada. Canadian Center for Electron Microscopy (CCEM), McMaster University, Hamilton, ON, Canada, provided SEM training.

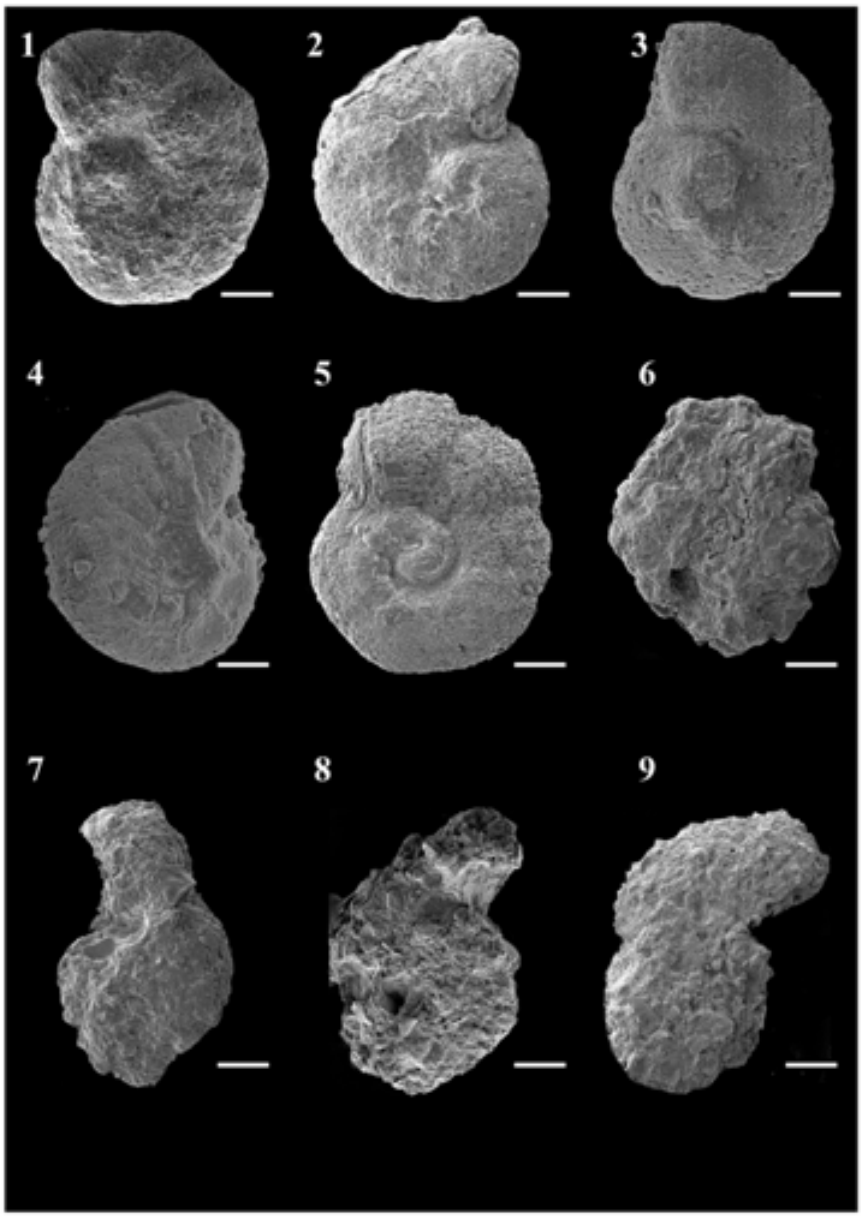

Plate 1: (1 - 2) *Gavelinella ammonoides* (Reuss, 1845), in umbilicalside view. (3-4) *Gavelinella lorneiana* (Cushman, 1938), (3) spire side view. (4) umbilical side view. (5) *Haplophragmoides sp.*, umbilical side view. (6) *Trochammina spp.* (7-9) *Ammobaculites subcretaceus* (Cushman andAlexander, 1930). Scale bars = 50 μm.

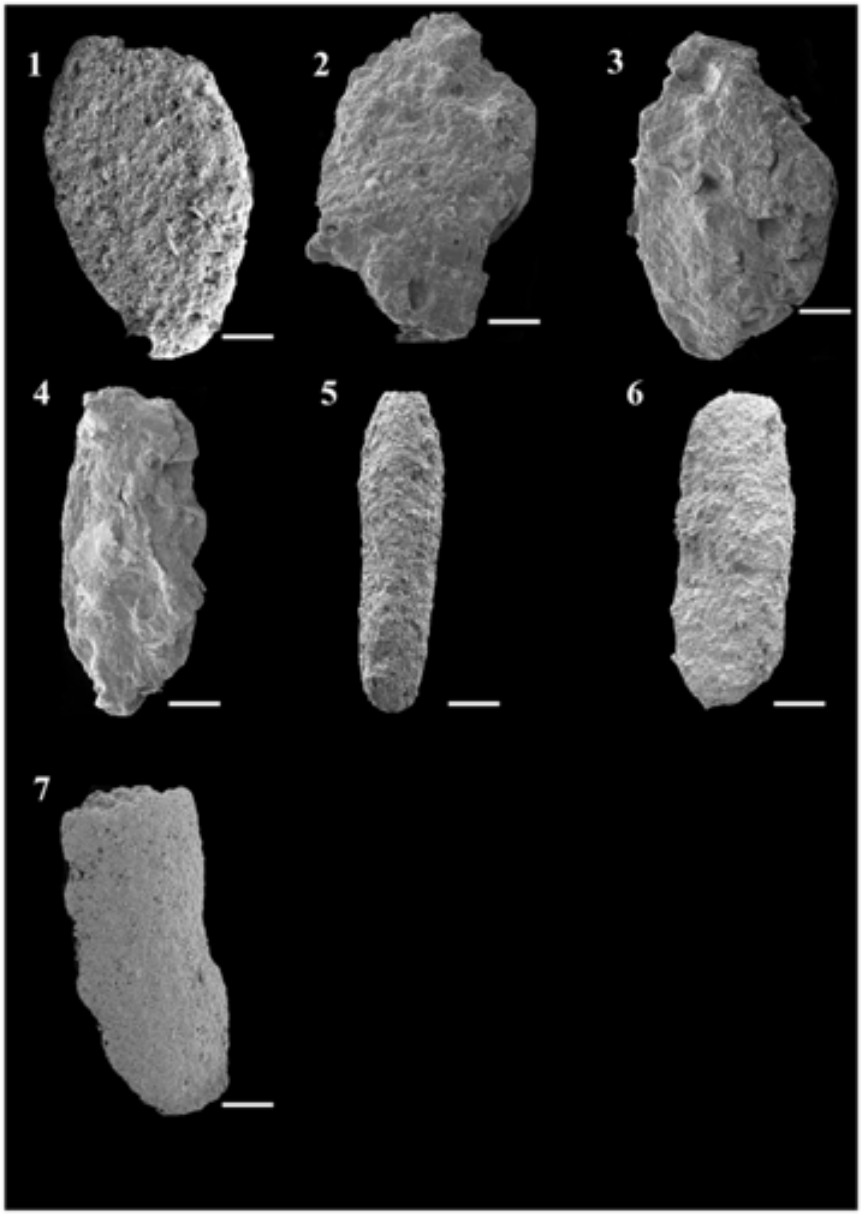

Plate 2: (1-4) *Miliammina spp.*, chamber side view, tests are flattened and deformed (5-6) *Reophax spp.* (7). *Bathysiphon spp.* (Sars, 1872),in edge view. Scale bars = 50μm.

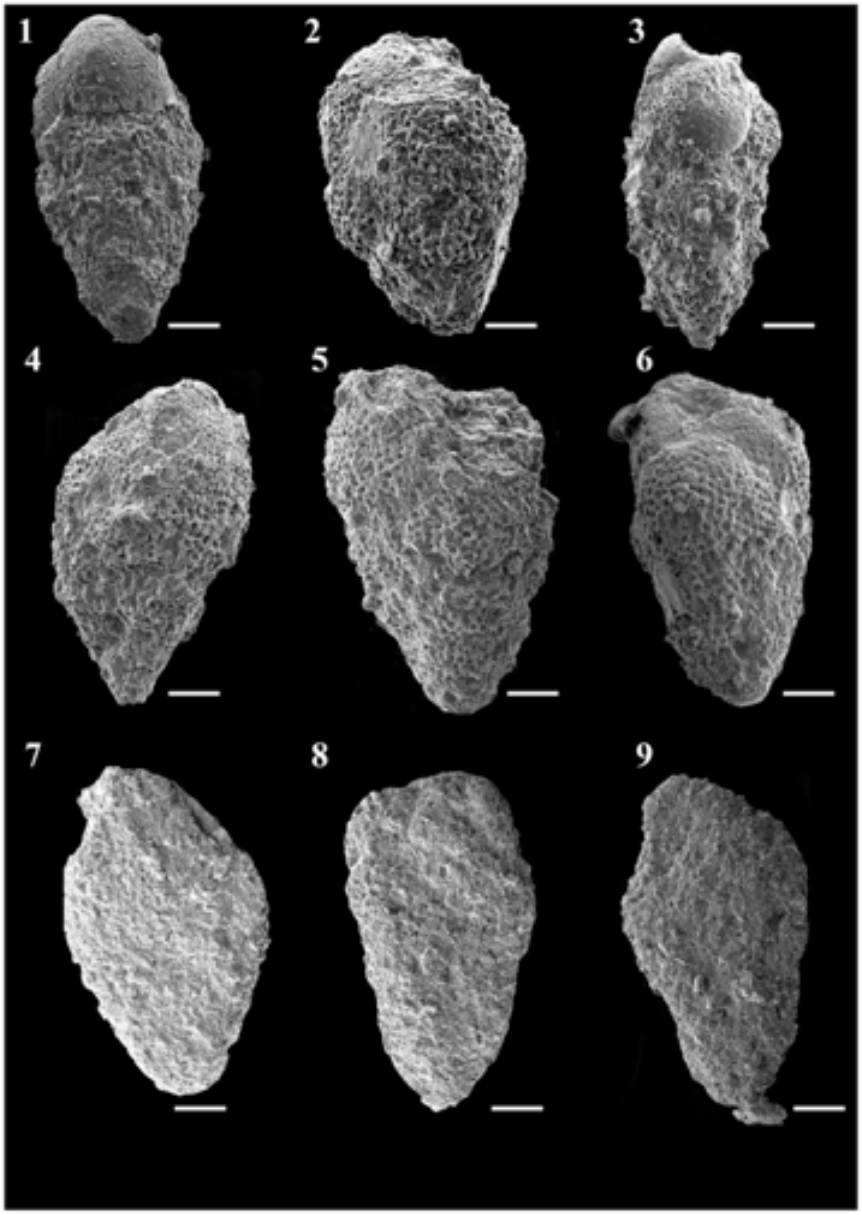

PLATE 3: (1-4(6)) lateral view of *Neobulimina albertensis* (Stelck and Wall, 1954). (1-4(6)) tri-serial arrangement of *N. albertensis*. (5 - 9) biserial arranged chambers deformed (by dissolution) and flattened tests of *Textularia spp.* Scale bars = 50μm.

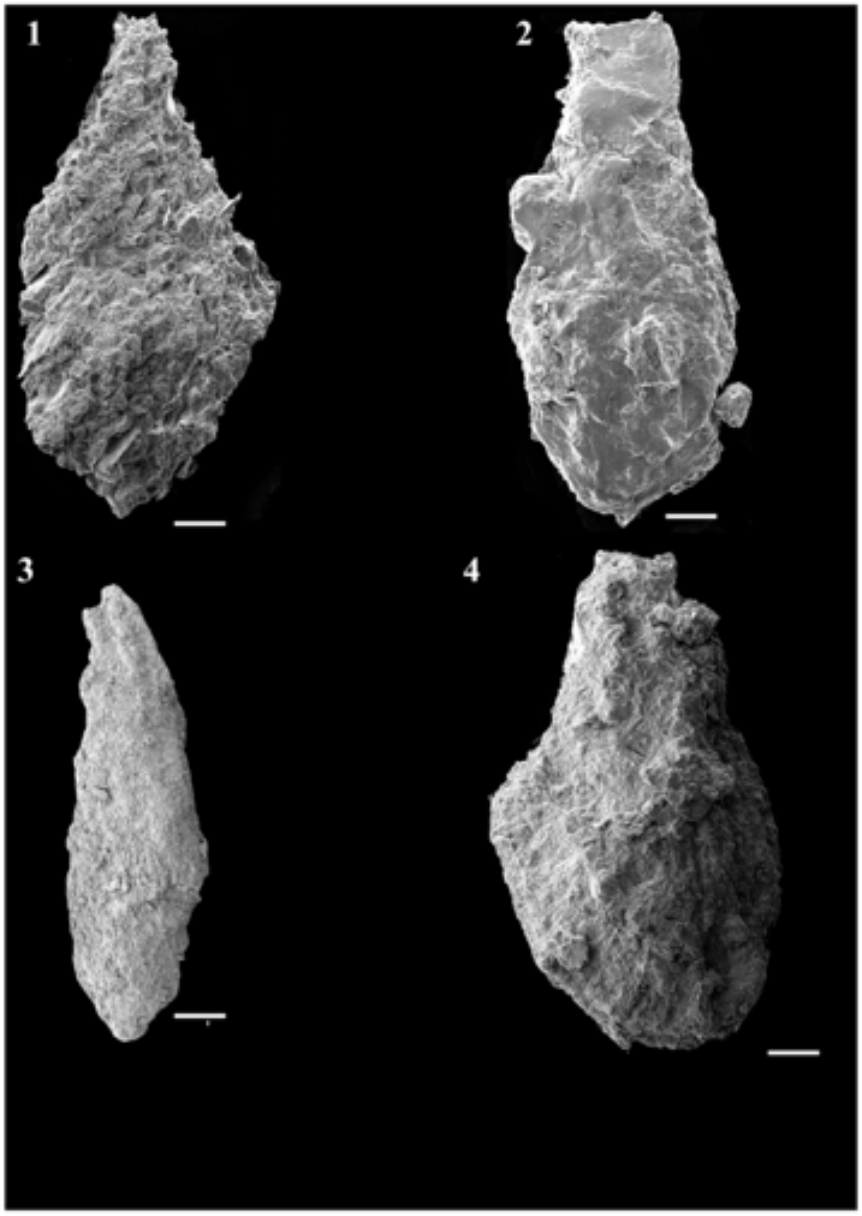

Plate 4: (1-4) *Difflugia oblonga* (Ehrenberg, 1832), in sideviews of different morphotypes of the species. Scale bars = 50 μm.

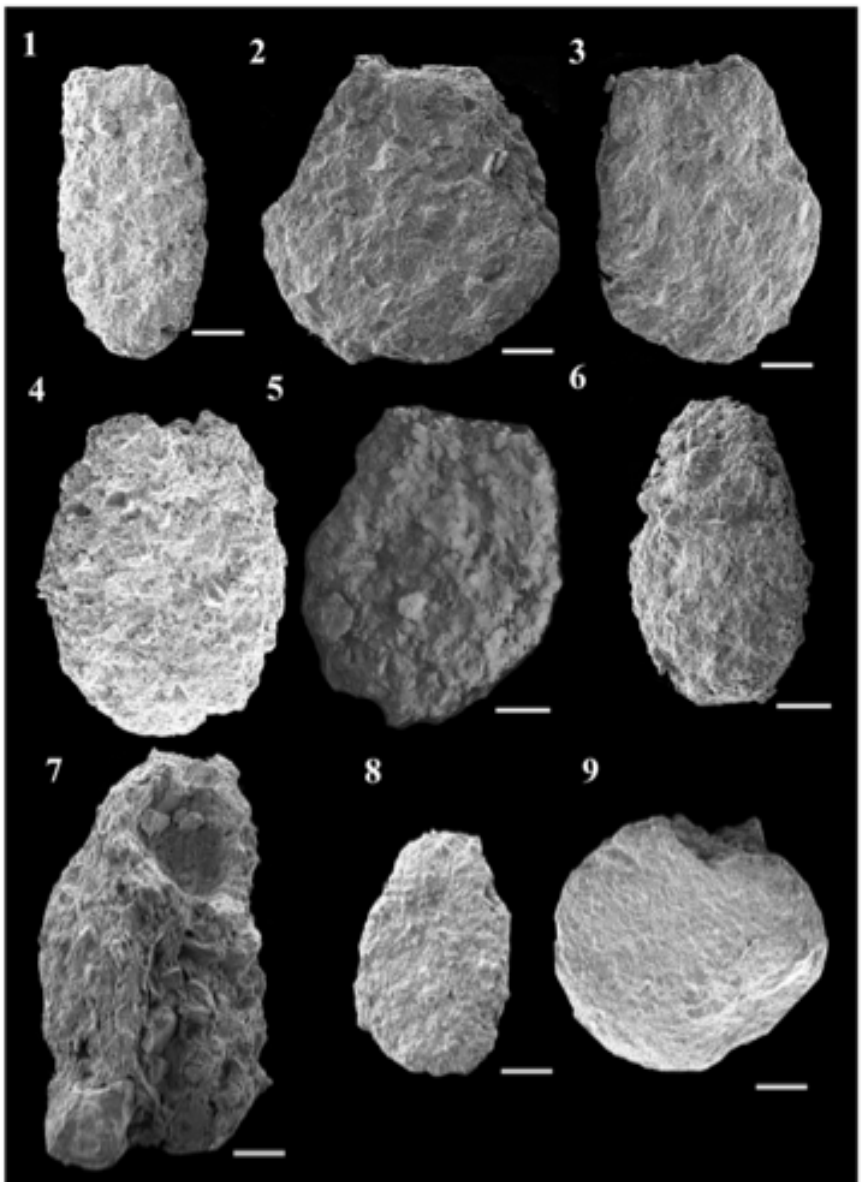

Plate 5: (1) *Difflugia proteiformis* (Lamarck, 1816), (2) *Difflugia corona* (Walich),(3 - 5) *Difflugia urceolata* (Carter). (6) *Lagenodifflugia cf. vas* (Leidy, 1874). (7-8) *Centropyxis aculeate* (Ehrenberg). (9) *Centropyxis constricta*. All specimens are in sideviews. Scale bars =50μm.

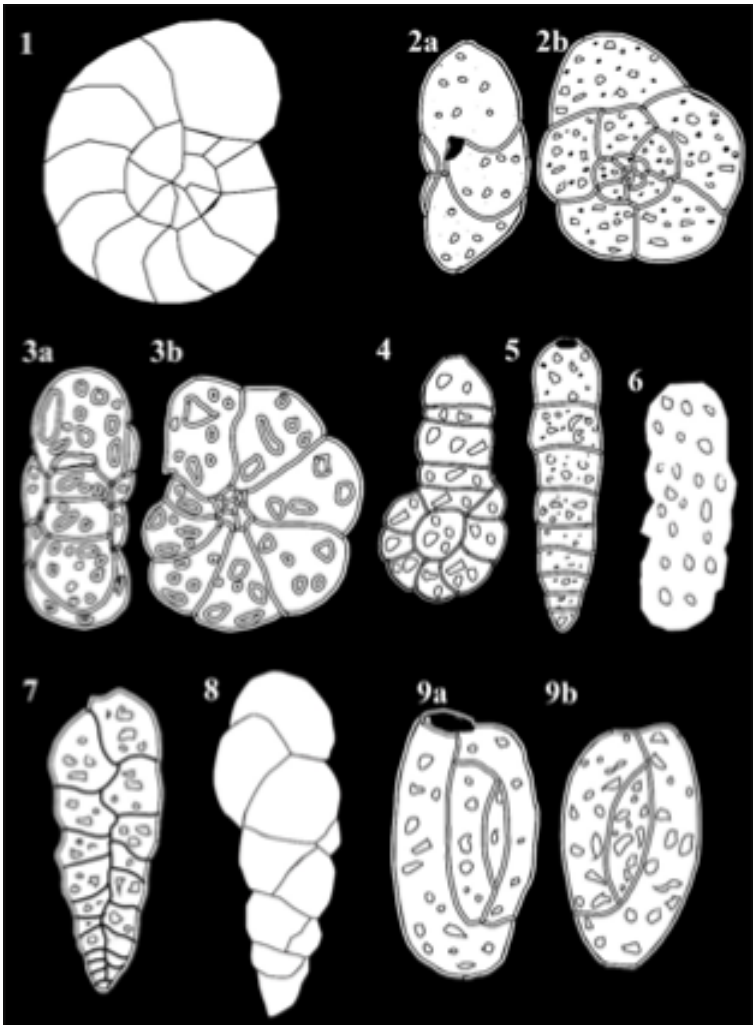

Figure 2.5: Line drawings of modern and Cretaceous foraminiferal species as representative for the present study species. Modified and redrawn from Scott et. al. 2005. (1) *Gavelinella spp.*, (2) *Trochammina inflata*, 2a.ventral view, 2b. edge view. (3) *Haplophragmoides spp.* 3a. apertural view, 3b. side view. (4) *Ammobaculites spp.* (5) *Reophax spp.* (6) *Bathysiphon spp.* (7) *Textularia spp.* (8) *Neobulimina albertensis* (9) *Miliammina fusca.* 9a, side view, 9b, opposite sideview.

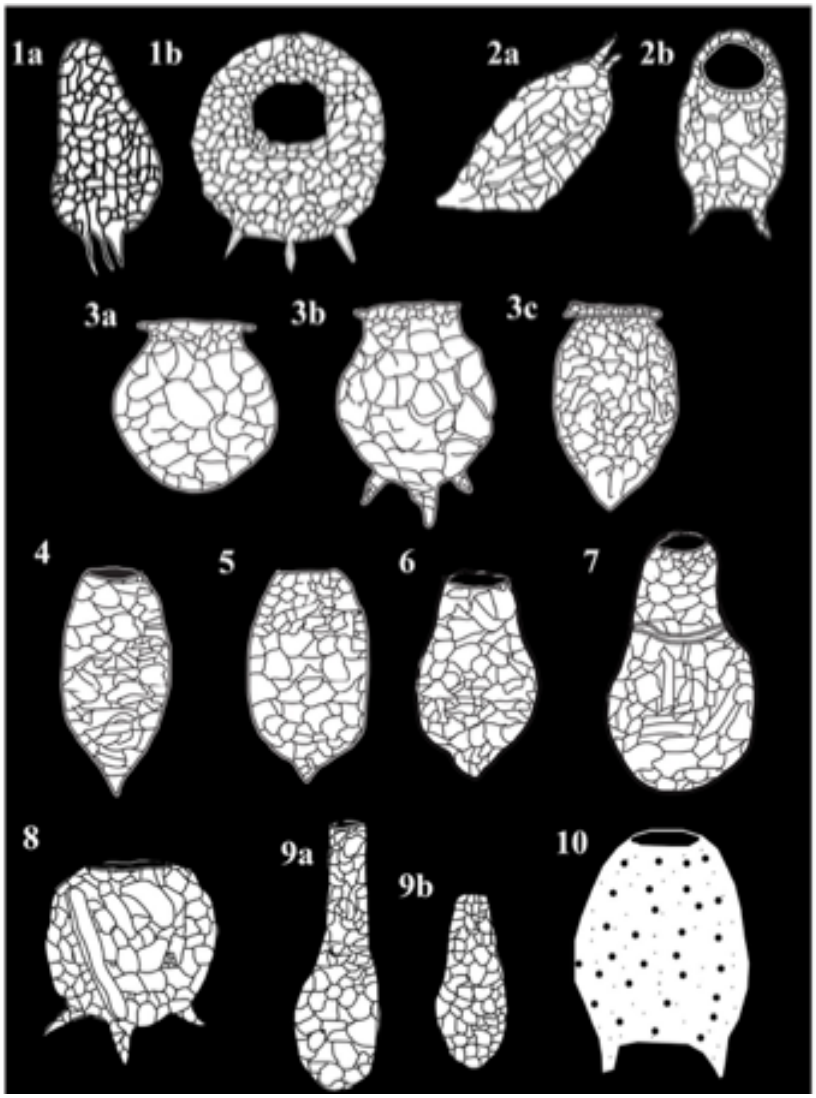

Figure 2.6: Line drawings of modern testate amoebae species as representative for the present study species. Modified and re-drawn from Scott et. al. 2005. (1) *Centropyxis aculeata*, 1a. edge view,1b. aperture view. (2) *Centropyxis constricta*, 2a. lateral apertural view, 2b.edge view. (3 & 10) *Difflugia urceolata*, 3a-b, morphological variations, and 3c, aperture view. (4-6) *Difflugia proteiformis*. (7) *Lagenodifflugia vas*.(8) *Difflugia corona* (9) *Difflugia oblonga*, 9a-b, side views.

Chapter 3

Foraminifera and Testate Amoebae Morphogroup Analysis and Biofacies of the Upper Cretaceous (Turonian) Ferron-Notom Delta, Utah, USA.

Majed N. Turkistani*, Eduard G. Reinhardt*, David Kynaston* and Janok P. Bhattacharya*

*School of Earth, Environment and Society, McMaster University, 1280 Main Street West, Hamilton, ON L8S 4K1 Canada

This paper will be submitted to *Cretaceous Journal* and will included in its published form once accepted

Abstract

Morphogroup and biofacies analysis was conducted on strata of the Upper Cretaceous (Turonian) Ferron-Notom delta, Central Utah, USA. This study investigates associations between ancient deltaic environments and foraminiferal and testate amoebae assemblages with an assessment of their ecological zonation based on their extant Holocene counterparts. Sixty-six hand specimens of mudstone were collected from the three outcrops along strike and dip profiles. Previous, morphogroup analysis showed four morphogroups and eleven morphotypes of foraminifera and testate amoebae indicating relationships between test morphology and depositional environment. Based on this preliminary analysis, we use the morphotypes to define four main biofacies using cluster analysis, and biodiversity indices. However, because of fossilization biases and the partial loss of the calcareous fraction, the biodiversity indices are only used as relative measures. Despite this taphonomic bias, the agglutinated foraminifera and testate amoebae morphogroups show trends with salinity both among the outcrops and stratigraphically within the outcrops. The Blue Hills outcrop represents the most landward and thus the lowest salinity environment (tidally-influenced backwater), Steamboat is more coast proximal with a higher salinity found in the delta front and fluvial estuarine environment, and the Caineville North outcrop represents the most coast proximal with variable low - medium salinity of the prodelta/delta front and fluvial/estuarine environment. It appears that landward and coastward transport of tests led to a taphonomic bias. Nonetheless, the assemblages provide useful information that correlates with previously documented lithofacies data. A salinity index which is a ratio of trochospiral taxa versus testate amoebae taxa provides a useful measure of coastal proximity that matches lithofacies trends. In addition, an OM index, which is the ratio of "bolivind-type" taxa versus trochospiral taxa shows relationships with original organic content.

Keywords: Ferron Sandstone delta, Upper Cretaceous, Morphogroup analysis, Biofacies, Foraminifera, Testate amoebae, Paleoenvironments

3.1 Introduction

Marginal marine settings include deltas, estuaries, lagoons, and tidal flats, where waves, rivers, currents, and tides dominate, and are often classified based on physiochemical criteria (e.g. salinity, pH, temperature, etc). However, these criteria are missing in ancient rock strata and can only be estimated using lithological, fossil or geochemical evidence (Scott et al., 2005). Fossil assemblages and comparisons with modern analogs can offer insight into how these systems formed and

more importantly, provide information on paleo-salinity which can be important for reconstructing sea-level and proximity to the shoreline (Bhattacharya and Tye, 2004; Scott et al., 2005; Akyuz et al., 2015). For decades foraminiferal assemblages have been used as paleoenvironmental indicators throughout geological time periods (mostly Mesozoic-Cenozoic), while testate amoebae have been more widely applied in Quaternary and Holocene strata (Scott et al., 2005). Their combined ecological range from the deep sea to marginal marine settings (foraminifera) and freshwater environments (testate amoebae, lakes, rivers, and wetlands; Scott et al., 2005), make their combined application useful proxies for determining sea-level fluctuations (Haynes, 1973; Scott et al., 1976; Scott and Medioli, 1978; Houghton et al., 1990; Scott and Medioli, 1980b; Scott et al., 1995b), estuarine classification (Nichols, 1977) and the lateral movement of freshwater/marine transitions (Schafer, 1974; Scott et al., 1977; Scott and Medioli, 1980c; Haman, 1990; Patterson, 1990; Scott et al., 1991; Collins, 1996). These Holocene examples show their potential for reconstructing paleoenvironment conditions, and foraminifera and testate amoebae can often determine sea-level changes up to centimeters in resolution (e.g. Houghton et al., 1990). Ecologically, testate amoebae appear to be static in terms of their ecological constraints over the Phanerozoic. Testate amoebae have been recorded from marine to freshwater settings from the Mesozoic (van Hengstum et al., 2007; Turkistani et al., submitted), Palaeozoic (Farooqui et al., 2010) and Pre-Cambrian (Porter and Knoll, 2000).

Turkistani et al. (submitted, Chapter 2), proposed a morphogroup framework for foraminifera and testate amoebae in the mudstones of the Ferron-Notom delta (Figs. 3.1,3.2). In this study, we use the morphotypes defined in the morphogroup analysis to identify biofacies in three outcrops (Caineville North, Steamboat, Blue Hills). The concept of morphogroup analysis was first introduced by Jones and Charnock (1985), which used test morphology of agglutinated foraminifera to determine paleoenvironments (e.g. marine, marshes, estuaries), but also calcareous foraminifera (Reolid et al., 2008). The advantages of morphogroup analysis are: 1) increased sample size by combining individual species, and 2) reduction of fossilization biases and taxonomic uncertainty with species identification (Nagy, 1992). Morphogroup analysis shows significant potential in paleoenvironmental studies in Paleozoic and Mesozoic contexts. Fossilization often inhibits the identification of taxa, but the data can still provide useful paleo-evnironmental information that would be otherwise unavailable (Nagy, 1992; Nagy et al., 1995; Reolid et al., 2008; Turkistani et al., submitted).

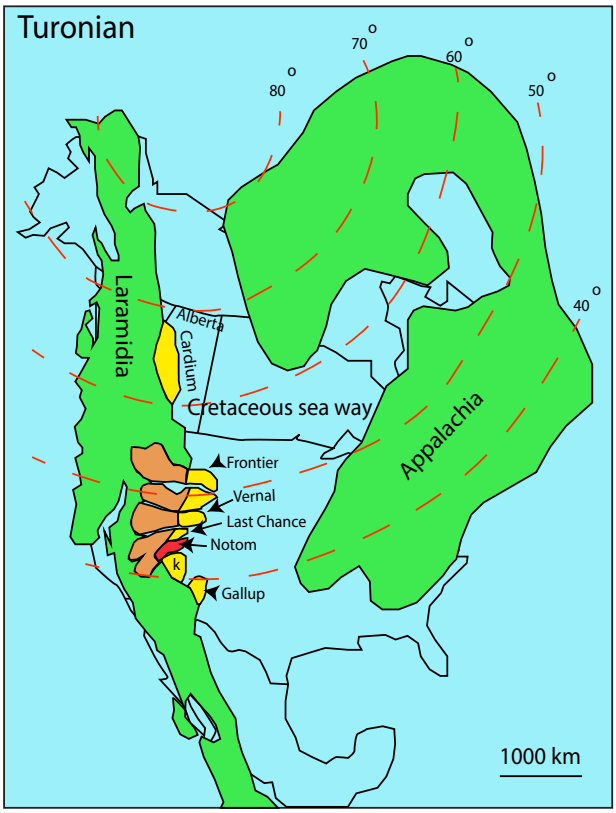

Figure 3.1: Map of the North American continent during the Upper Cretaceous (Turonian), where the Western Interior Seaway split the continent into two subcontinents (after Bhattacharya and Tye, 2004; Zhu et al., 2012)

3.1.1 Holocene Foraminifera and Testate Amoebae Environmental Distributions

Foraminifera and testate amoebae have been used as proxies in Quaternary environments for the identification of estuaries, lagoons, and marshes because they are sensitive to salinity and temperature and because they have mineralized tests, which preserve well as fossils (Fig. 3.3 Murray, 1973; Scott et al., 2005). Generally, calcareous foraminifera are relatively dominant in warm water with a minimum salinity of 10 ppt, whereas calcareous foraminifera in cold water are generally found in salinity $>$ 20 ppt (i.e. open sea; Scott et al., 1980; Gupta, 2003; Scott et al., 2005). Agglutinated foraminifera are predominantly found in a range of salinities between $<$ 20 ppt and $>$ 30 ppt (Scott et al., 1980; Alve, 1990). Testate amoebae are freshwater taxa, and can only tolerate lower salinity ($<$ 5 ppt), thus they are useful indicators of freshwater influx, such as runoff from rivers and streams

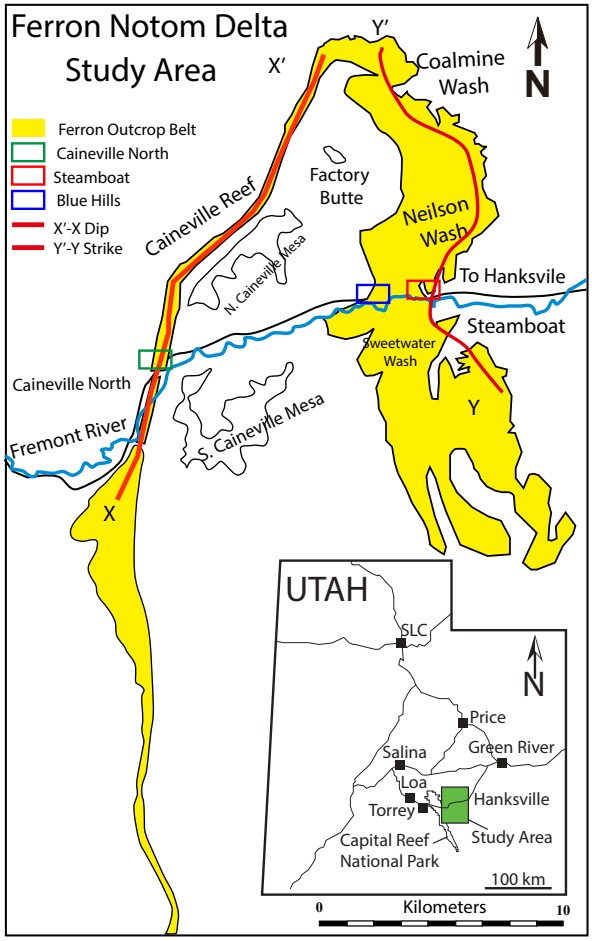

FIGURE 3.2: Map of the Ferron-Notom delta showing the five outcrops of the current study, and the Caineville North outcrop on the western part (after Li and Bhattacharya, 2013; Zhu et al., 2012; Akyuz et al., 2015)

in coastal areas. Taphonomically, they are also useful indicators of freshwater transport with rainfall (Scott et al., 2005; Babalola, 2009).

Estuaries

Estuaries are influenced by riverine and tidal conditions, which affects circulation patterns and salinity (Scott et al., 1980; Scott et al., 2005; Ghosh and Filipsson, 2017). The classification of eastern Canadian estuaries by Scott et al. (1980) provides an example of how benthic foraminifera can be used to indicate salinity zonation. Scott et al. (1980) subdivided the estuaries of Miramichi River, Restigouche Estuary, and Chezzetcook Inlet into four zones, which vary in salinity,

depth, and marine influence. Based on the Scott et al. (1980) classification scheme, estuaries can be subdivided into zones as follows:

Upper estuarine/Riverine. This zone has the lowest salinity, typically < 16 ppt and high organic content sediment with species diversity that tends to be low and mostly made up of agglutinated taxa (Scott et al., 1977). *Milimmina fusca* (morphotype-Mi; Chapter 2; Turkistani et al., submitted) is commonly dominant in the upper estuary among other taxa, such as *Ammobaculites spp., Ammotium salsum* (morphotypes PS/UnS and PS). *M. fusca* can also be found within intertidal, shallow and deep subtidal salinity transition zones (Fig. 2.3). Testate amoebae, such as *Difflugids and Centropyxids*, (morphotypes Ta-F, Ta-D, Ta-S) mark the extent of marine influence inland (Gehrels et al., 2001; Scott et al., 2005; Charman et al., 2010; Shaw, 2013; Châtelet et al., 2018; Müller-Navarra, 2018).

Mid-estuarine. This zone is where mixing of river and marine water occurs (Scott et al., 1977; Scott et al., 1980), and normally has a salinity range from 16 ppt to 26 ppt (Alve and Nagy, 1986; Fernandes et al., 2019). Foraminiferal assemblages tend to be higher in diversity and include more, or mostly calcareous taxa in this zone, including *Elphidium, Ammonia, and Ammotium* (morphotypes PS and TS; Fig. 3.3; Chapter 2; Turkistani et al., submitted).

Lower estuarine. This zone is characterized as the most seaward part of an estuary, and the salinity is close to normal marine (33-35 ppt). Calcareous foraminifera, such as *Ammonia* and *Elphidium* (morphotypes TS, PS) tend to be dominant but agglutinated taxa maybe common (Fig. 3.3; Scott et al., 1980), organic content is high, and "bolivinid-type" taxa may also be found (e.g. BiS, TrS; Turkistani et al., submitted).

Lagoon

Lagoons are characterized by brackish to hyper-salinity with lesser freshwater input, from stream or groundwater and barriers often form through longshore sediment drift (Scott et al., 2005; Alday et al., 2013). Lagoons are found worldwide but commonly form on warm and arid coasts, such as in the Arabian Gulf, the Mediterranean, and on the Australian coastlines (Scott et al., 2005). Calcareous foraminifera taxa tend to dominate lagoons with normal to hypersaline conditions but agglutinated taxa can also be present in brackish settings (Scott et al., 2005; Alday et al., 2013). Foraminiferal assemblages commonly found in a lagoon environment are *Ammonia tepida, Quinqueloculina seminula, Trochammina amnicola, Rosalina sp., and Ammobaculites exiguus*, and diversity can range from high to low depending on salinity (Culver et al., 2012). Brackish, marginal marine, and open marine taxa, such as *Ammonia beccarii, Haynesina depressula, Milimmina fusca,*

Textularia spp., Elphidium charlottensis, Bolivina and Quinqueloclina, Trochammina inflata and *Elphidium excavatum* (morphotypes PS, Mi, BiS, TS; Hayward and Hollis, 1994; Hayward et al., 2011) dominate depending on the salinity.

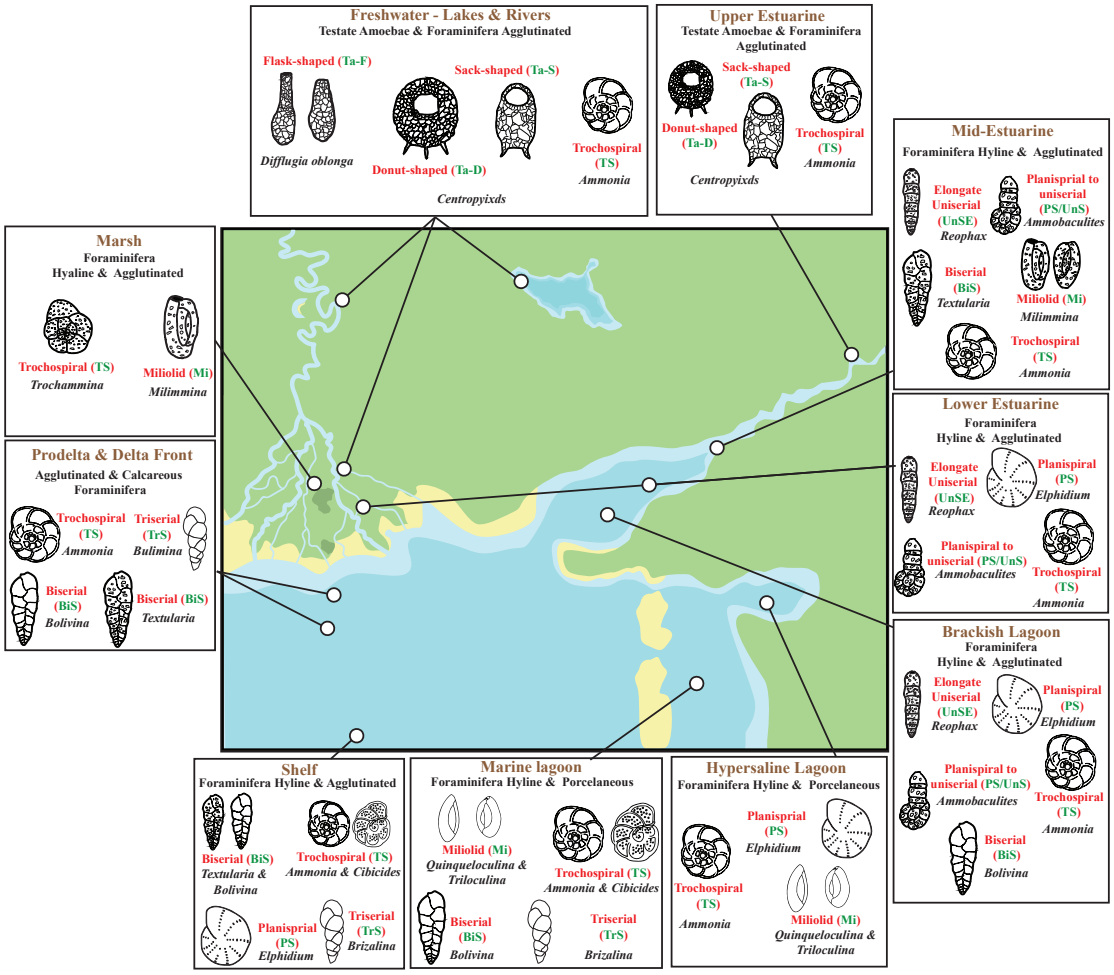

Figure 3.3: Typical Holocene distribution of foraminiferal and testate amoebae in modern coastal environments. (after Scott et al., 2005)

.

Marshes

Marshes form on the protected margins of estuaries and lagoons, and are zoned according to tidal elevation that controls inundation and salinity (low and high marsh). As such, the marsh zones have a range of salinity, temperature, and *pH* (high, mid, low marsh; Phleger and Bradshaw, 1966). In such environments, occurrences of foraminifera and testate amoebae are primarily controlled by variations

in these physiochemical criteria (Scott et al., 2005). Agglutinated taxa, including foraminiferal and testate amoebae exclusively dominate the high marshes (Fig. 3.3; Scott et al., 2005). Calcareous foraminifera are unlikely to live, or be preserved in the high marsh environment due to the low *pH*, while agglutinated foraminifera tend to dominate as they are adapted to low oxygen and low *pH* conditions (Scott and Medioli, 1980a; Scott et al., 2005). In the upper reaches of a high marsh, testate amoebae, such as *Centropyixds, and Difflugids* (morphotypes Ta-F, Ta-D, Ta-S) occupy the most inland area, where the flood tide inundates the area only a few days annually (Ozarko et al., 1997; Gehrels et al., 2001; Shaw, 2013; Châtelet et al., 2018; Müller-Navarra, 2018). Common high marsh foraminifera taxa are *Trochammina*, and *Jadammina macrescens* (morphotype TS; Gehrels et al., 2001; Shaw, 2013; Châtelet et al., 2018; Müller-Navarra, 2018). In the low marsh, agglutinated *Ammobaculites spp.* (morphotype PS/UnS), *Miliammina spp.* (morphotype Mi), *Haplophragmoides welberti* (morphotype PS), and calcareous *Ammonia beccari* (morphotype PS) foraminifera commonly are found (Ozarko et al., 1997; Gehrels et al., 2001; Shaw, 2013; Châtelet et al., 2018; Müller-Navarra, 2018).

Prodelta, Delta front, and Shelf

The prodelta environment is characterized by medium to normal marine salinity depending on riverine outflow, and is strongly influenced by episodic river floods (Tesi et al., 2011). Calcareous foraminifera taxa found in the prodelta typically are *Ammonia, Bulimina, Bolivina, Elphidium, Rectuvigerina* and *Lenticulina* (morphotypes TS, TrS, BiS, PS, UnSE), and alggutinated foraminifera, such as *Reophax, Bigenerina, Textularia,* and *Cribrostomoides* (mophotypes UnSE, BiS, PS). The delta front is characterized by brackish conditions and is frequently affected by waves and river flooding (Coleman, 1982). In the delta front, like the prodelta, calcareous foraminifera taxa dominate, such as *Cibicides, Quinqueloculina, Bolivina,* and *Elphidium* (morphotypes PS, Mi, BiS; Corner et al., 1996; Cearreta et al., 2016), but there are also agglutinated taxa, such as *Textularia, Trochammina, Eggerelloides* and *Jadammina* (morphotypes BiS, TrS, TS; Corner et al., 1996; Cearreta et al., 2016). The shallow shelf has normal marine salinity, and foraminifera in this environment are controlled by bottom water conditions including depth, oxygen levels, nutrient, substrate, water currents, and temperature (Gupta, 2003; Culver et al., 2012; Anbuselvan et al., 2018). In deeper shelf environments, diversity generally increases with a wide range of taxa (morphotypes PS, TS, BiS, TrS, Mi; Anbuselvan et al., 2018).

Taphonomy

Foraminifera and testate amoebae can be transported either landward or seaward during river flood events and through waves with large storms in the basin. Fossil

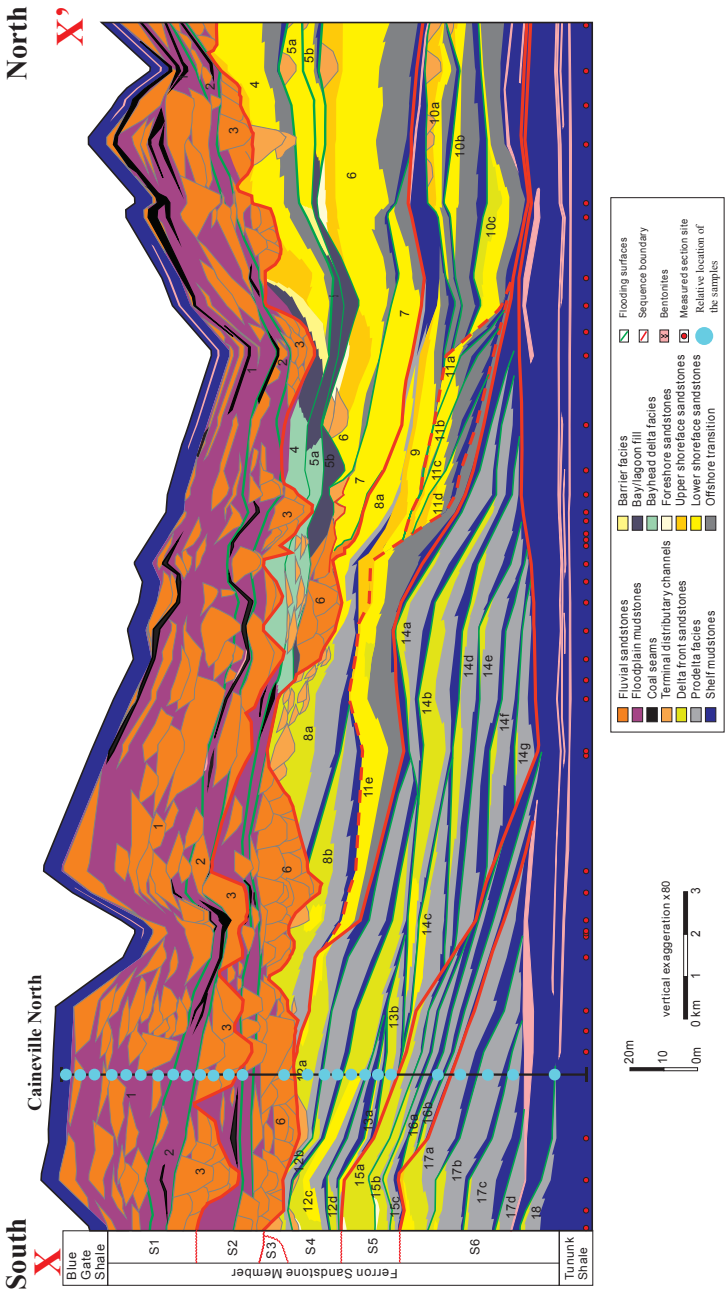

FIGURE 3.4: Strikecross section Y-Y' (Fig.3.2), showing the sample intervals (vertical black line). Approximate location of the Caineville outcrop is shown (from Li et al., 2010; Zhu et al., 2012)

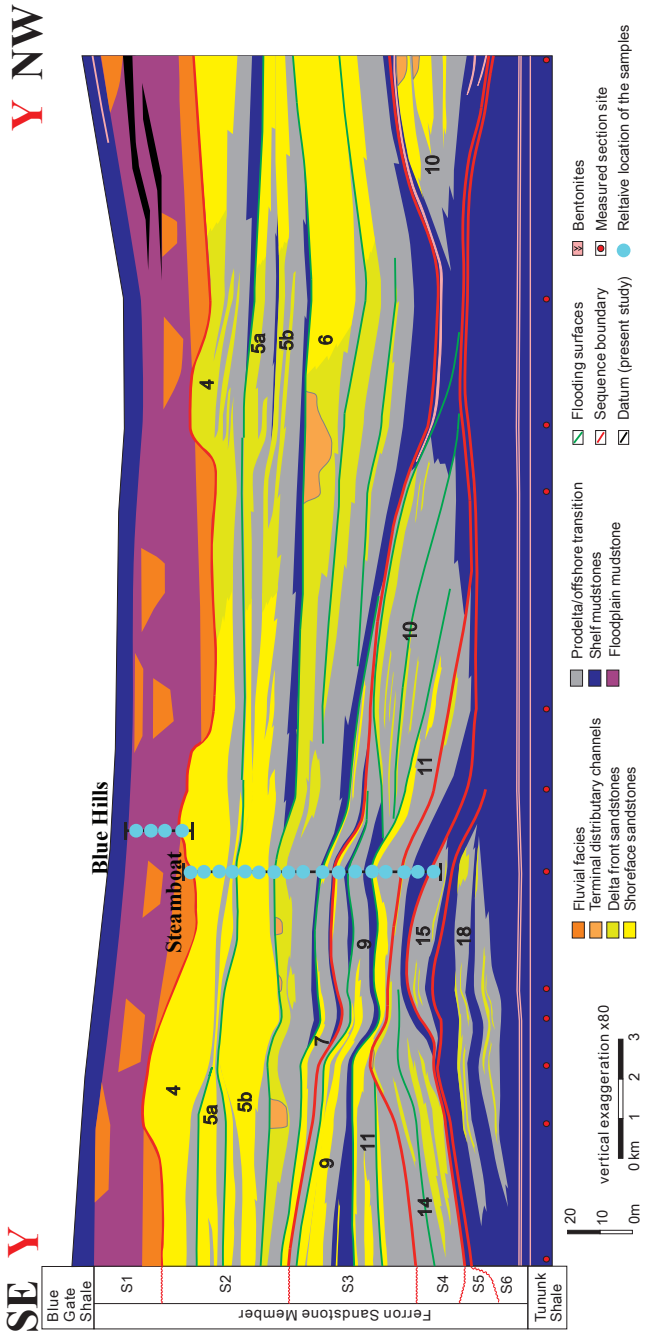

FIGURE 3.5: Dip oriented cross-section X-X' (Fig.3.2), showing the sample intervals (vertical black line). Approximate location of the Steamboat and Blue Hills outcrops are shown (from Zhu et al., 2012; Richards and Bhattacharya, 2018)

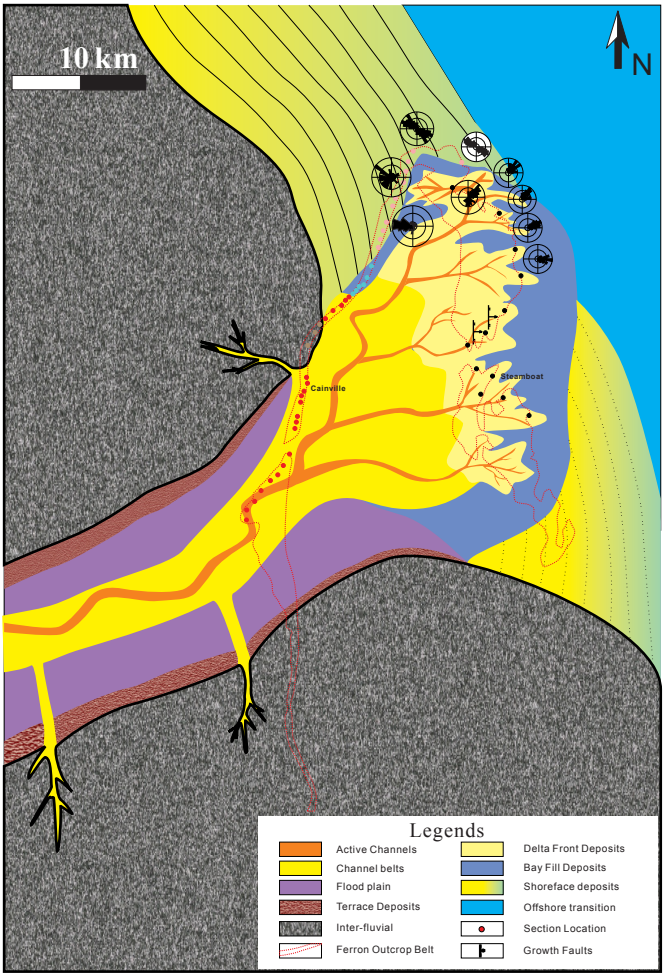

Figure 3.6: Paleogeographic reconstruction map of the Ferron-Notom delta (PS 6) showing the symmetric-delta model proposed by Li et al. (2018). It shows a valley-fed delta prograding to the northeast, and paleocurrent plots show the relative proportion of river-dominated versus wave- and storm-dominated facies (Li et al., 2015)

.

tests can also be eroded from older sediments in the watershed and incorporated with the exisiting living taxa (biocenosis vs. taphocenosis; Scott et al., 2005; Babalola, 2009; Farr et al., 2020). However, this is thought to be more prevalent for calcareous taxa, because with extensive lateral transport or wave action, agglutinated tests (foraminifera and testate amoebae) tend to break apart (Murray and Alve, 1999a). There are numerous examples of transport of calcareous taxa. Planktic foraminifera were eroded out of Miocene/Pliocene rocks in an incisied

river valley in southern Italy and transported offshore by hyperpycnal floods and incorporated into Holocene sediments (Farr et al., 2020). Transported specimens were pristine in condition, and were found to be indistinguishable from modern taxa except they were iron-stained. Other studies have demonstrated the transport of foraminifera inland by tides in Trinidad Island, located on the northeast coast of Venezuela, where marine taxa *Neoeponides antillarum* (morphotype PS), was transported from the shelf to the Godineau River (Laut et al., 2017). However, in the same study, agglutinated testate amoebae, such as *Difflugids* and *Centropyixds* were also transported from inland areas to the estuary (Laut et al., 2017). Testate amoebae were also documented in Holocene cores from an inlet in British Columbia and were associated with agglutinated foraminifera *Eggerella advena* (morphotype TrS). The testate amoebae were interpreted as being transported to the deep shelf from freshwater runoff that eroded soils (Babalola, 2009; Riveiros and Patterson, 2009), so agglutinated foraminifera and testate amoebae can be transported offshore in some instances.

The preservation of calcareous foraminifera depends on several factors, such as temperature, *pH* level, and salinity (Murray and Alve, 1999a; Murray and Alve, 1999b; Scott et al., 2005). Calcareous foraminifera preservation is dependent on *pH* and thus are not preserved in temperate salt marshes, while agglutinated taxa are preserved (Goldstein, 1988; Murray and Alve, 1999a; Murray and Alve, 1999b; Scott et al., 2005). Fossilization of agglutinated foraminifera and testate amoebae tests tends to be accompanied by flattening, but taxa can often still be identified as the study of testate amoebae from the Cretaceous Dakota Formation near Lincoln, Nebraska, USA (van Hengstum et al., 2007).

3.1.2 Ferron-Notom delta Geological Settings

The Cretaceous Western Interior Seaway (KWIS) split the North American continent into two sub-continents (Figs. 3.1-3.2). During that time, three progradational complex wedges deltas formed comprising the Ferron Sandstone Member of the Mancos Shale Formation (Notom, Ventral, and Last Chance; Li et al., 2011a; Zhu et al., 2012; Akyuz et al., 2015; Wu and Bhattacharya, 2015). The climate during the formation of the Ferron-Notom delta has been described as subtropical to tropical based on pollen analysis (Akyuz et al., 2015). These deltaic deposits overlie the Tununk Shale Member and the Bluegate Shale Member is on top (Li et al., 2010; Zhu et al., 2012; Akyuz et al., 2015).

Sequence stratigraphic analysis of the Ferron-Notom delta separates its clastic wedge into forty-eight parasequences, divided into eighteen fluvio-deltaic to shoreface marine parasequences sets (PSS18 -PSS1 in Figs. 3.4-3.6) (Li et al.,

2010; Zhu et al., 2012) within six sequences bounded by regionally extensive sequence boundaries. Compound incised valleys incise the upper two sequences, and range in depositional environments from the trunk and tributary fluvial-channels to tidally influenced fluvial-channels and distributary fluvial-channels (Li et al., 2010; Zhu et al., 2012). Parasequences sets (PSS) PSS4 and PSS5 are fluvial channel belts and floodplain mudstones with coal, and they are truncated by other incised valleys (PSS3). PS2 and PS1 are sandy to conglomeratic fluvial channels and their respective floodplain deposits represent an extensive regionally transgression landward and progradation of the system (Figs. 3.4-3.6). The six sequence boundaries identified (Zhu et al., 2012) are associated with negative shoreline trajectories (SB 3, SB4, and SB5) following relative sea-level fall (typically 30m), and SB2 and SB1 are associated with incised valleys that extended laterally as erosional surfaces truncating into delta front/shoreface sandstone or prodeltaic mudstones and were filled with multistory channels and estuarine facies (Figs. 3.4-3.6). Detailed facies associations of the Ferron-Notom delta were described in Li et al. (2010).

Li et al. (2018) proposed a paleogeographic reconstruction map (Fig. 3.6) based on paleocurrent data, clinoform data, depositional facies, and facies architecture analysis. The Ferron-Notom delta's paleogeographic shows the delta (river-dominated) prograded northeast, and the west lobe of the delta significantly prograded to the northeast (Li et al., 2018). Wave-dominated shorefaces surrounded the river-dominated delta from the northwest and southeast, and distributary channels branched from the river trunk to the northwest feeding the river-dominated delta lobe in the west to the northwest (Li et al., 2018). The delta was fed by an incised valley system to the west, and was protected from waves by a barrier system in the northwest (Li et al., 2018).

3.2 Methodology

3.2.1 *Samples collection and preparation*

Sixty-six mudstone ($\approx$ 50 x 100 cm^3) samples were collected from three outcrops (Figs. 3.2, 3.4, 3.5) within the Upper Cretaceous (Turonian) Ferron-Notom delta. Twenty-nine samples were collected from the Caineville North area representing the full six sequences, while twenty-one samples were collected from the Steamboat area representing four sequences (SQ 1 - 4). Fifteen samples were collected from Blue Hills tributary valley fills, representing one sequence (SQ 1), and the uppermost part of the Ferron-Notom delta.

Subsamples ($\approx$ 10 cm^3) were soaked in distilled water overnight for disaggregation and were sieved using a 63μm mesh and dry split (1/8) using standard

techniques (Scott et al., 2001). Specimens were examined using a binocular microscope (100x) and were picked and categorized based on their overall test morphology, using morphogroup analysis (Chapter 2; Turkistani et al., submitted). Approximately 300 specimens were counted according to Fishbein and Patterson (1993). *Bathysiphon spp.*, and *Reophax spp.* were grouped together due to difficulty in recognizing them individually using a binocular microscope, and they were only identifiable using a Scanning Electron Microscope (SEM). Similarly, *Difflugia* species were grouped into one morphotype (Ta-F). Overall, the samples are divided into four morphogroups and ten morphotypes, where letters and numbers are assigned to each morphotype (Chapter 2 Turkistani et al., submitted; Nagy et al., 1995; Reolid et al., 2008). Agglutinated benthic foraminifera and testate amoebae morphogroups and subgroups were organized based on the test morphology, coiling pattern (or direction), chamber arrangement, and the number of chambers (if present). Selected specimens were picked and mounted on studs for SEM analysis at the Canadian Center for Electron Microscopy (CCEM), McMaster University. Many of the species have undergone flattening and deformation, as found in van Hengstum et al. (2007).

3.2.2 *Statistics*

The relative abundances (equation 3.1) were calculated for each morphotype, with respect to the total count of both microfossil assemblages (foraminifera and testate amoebae), such that

$$F_i = \frac{C_i}{N_i} \tag{3.1}$$

Where Ci is the count of thr individual morphotypes, and Ni is the total test count number. The statistical significance of each morphotype can be determined by calculating each morphotype abundance (%) standard error (equation 3.2) as follows:

$$S_{F_i} = 1.96\sqrt{\frac{F_i(1-F_i)}{N_i}} \tag{3.2}$$

According to Fishbein and Patterson (1993), if a taxa standard error is more than its relative abundance in all samples, then this taxa is statistically insignificant and should be excluded from the multivariate analysis. Identification of biofacies is based on morphotype, their relative abundances, and biodiversity indices, specifically Shannon-Weaver (SDI) and Fisher's alpha (Fα). Shannon-Weaver index (SDI), Fisher Index (Fα) Evenness (SDI/S) Dominance (D), species richness, and Simpson index (1-D) are calculated using PAST (Hammer et al., 2001). The

Shannon-Weaver Diversity Index (SDI) is used to measure the environment stability for each sample, and it establishes a relative diversity measure based on the abundance of each taxa and the species richness of each sample (Leckie, 1985). Fisher's alpha and Shannon-Weaver indices as applied by Jain and Farouk (2017) shows that Fisher values lower than 5 and Shannon values between 0 and 2.5 are an indication of restricted environments, while Fisher values greater than 5 and Shannon index values > 2.5 are an indication of open marine conditions. However, because this study combines species into morphotypes, and because fossilization has biased the assemblage (dissolution of calcareous taxa) these indices can only be used as a relative measure of diversity.

Cluster analysis of morphotypes was then used to establish the biofacies in the Ferron-Notom delta. Dendrograms were produced using R packages, Vegan (Oksanen et al., 2019) and paleotree (Bapst, 2012), using a total of sum of squares for standardization, Euclidean distance was calculated using Ward's Linkage Method. Based on results of the multivariate analysis, a salinity index was derived by dividing the trochospiral foraminifera morphotype (TS) versus the total sum of testate amoebae morphotypes (Ta-F+Ta-D+Ta-S; Fig. 3.13). Similarly, an OM (eutrophication) index was derived by dividing the "bolivind-type" foraminifera morphotypes (BiS, TrS) versus the trochospiral foraminifera morphotype (Fig. 3.13).

3.3 Results and Discussion

We applied the morphogroup analysis (Jones and Charnock, 1985) to foraminifera and testate amoebae assemblages recovered from the samples. The foraminiferal and testate amoebae morphotypes were identified based on test morphology in relation to environment and compared to modern examples. Seven foraminifera morphotypes, and three testate amoebae morphotypes were identified, and the morphogroup analysis is discussed in detail in Turkistani et al. (submitted, Chapter 2). The planispiral (PS) morphotype comprises two foraminifera species *Gavelinella ammonoides*, *Gavelinella lorneiana*. Morphotype (PS/UnS) includes taxa with a test form of planispiral to uniserial, such as *Ammobaculites subcretaceus*. *Trochammina spp.* is a species with flattened trochospiral form, which is the third morphotype (TS). The miliolid morphotype included mostly *Miliammina fusca* (morphotype-Mi). Four "bolivind-type" morphotypes were also defined including: *Bathysiphon spp.* (Uniocular-tubular, UnLT), *Reophax spp.* (elongated uniserial, UnSE), *Neobulimina albertensis* (tri-serial, TrS) and *Textularia spp.* (bi-serial, BiS). Testate amoebae taxa had three morphotypes. Several taxa were included in Ta-F morphotype, namely, *Difflugia oblonga*, *Difflugia proteiformis*, *Difflugia corona*, *Difflugia urceolata* and *Lagenodifflugia vas.*, and the other morphotypes are *Centropyix constricta* (Ta-S) and *Centropyxis aculeata* (Ta-D). There were

only a few calcareous species belonging to morphotypes PS and TrS, and they were excluded because of the low abundance. As discussed previously, morphotypes UnLT and UnSE were grouped because they were indistinguishable under a binocular microscope.

3.3.1 Foraminiferal and Testate Amoebae Biofacies

Overall, the distribution of microfossils between the three outcrops showed little variation with little difference in the presence/absence of taxa between lithofacies. It appears that landward and basinward transport of tests was a dominant process (Fig. 3.12). The loss of the calcareous fraction through dissolution has also created a bias, thus hindering the recognition of biofacies. Normally, the abundance and diversity of calcareous taxa would increase with marine influence and salinity, but this is not the case in the samples from the Ferron-Notom delta, where there is only a record of the agglutinated taxa. Calcareous foraminifera are only found in the more distal facies of the Tununk (Li and Schieber, 2018). However, despite the lack of calcareous taxa, there are differences in the abundance of agglutinated morphotypes that do show trends with cluster analysis. Cluster analysis using the morphotypes distinguished four major Biofacies I, II, III, and IV that seem to vary with salinity. The bolivind-type foraminifera are found throughout the biofacies and vary with original OM, and typify estuarine deltaic facies.

Biofacies-I. This biofacies is characterized as the lowest salinity with high OM (Figs. 3.7-3.11; Tables 3.1, 3.2, 3.3). The three most dominant morphotypes show the highest average abundance 23% (UnLT+UnSE) and 20% TrS, followed by PS (18%) and Ta-F (15%). Morphotypes TS and BiS are also present, but are lower than 10%. Other morphotypes are very low including Ta-D, Ta-S, Mi, and PS/UnS, which have an average abundance of <5% (Figs. 3.7-3.8). The diversity of testate amoebae morphotypes, Ta-F, Ta-D, Ta-S indicate a lower water salinity relative to the other biofacies, where they are lower in abundance or not present. Foraminiferal morphotypes including TrS, BiS, UnLT and UnSE are an indication of high OM, and the presence of the wetland morphotype, such as Mi in some units indicates a floodplain-backwater or possibly a wetland environment. In comparison with the other biofacies, Biofacies I shows higher presences of testate amoebae than Biofacies II, III, and IV. Biofacies I represents low salinity with high OM in a tidally influenced backwater environment. Biofacies I was found in several facies within the Caineville North, Steamboat and Blue Hills outcrops. In Caineville North, Biofacies I was found in a few samples from the shelf mudstone of the Tununk Shale (prodelta and Bluegate Shale, Shelf; CN 26, 2), fluvial sandstone (CN 14, 8, 9), and floodplain mudstone (CN 11 and 4) of the fluvial channels (Ferron Sandstone). In Steamboat, samples of Biofacies I include two samples from the shelf mudstone of the delta front (SB 8, 11), and in the fluvial channels

(SB 6). In Blue Hills, Biofacies I dominates the whole outcrop all within the fluvial mudstone.

Biofacies-II. This biofacies is characterized by slightly lower OM, and slightly higher salinity relative to Biofacies I (Figs. 3.7-3.11; Tables 3.1, 3.2, 3.3). The PS, TS, and Ta-F are the most abundant morphotypes with average abundance 26%, 14% and 23% respectively. Unlike Biofacies I, Biofacies II is missing the testate amoebae morphotype Ta-D, and Ta-S is only present in low abundance (<5%). However, the presence of testate amoebae morphotypes Ta-F and Ta-S still indicates freshwater influence but less so than Biofacies I. Foraminiferal morphotypes TrS, BiS, UnLT, UnSE, Mi, and PS/UnS are all lower than 10% compared to Biofacies I, thus suggesting lower OM contents. Therefore, Biofacies II shows a slightly higher salinity with low OM that would typify a brackish lagoon/estuarine environment. There is only one Biofacies II sample in Caineville North (CN 21) within the marine sandstone of the delta front, while in Steamboat, Biofacies II dominates the outcrop, which is in the marine and shelf mudstone of the delta front and fluvial channels (SB 3-4, 9-10, 12-22).

Biofacies-III. This biofacies shows slightly higher salinity relatively to Biofacies II and higher OM content (Figs. 3.7-3.11; Tables 3.1, 3.2, 3.3). PS, TS, UnS (UnLT+UnSE), and TrS morphotypes dominant Biofacies III with average abundances of 28%, 12%, 18% and 16% respectively. TrS, BiS, UnLT and UnSE morphotypes are slightly higher compared to Biofacies II, which indicates higher OM content. The morphotypes BiS and Ta-F have average abundance of 6% and 11%, and morphotype Mi is absent, while other morphotypes including Ta-S and PS/UnS are lower than 5%. The testate amoebae morphotype Ta-D is absent in Biofacies III but overall is not generally different than Biofacies II. Biofacies III indicates low to medium salinity lagoon/estuary environments with slightly higher OM. Biofacies III is found only in the Caineville North, delta front (marine and shelf mudstone; CN 5-6, 10, 12, 13, 15-20, 22-24).

Biofacies-IV. This biofacies is characterized by medium to normal marine salinity and higher OM (Figs. 3.7-3.11; Tables 3.1, 3.2, 3.3). Unlike the other biofacies, Biofacies IV is dominated by foraminiferal morphotypes TrS, UnLT, UnSE, TS, and BiS, with average abundance of 25%, 18% (UnLT+UnSE), 7% and 9% respectively, which indicates high OM content. Testate amoebae (e.g. Ta-F, Ta-S, Ta-S) and some foraminifera morphotypes (e.g. PS/UnS, Mi) are absent in Biofacies IV. This biofacies represents a shallow shelf to prodelta environment. Similar to Biofacies III, Biofacies IV is only found in Caineville North within the Tununk Shale prodelta (CN 27-29), fluvial channels (CN 9), and in the Bluegate Shale shelf mudstone (CN 3, 1). Calcareous foraminifera morphotypes TrS and PS are found in Biofacies IV but only in two samples from Caineville North (CN

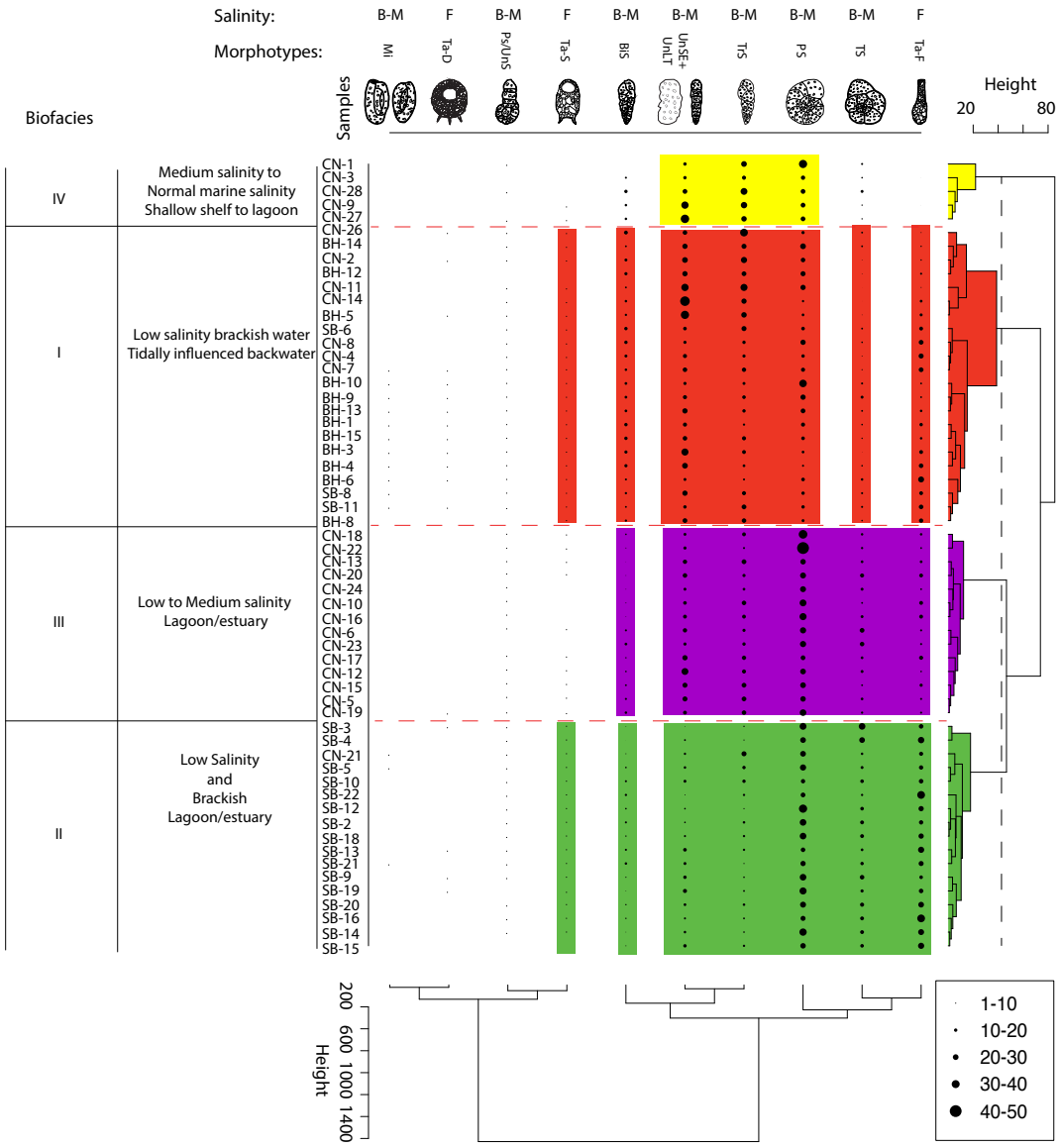

Figure 3.7: Dendrogram from the cluster analysis using Ward's linkage and Euclidean distances of foraminiferal and testate amoebae morphotypes. Biofacies I to IV represents a gradient from fresh to marine influence, where I is the most fluvially influenced, and IV is the most marine.

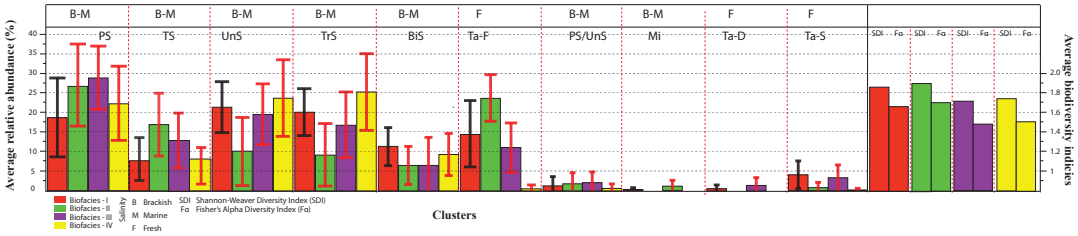

FIGURE 3.8: Bar plots of morphotypes and their average relative abundance in each biofacies with standard error bars.

27 and 3).

TABLE 3.1: Table showing morphotype relative abundance and standard error in the Caineville North outcrop, Ferron-Notom delta. B= Brackish, M= Marine, F= Fresh, SDI = Shannon-Weaver Index, and Fα= Fisher's Alpha Index.

Salinity:	**B-M**	**B-M**	**B-M**	**B-M**	**B-M**	**B-M**	**B-M**	**F**	**F**	**F**	**Diversity Index**		**Biofacies**
Samples	**PS**	**PSUnS**	**TS**	**Mi**	**UnLT-UnSE**	**TrS**	**BiS**	**Ta-F**	**Ta-D**	**Ta-S**	**SDI**	**Fα**	
CN-1	36±12	-	9±6	-	15±7	25±10	-	-	-	-	1.3	0.9	IV
CN-2	20±9	2±3	3±4	-	25±10	27±10	13±7	6±5	-	4±4	1.8	2.0	I
CN-3	19±9	1±2	7±5	-	15±8	18±8	9±6	1±2	-	4±4	1.7	2.3	IV
CN-4	15±8	2±3	4±4	-	18±8	14±7	13±7	22±9	-	4±4	1.9	2.1	I
CN-5	24±10	2±3	12±7	-	22±9	21±9	9±6	9±6	-	1±2	1.8	2.0	III
CN-6	27±10	1±2	21±9	-	19±8	14±7	9±6	9±6	-	1±1	1.8	2.0	III
CN-7	18±8	1±2	5±4	-	20±9	19±8	11±6	21±9	-	5±4	1.9	2.0	I
CN-8	23±9	1±2	7±5	-	14±7	15±7	15±7	21±9	-	5±4	1.9	2.0	I
CN-9	21±9	1±2	6±5	-	32±11	28±10	11±6	1±2	-	-	1.6	1.7	IV
CN-10	30±11	3±4	8±6	-	16±8	20±9	4±4	17±8	-	-	1.8	2.1	II
CN-11	23±9	-	1±2	-	32±11	31±11	8±6	4±4	-	1±2	1.5	2.0	I
CN-12	25±10	1±2	13±7	-	30±11	18±8	7±5	7±5	-	-	1.7	1.7	III
CN-13	24±10	3±3	12±7	-	19±9	21±9	2±3	12±7	-	1±2	1.8	2.1	III
CN-14	10±6	1±2	1±2	-	42±13	23±9	11±6	12±7	-	1±2	1.5	2.0	I
CN-15	25±10	1±2	8±5	-	22±9	21±9	8±6	14±7	-	2±3	1.8	2.1	III
CN-16	31±11	1±2	13±7	-	17±8	17±8	3±3	17±8	-	-	1.7	2.0	III
CN-17	21±9	-	12±7	-	23±9	19±9	6±5	18±8	-	1±2	1.8	1.7	III
CN-18	38±12	2±3	11±6	-	13±7	17±8	7±5	11±6	-	1±2	1.7	2.0	III
CN-19	29±10	3±4	10±6	-	17±8	20±9	11±6	9±6	-	1±2	1.8	2.0	III
CN-20	26±10	1±2	18±8	-	20±9	14±7	3±3	17±8	-	1±2	1.8	2.0	III
CN-21	25±10	3±4	11±7	-	10±6	22±9	4±4	18±8	-	5±4	1.9	2.0	II
CN-22	52±14	1±2	10±6	-	14±7	9±6	4±4	8±6	-	2±3	1.5	2.0	III
CN-23	27±10	3±3	20±9	-	14±7	15±8	12±7	9±6	-	1±2	1.8	2.0	III
CN-24	26±10	2±3	13±7	-	13±7	12±7	3±4	8±6	-	-	1.7	1.9	III
CN-25	-	-	-	-	-	-	-	-	-	-	-	-	-
CN-26	14±7	2±3	8±5	-	20±9	34±11	17±8	4±4	-	2±3	1.7	2.0	I
CN-27	21±9	-	6±5	-	37±12	24±10	11±6	0±1	-	1±2	1.5	2.0	IV
CN-28	21±9	-	13±7	-	21±9	30±11	15±8		-	-	1.6	1.1	IV
CN-29	-	-	-	-	-	-	-	-	-	-	-	-	-

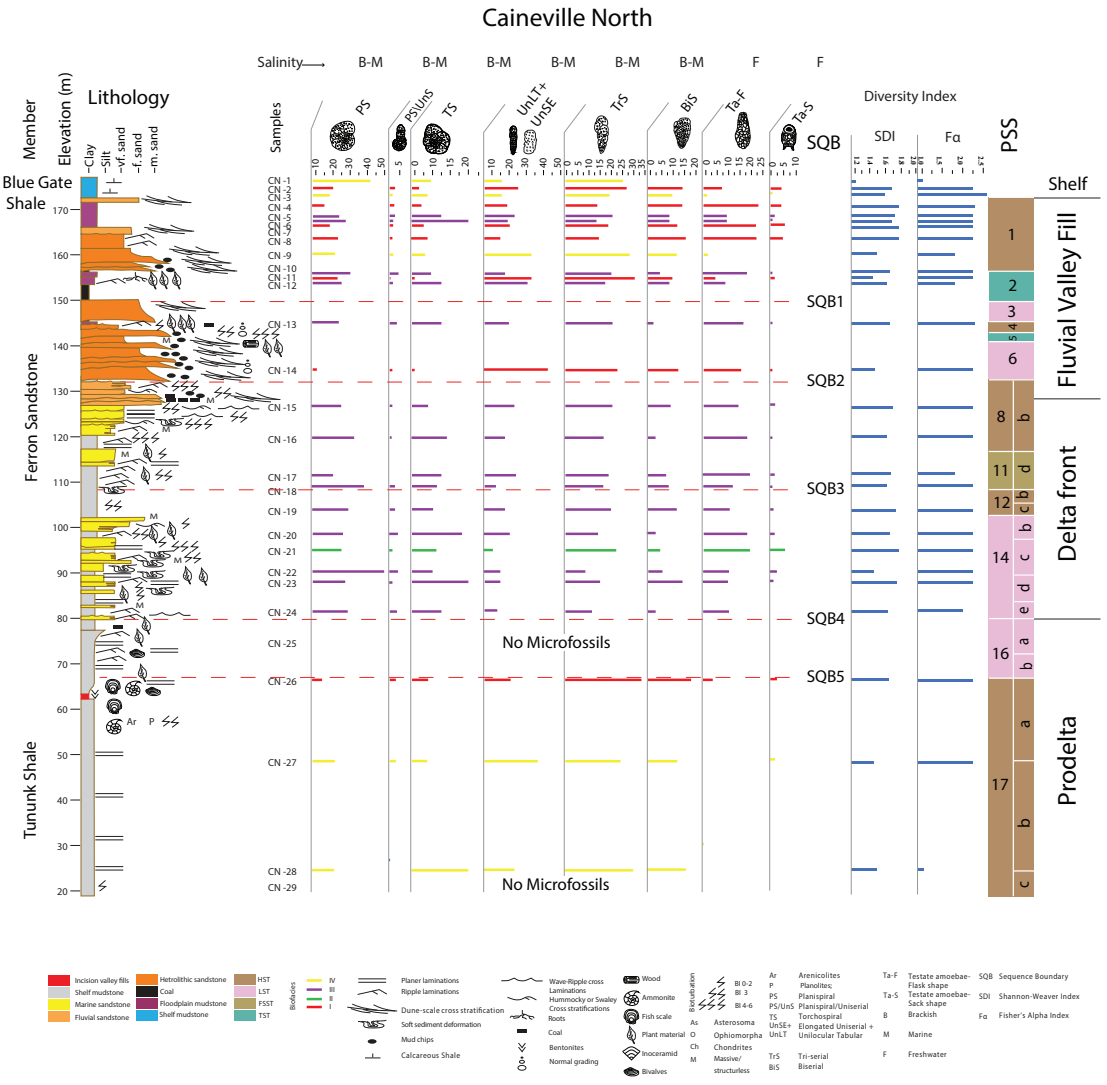

FIGURE 3.9: Figure showing the lithofacies of the Ferron-Notom delta in Caineville North, along with biofacies, morphotype relative abundance (Percent foraminifera and testate amoebae), parasequences and system tracts

3.3.2 Relationships with Lithofacies

Caineville North

The lower part of the Caineville North outcrop (Figs. 3.9, 3.12, 3.13) is the Tununk Shale prodelta that was deposited during a highstand and lowstand system tracts (HST, LST; PSS 17, 16; SQB 4-5), and it represents the inner shelf area of the Ferron-Notom delta. The prodelta samples (CN 25-29; Fig. 3.9) are mainly from

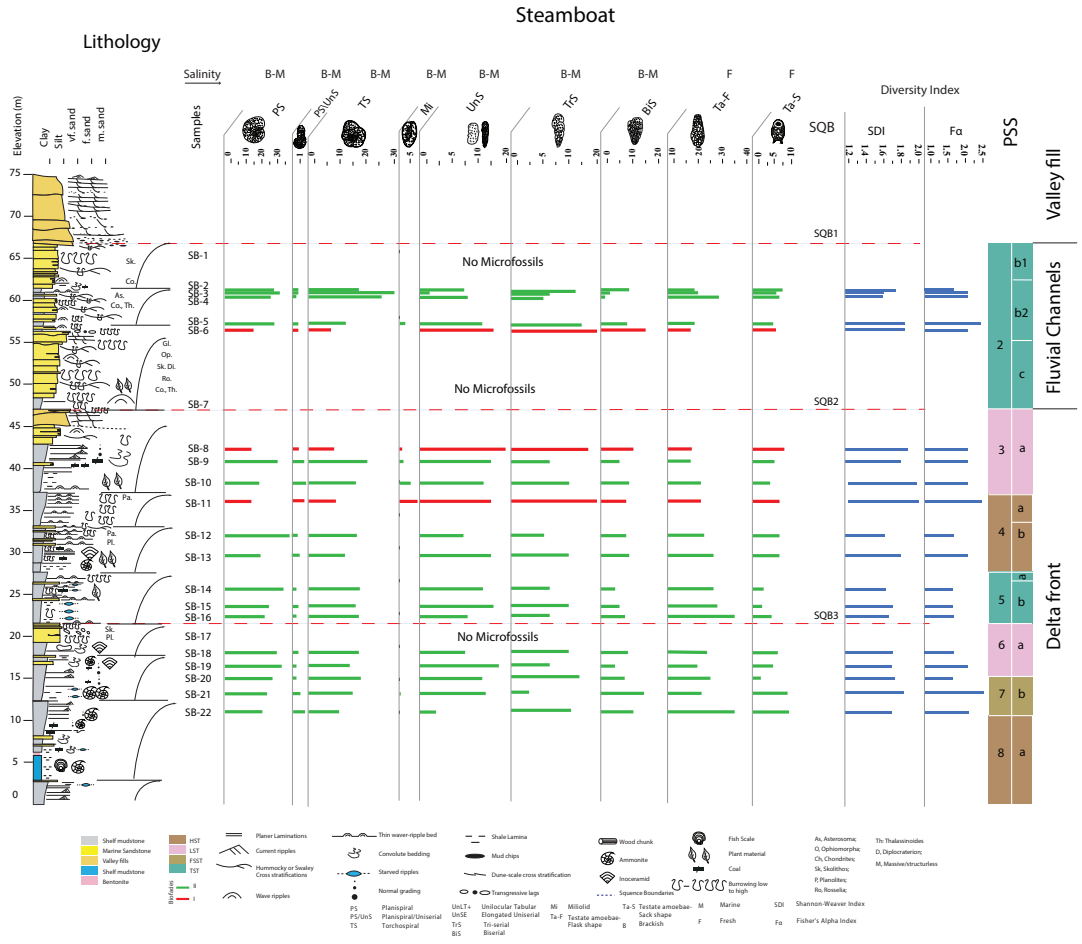

FIGURE 3.10: Figure showing the lithofacies of the Ferron-Notom delta in Steamboat, along with biofacies, morphotype relative abundance (Percent foraminifera and testate amoebae), parasequences and system tracts

a shelf mudstone showing planer laminations. Fish scales, ammonite and burrows are present at the top of the prodelta with low bioturbation (samples CN 25-26; Zhu, 2010; Zhu et al., 2012; Wu et al., 2012). The Tununk Shale is dominated by the morphotypes TrS, BiS, UnLT and UnSE of Biofacies IV, which indicates a prodelta with medium to normal marine salinity and high OM. The top of the Tununk Shale prodelta shows a fully freshwater biofacies (Biofacies I; CN-26) that coincides with the beginning of a sea-level fall (LST; PSS 16) and the above SQB 5. Li and Schieber (2018) investigated the middle and distal shelf facies of the Tununk Shale, and out of four facies, three facies were rich in calcareous particles, including planktic foraminifera, coccoliths, and fecal pellets. Also, macrofossils, such as

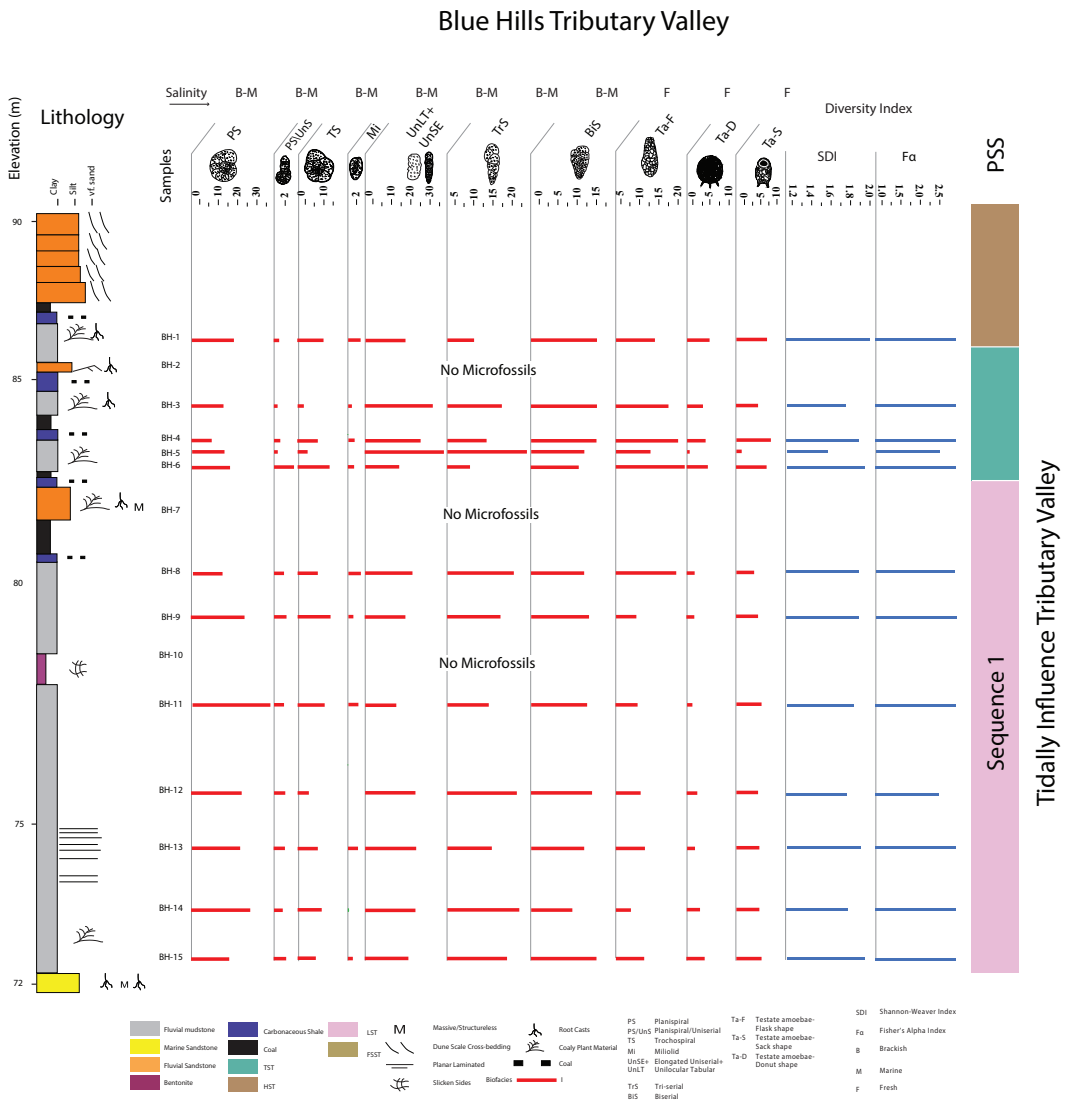

FIGURE 3.11: Figure showing the lithofacies of the Ferron-Notom delta in Blue Hills, along with biofacies, morphotype relative abundance (Percent foraminifera and testate amoebae), parasequences and system tracts

ammonites (e.g. *Prionocyclus hyatti*, *Collignoniceras woollgari*) and mollusks (e.g. *Inoceramidae*) were found in calcareous facies of the study (Li and Schieber, 2018). The salinity index shows higher salinity in the prodelta lithofacies compared to the delta front, which would be expected moving closer to the input of river water and the shoreline. The salinity index shows higher salinity associated with sea-level

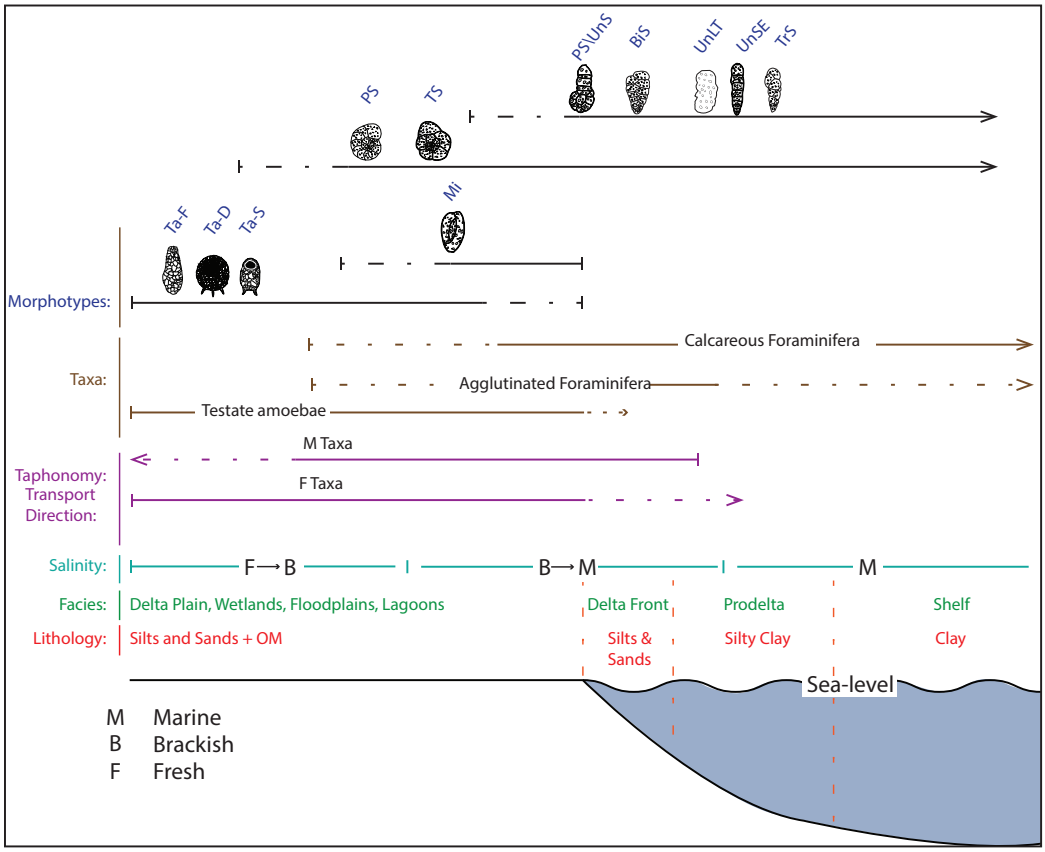

FIGURE 3.12: Figure showing the lithology, facies, salinity, taphonomy, taxa, and morphotypes from offshore to inland environments

rise (HST; CN 26 - 29; PSS17; SQB5), and a decrease in salinity corresponding to sea-level fall in the LST (PSS16; SQB4).

The delta front samples (CN 15 - 24; Fig. 3.9) of the Ferron were deposited during LST (PSS 14), FSST (PSS 11), and HST (PSS 12 and 8b). Sedimentary structures observed in the delta front facies include planar laminations, ripple laminations, and soft sediment deformation structures as well as massive structureless sandstone beds. Plant material is also common, and bioturbation is relatively high (Zhu, 2010; Zhu et al., 2012; Wu et al., 2012; Wu, 2013). The biofacies show an overall decreasing marine influence, which is concurrent with the relative sea-level fall that dominates PSS 14 (samples CN 20 - 24; Figs. 3.9, 3.13). The salinity remains relatively low during the FSST and HST and shows sea-level fall followed by relative sea-level rise (samples CN 17 - 19; SQB3). The delta front is dominated by Biofacies III suggesting a change from medium/normal marine salinity (Biofacies

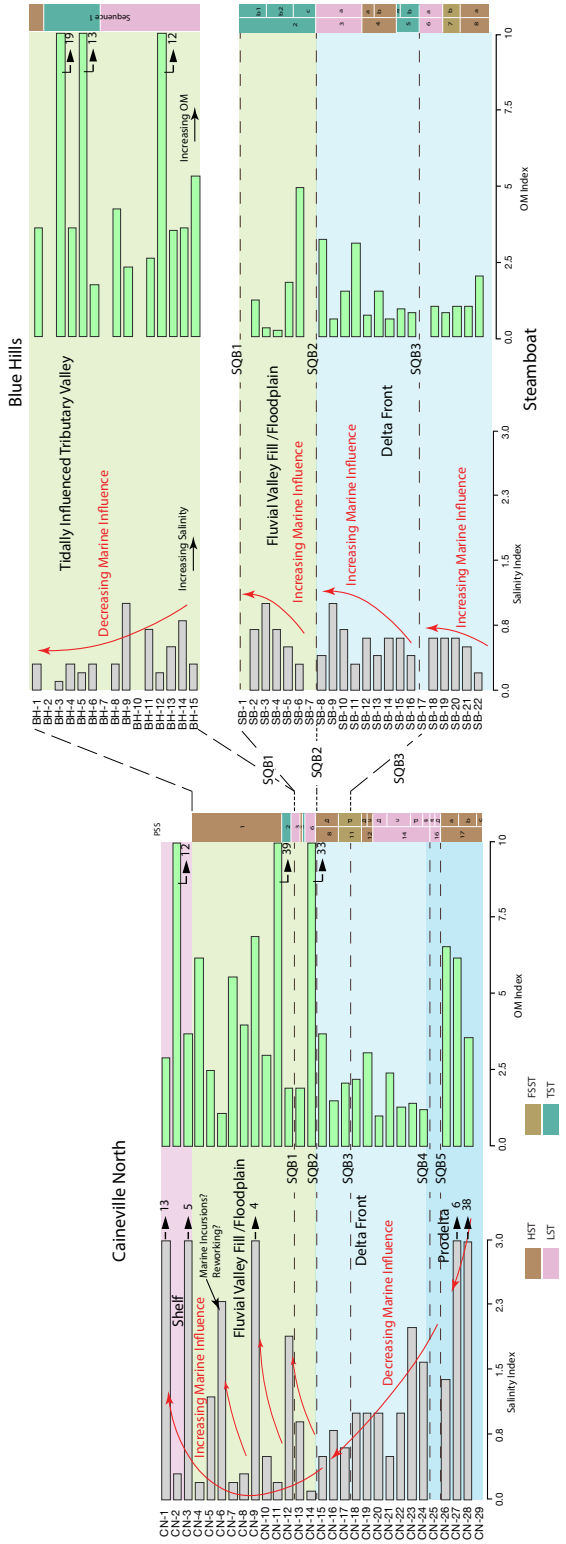

FIGURE 3.13: Salinity index plot based on a ratio of trochospiral foraminifera and testate amoebae (TS/(Ta-F + Ta-D + Ta-S) morphotypes showing the increase and decrease of marine influence. OM index plot based on a ratio of "bolivind-type" taxa and trochospiral morphotypes ((BiS+TrS)/TS)) showing the increase and decrease OM in the Caineville North, Steamboat, and Blue Hills outcrops.

IV) to slightly low to medium salinity based on the presence of testate amoebae morphotype Ta-F. The OM is high similar to the prodelta, which is interpreted based on the abundance of foraminifera morphotypes TrS, BiS, UnLT, and UnSE (Figs. 3.7-3.11; Tables 3.1, 3.2, 3.3). Within the delta front only one sample (CN 21) belongs to Biofacies II (PSS 14C) indicating a period of low salinity with low OM.

In Sequences 1-2 (PSS 1-6; samples CN 4 - 14; Fig. 3.9), fluvial and heterolithic sandstones were deposited in multistory fluvial channels, with ripple lamination, dune-scale cross-bedding and mud-chips (Zhu, 2010; Zhu et al., 2012; Wu et al., 2012; Wu, 2013). Plant material, wood, and coal were also found in Sequences 1 and 2, and the bioturbation is moderate to high (Famubode and Bhattacharya, 2016). Sequences 2 and 1 were deposited in a LST, TST and HST (Fig. 3.9), but also include short-term sea-level fluctuations. The salinity index shows an overall increasing marine influence, but the salinity remains low. Sequences 1 and 2 (PSS 1 - 6) are dominated by two Biofacies III (samples CN 5, 6, 10, 13), Biofacies I (samples CN 4, 7, 8, 11 and 14), and one sample (CN 9) of Biofacies IV suggests a fluctuation in salinity (Biofacies III to Biofacies I), and from low to high OM. Unlike the prodelta and delta front, testate amoebae morphotypes Ta-F, Ta-S, and Ta-D increased indicating a freshwater influx. Based on Biofacies I, Sequence 1 is interpreted as a low salinity tidally-influence backwater, while Sequence 2 is a low to medium salinity lagoon/estuary. Within the fluvial channel facies marine incursions and reworking of foraminifera are possible.

The Bluegate Shale samples (CN 1 - 3; Fig. 3.9) show a salinity index with increased marine influence, which matches the shelf lithofacies (Biofacies IV), and has high OM contents. This matches the transition from a full fluvial environment to marine. Foraminifera morphotypes PS, TS, UnLT, UnSE, TrS and BiS dominated, and testate amoebae morphotypes are absent relative to the brackish salinity of Biofacies I and III.

Steamboat

Steamboat consists of two lithofacies, the delta front and fluvial channels (Figs. 3.10, 3.12, 3.13). The delta front (samples SB 8 - 22; Fig. 3.10) shows normal grading from a shallow marine sandstone to a shelf mudstone (Zhu, 2010; Zhu et al., 2012; Wu et al., 2012; Wu, 2013). The mudstone shows laminations, current ripples, starved ripples, and convoluted bedding. Ammonites, fish scales and inoceramids are also found within the mudstone (samples SB 13 - 22). The sandstone of the fluvial channels show thin wave-rippled beds at the top with high amounts of burrowing activity (samples SB 1-7; Fig. 3.10 Zhu, 2010; Zhu et al., 2012; Wu

Table 3.2: Table showing morphotype relative abundance and standard error in the Steamboat outcrop, Ferron-Notom delta. B= Brackish, M= Marine, F= Fresh, SDI = Shannon-Weaver Index, and Fα= Fisher's Alpha Index.

Salinity:	B-M	B-M	B-M	B-M	B-M	B-M	B-M	F	F	F	Diversity Index		Biofacies
Samples	PS	PSUnS	TS	Mi	UnLT-UnSE	TrS	BiS	Ta-F	Ta-D	Ta-S	SDI	Fα	
SB-1	-	-	-	-	-	-	-	-	-	-	-	-	
SB-2	29±11	1±2	17±8	-	7±5	11±7	9±6	19±9	-	6±5	1.7	1.8	II
SB-3	30±11	1±2	29±11	-	3±3	6±5	3±4	20±9	3±3	5±4	1.6	2.1	II
SB-4	25±10	1±2	25±10	-	8±6	5±4	1±2	28±10	2±3	6±5	1.6	2.1	II
SB-5	27±10	1±2	13±7	1±2	11±7	15±8	7±5	19±9		4±4	1.8	2.4	II
SB-6	16±8	1±2	8±5	-	16±8	22±9	15±8	17±8	1±2	5±4	1.8	2.1	I
SB-7	-	-	-	-	-	-	-	-	-	-	-	-	
SB-8	15±7	2±3	9±6	1±2	23±9	18±8	10±6	17±8	-	7±5	1.8	2.1	II
SB-9	29±11	2±3	20±9	1±2	15±7	7±5	5±4	16±8	-	5±4	1.8	2.1	I
SB-10	19±9	2±3	16±8	3±3	13±7	15±8	9±6	20±9	-	4±4	1.9	2.1	II
SB-11	15±7	1±2	9±6	4±4	15±8	21±9	8±5	20±9	1±2	6±5	1.9	2.4	I
SB-12	36±12	1±2	16±8	-	7±5	5±4	7±5	23±9	-	6±5	1.6	1.7	II
SB-13	20±9	1±2	12±7	-	16±8	10±6	9±6	27±10	-	6±5	1.8	2.1	II
SB-14	32±11	1±2	17±8	-	11±6	7±5	3±4	26±10	-	2±3	1.6	1.7	II
SB-15	24±10	1±2	16±8	-	15±8	10±6	4±4	27±10	-	2±3	1.7	1.7	II
SB-16	22±9	1±2	17±8	-	9±6	8±5	6±5	34±11	-	4±4	1.6	1.7	II
SB-17	-	-	-	-	-	-	-	-	-	-	-	-	
SB-18	29±10	1±2	17±8	-	9±6	10±6	6±5	23±9		5±5	1.7	1.7	II
SB-19	31±11	1±2	14±7	-	18±8	8±5	3±4	20±9	1±2	4±4	1.7	2.1	II
SB-20	26±10		18±8	-	12±7	11±7	6±5	25±10	1±2	2±3	1.7	1.7	II
SB-21	23±9	1±2	15±8	-	13±7	5±4	11±6	22±9	1±2	8±6	1.8	2.5	II
SB-22	21±9	2±3	10±6	-	4±4	10±6	10±6	34±11	-	8±5	1.7	2.1	II

Table 3.3: Table showing morphotype relative abundance and standard error in the Blue Hills outcrop, Ferron-Notom delta. B= Brackish, M= Marine, F= Fresh, SDI = Shannon-Weaver Index, and Fα= Fisher's Alpha Index.

Salinity	B-M	B-M	B-M	B-M	B-M	B-M	B-M	F	F	F	Diversity Index		Biofacies
Samples	PS	PSUnS	TS	Mi	UnLT-UnSE	TrS	BiS	Ta-F	Ta-D	Ta-S	SDI	Fα	
BH-1	18±8	2±3	7±5	3±4	18±6	10±6	15±8	15±7	5±5	6±5	2.1	2.8	I
BH-2	-	-	-	-	-	-	-	-	-	-	-	-	-
BH-3	12±7	1±2	2±3	1±2	31±8	17±8	14±7	17±8	2±3	4±4	1.9	2.8	I
BH-4	9±6	2±3	7±5	2±3	25±7	12±7	14±7	20±9	2±3	7±5	2.0	2.8	I
BH-5	12±6	1±2	3±2		36±8	24±9	10±8	13±8		1±3	1.7	2.4	I
BH-6	16±8	5±5	11±6	2±3	13±5	9±6	9±6	26±10	3±3	6±5	2.1	2.8	I
BH-7	-	-	-	-	-	-	-	-	-	-	-	-	-
BH-8	13±6	3±3	7±4	3±4	21±6	20±9	10±7	19±8	1±3	3±5	2.0	2.8	I
BH-9	23±9	3±4	13±7	1±2	18±6	16±8	12±7	8±5	1±2	4±4	2.0	2.8	I
BH-10	33±11	3±3	9±6	3±3	14±5	13±7	12±7	8±6	1±2	5±4	2.0	2.8	I
BH-11	-	-	-	-	-	-	-	-	-	-	-	-	-
BH-12	22±9	3±3	3±3		23±7	21±9	14±7	9±6	1±2	3±4	1.9	2.4	I
BH-13	21±9	3±3	8±5	3±3	23±7	15±8	12±7	11±6	1±2	4±4	2.0	2.8	I
BH-14	25±10	2±3	8±6		23±6	22±9	8±6	6±5	2±3	4±4	1.9	2.8	I
BH-15	16±8	3±4	6±5	1±2	20±6	18±8	15±8	11±6	4±4	5±4	2.1	2.8	I

et al., 2012; Wu, 2013). Overall compared to Caineville North, Steamboat biofacies are characterized by a lower salinity, but are still within a lagoon/estuary environment (Figs. 3.7-3.8). However, the salinity shows intervals of increasing

marine influence that coincides with the sequence boundaries (Fig. 3.13).

Foraminiferal morphotypes Tr, BiS, UnLT and UnSE are slightly lower compared to Caineville North and thus have a lower OM content. The foraminiferal wetland morphotype Mi (Biofacies I) is rare in Steamboat, but present within PSS 3, suggesting a floodplain-backwater condition in the LST (PSS 3; samples SB 6, 8, and 11). Testate amoebae morphotype Ta-D is absent, while Ta-F and Ta-S have moderate abundance, which is indicative of less marine influence compared to Caineville North. A transition from low salinity to slightly higher salinity (to Biofacies II) is detected from PSS 3 to PSS 2 (samples SB 1 - 5, 9 - 10, and 12 - 22). Like Caineville North, Steamboat has high abundance of high marsh morphotype TS, and testate amoebae morphotypes Ta-F and Ta-S within Sequence 2, and this may provide evidence of the extent of sea-level rise inland.

Blue Hills

The Blue Hills outcrop represents the very top sequence of the Ferron-Notom delta (e.g. SQ 1; Fig. 3.11, 3.12, 3.13), and the salinity index shows a general decrease in marine influence compared to Caineville North and Steamboat, but there is also an upward trend in the outcrop. This outcrop is dominated by a fluvial mudstone deposited in the HST, LST and TST (Zhu, 2010; Zhu et al., 2012; Wu et al., 2012; Wu, 2013; Kynaston and Bhattacharya, 2019). The fluvial mudstone is mostly planer laminated with coaly plant material (samples BH 1 - 7). The fluvial sandstone is massive and structureless with coaly plant material and roots found within the beds (sample BH 7). Coal and carbonaceous shale beds are also found within the upper part of the outcrop.

Biofacies I (samples BH 1 - 15) dominates the sequence. In terms of morphotype trends, the lagoon/estuary morphotypes (e.g. UnLT, UnSE, BiS) are lower than in the other two outcrops (Caineville North and Steamboat), and freshwater morphotype *Difflugids* (Ta-F) have increased. Similarly, morphotypes Ta-D, and Ta-S have higher abundance relative to Caineville North and Steamboat. Biofacies I is indicative of a low salinity tidally-influenced backwater with high OM contents (e.g. Kynaston and Bhattacharya, 2019). The presence of wetland foraminifera morphotype Mi (in Biofaices I) suggests a floodplain-wetland environment. Other foraminiferal morphotypes (TrS, BiS, UnLT, and UnSE) maybe transported. The salinity index shows an overall decreasing marine influence moving upward with relatively high but variable OM content, which is corroborated with the Mi morphotype (samples BH 3, 5, and 13; Fig. 3.13). In this case, the tributary valleys could be incising into older marine strata causing redepositing of foraminifera within freshwater strata and/or transport of foraminifera inland during storm surges.

3.3.3 Utility of the Salinity Index and OM Index

Based on the biofacies analysis we use some of the morphotypes to develop a salinity index and an organic matter (OM) index (Fig. 3.13). The salinity index is calculated as TS/(Ta-F+Ta-D+Ta-S). The trochospiral taxa (TS) are generally the most prevalent taxa going from low-brackish to marine salinity, so dividing them by all the testate amoebae (Ta) morphotypes which are a freshwater indicator, provides a good salinity index. Despite the taphonomic mixing with landward to shoreward transport, this process would intensify with coastal proximity, so the index would still follow relative salinity trends. The OM index uses the ratio of "bolivind-type" taxa vs trochospiral ((BiS+TrS)/TS). BiS and TrS are indicative of OM and nutrient loading in deltas and estuaries (Fig. 3.13; Gupta, 2003), and when ratioed with other morphotypes, such as TS, they provide a relative measure of the original OM content of the sediment and eutrophication. Our OM index largely follows the lithofacies in the three outcrops.

The salinity index in Caineville North shows an overall decreasing marine influence upward from 38.0 to 0.1 and then increases towards the top of the outcrop from 0.2 to 13. The OM index in the prodelta (Tununk Shale) is high (3.6 to 6.6; e.g. fine OM) due to relative sea-level rise associated with the HST which is associated with an increase in sedimentation rate, runoff, nutrient supply and decreases in microfossils upward (Leckie and Olson, 2003). The delta front consists of several system tracts including LST, HST and FSST. The delta front shows salinity decreasing upward from 0.1 to 2.0, and OM increasing upwards from 1.0 to 33.7, which is concurrent with a relative sea-level rise and fall (Figs. 3.9-3.13). The shallower delta front is where there is higher wave and current reworking of sediments, and here the OM index values are moderate and fairly consistent (1.0 to 3.7). The valley fill deposited in LST, TST and HST, shows salinity increasing upwards from 0.2 to 4.3 (samples CN 12, 9, 6; Fig. 3.13). The fluvial floodplain/wetland environment can have high OM content generally (1.9 to 39.3), but can be variable depending on the sub-environment. Correspondingly, our OM index values are highly variable (low to high). High OM content (samples CN 14, 11; Fig. 3.13) is concurrent with the HST, and relative sea-level rise with increases in sedimentation and nutrient supply. The Bluegate Shale shows high salinity (0.5 to 13.0) with high OM content (2.9 to 12.1) concurrent with the normal marine shelf/prodelta conditions with the lithofacies.

In Steamboat, marine influence slightly increases upward (0.2 to 1.0) through the outcrop but more prominently there are "pulses" of increasing/decreasing salinity. Because the sampling resolution is higher between the sequence boundaries compared to Caineville North, we are observing shorter term trends. Salinity and

OM are relatively low to moderate, and it shows increasing pulses in salinity upwards, although they are not pronounced (Fig. 3.13). OM content is low in the Steamboat delta front facies (0.3 to 6.0), and it increases upward, with fluvial channels deposited in the TST (samples SB 6, 8, 11; Fig. 3.13). The salinity index in Caineville North between SQB1 and 2 varies from 0.1 to 0.9 and 0.3 to 1.0 in Steamboat which is very similar indicating a common salinity environment which is in keeping with the lithofacies. The values slightly decrease in Cainville (0.1 to 0.9), but are relatively constant and show some shorter term variability in Steamboat. We have a higher resolution sampling in Steamboat and thus it maybe documenting shorter term trends that are not observed in Caineville North. The OM index values between SQB1 and 2 in Caineville North are higher (1.9 to 33), but there are only two very high values (i.e. 33). Steamboat has OM index values (0.3 to 6.0) decreasing upward indicating a decreasing amount of OM content possibly caused by less rainfall, and runoff transporting OM content basinward. Between SQB2 and 3 salinity index values in Caineville North are 0.5 to 0.8 and 0.3 to 1 in Steamboat, which shows similar trends as the interval between SQB1 and 2 in both outcrops. The values slightly increase in Steamboat, but only gradually and are more variable (0.1 to 1.0) than in Caineville North (0.5 to 0.8). Both outcrops show increasing OM index values upward (1.5 to 3.7) in Caineville North and 0.6 to 3.1 in Steamboat, which might indicate a gradual increase in rainfall and runoff transporting OM content basinward. Steamboat shows a relative stable increasing salinity upward between SQB3 and SQB4 (0.2 to 0.6), while in Caineville North the salinity index is generally decreasing upwards (0.5 to 1.0), and two samples show the highest salinity index values 2.0 (CN 23) and 1.6 (CN 24). The OM Index in Steamboat within SQB3 and SQB4 is low (decreasing upward) with values between 0.8 to 2.0, while in Caineville North the OM index is higher than Steamboat (increasing upward) with values between 1.0 to 3.1.

Blue Hills consists of three system tracts including HST, LST and TST. In this outcrop, salinity decreases upward (0.3 to 1.0) indicating a decreasing in marine influence (Fig. 3.13). The Blue Hills also shows an overall lower salinity (0.3 to 1.0) compared to the other outcrops, which is consistent with the fluvial valley fill lithofacies. OM content is high (1.7 to 18.6) throughout the outcrop, which consistent with the TST and HST likely due to increases in rainfall, runoff. The Blue Hills shows an overall low salinity index (0.3 to 1.0), and decreased marine influence upward. This fits with the overall biofacies designations of low salinity brackish water, which indicates that Blue Hills had the lowest salinity followed by Steamboat and Caineville North. In SQ1, the Caineville North salinity index is higher and increasing upward (0.2 to 4.3) and in Blue Hills the salinity index is lower but decreasing upward (0.1 to 0.8), which maybe interpreted as a marine to brackish salinity in Caineville North and more brackish in Blue Hills. However,

the OM index in SQ1 shows high OM contents, where as in Blue Hills, the OM index increases upwards with values between 1.7 to 18.6, and in Caineville North OM, it is decreasing but remains high (1.1 to 39.3).

Overall, three outcrops are dominated by agglutinated foraminiferal and testate amoebae morphotypes, while calcareous foraminifera are rare or totally absent because of diagensis. Calcareous foraminifera are commonly more dominant in marine salinity (Scott et al., 2005; Armstrong and Brasier, 2013), and their abundance decreases in lower salinity (e.g. brackish). Calcareous foraminifera taxa are found in the Tununk and Bluegate Shales (Turkistani et al., submitted), and there are mollusca fossils (e.g. ammonite and inoceramids) preserved; however, in our samples the calcareous fraction is under represented. The high OM content may have created low-pH conditions that affected their preservation, but their lack of presence could be due to low salinity conditions that dominated the deltaic environment. Many studies have shown that the proximal shelves of the Cretaceous seaway were largely brackish and salinity may have been too low in the deltaic setting for calcareous taxa (Bhattacharya and MacEachern, 2009). The Ferron Member was interpreted to reflect deposition under hyperpycnal conditions, and ichnofacies showed a stressed environment with salinity fluctuating between normal and brackish conditions (Bhattacharya and MacEachern, 2009). Hyperpycnal muds have been reported to be transported over 250 km offshore by storm waves, which agitates the shelf mud and disperses it by wind driven currents (Varban and Plint, 2008; Bhattacharya and MacEachern, 2009). These frequent river-fed hyperpycnal flow events may have lowered the salinity within the inner shelf, and transported taxa (e.g. testate amoebae) basinward. This was observed in the current study, where testate amoebae were found within delta front and the prodelta facies. More detailed analysis in these sequences may show trends in taphonomic transport of testate amoebae with hyperpycnal events, which maybe useful for reconstructing relative periods of wetness/dryness.

3.3.4 Implications for "Marine" Based Testate Amoebae

In the Ferron-Notom delta, testate amoebae are found in freshwater lithofacies as in Holocene environments, but were also found in brackish marine lithofacies having been transported seaward during river floods. Several studies have documented transported testate amoebae into deep Holocene basins by river flood events (Babalola, 2009; Riveiros and Patterson, 2009; Laut et al., 2017; Farr et al., 2020). The oldest record of testate amoebae is from Neoproterozoic marine sediments of the Chuar Group, Grand Canyon, Arizona, where testate amoebae are described as vase-shaped microfossils (Porter and Knoll, 2000). Well-preserved testate amoebae (e.g. *Centropyxis*) have been also found in marine deposits of the Permian-Triassic Boundary in the Guryul Ravine Section, India (Singh et al.,

2015). From these studies, it would seem that earliest testate amoebae from the Pre-Cambrian to early-Permian inhabited shallow marine environments (Kumar et al., 2011). However, as discussed other studies including the present example have reported testate amoebae in shallow marine facies that were transported during river flood events and storms (Patterson et al., 2000; Kumar and Patterson, 2002; Babalola, 2009; Riveiros and Patterson, 2009; Kumar et al., 2011; Laut et al., 2017). Therefore, some of these previous studies with testate amoebae in marine context could have the same transport bias (e.g. transport of testate amoebae into the offshore) as in the Ferron-Notom delta and caution should be used when interpreting a marine context for testate amoebae (Singh et al., 2015).

3.4 Conclusion

Sixty-six samples collected from three outcrops within the Ferron-Notom delta show foraminifera and testate amoebae assemblages that are poorly to moderately preserved showing signs of burial compression and flattening. Agglutinated foraminifera and testate amoebae tests dominated the samples, while there were only a few calcareous foraminifera tests found within the Bluegate and Tununk shale samples. However, despite these taphonomic biases, morphogroup analysis has defined distinct biofacies in the Ferron-Notom delta stratigraphy, and show potential for interpreting paleoenvironments. The environments were assigned to each morphotype consistent with the studies of Nagy (1992) and Nagy et al. (1995), Reolid et al. (2008), Reolid et al. (2018); and discussed in Turkistani et al. (submitted) (Chapter 2).

Paleo-salinity was calculated based on the relationships between foraminifera morphotypes (TS) and testate amoebae morphotypes (Ta-F, Ta-D, Ta-S). The prevalent trochospiral taxa has a salinity range from low-brackish to marine, and using it with freshwater testate amoebae provides a good salinity index. The OM index was calculated using the "bolivind-type" morphotypes (BiS and TrS), which are good proxies for OM and nutrient and the trochospiral morphotype (TS), and they can provide a relative measure of the OM of the sediment. Both indices follow the lithofacies in the three outcrops. Overall, the salinity and OM indices show great potential as a paleoenvironmental indicator in ancient systems, and because these morphotypes belong to extant assemblages, these morphotypes are effective indicators of paleo-salinity and organic matter (OM), and could be used in similar studies.

3.5 Acknowledgment

This work was made possible through Natural Sciences and Engineering Research Council (NSERC) Discovery Grants (EGR — 2015-057250) and the Canada Foundation for Innovation John R. Evans Leaders Fund (CFI-JELF grant 105-04523). CRD to Dr. Bhattacharya, as well as BP Canada, and the Susan Cunningham Research Chair in Geology. King Abdulaziz University funded a scholarship through the Kingdom of Saudi Arabia Embassy, and the Kingdom of Saudi Arabia Cultural Bureau, Ottawa, ON, Canada. Canadian Center for Electron Microscopy (CCEM), McMaster University, Hamilton, ON, Canada, provided SEM training.

Chapter 4

μXRF Analysis of the Upper Cretaceous (Turonian) Caineville North, Ferron-Notom Delta, Utah, USA

Majed N. Turkistani*, Eduard G. Reinhardt*, Jeremy Gabriel*, David Kynaston* and Janok P. Bhattacharya*

*School of Earth, Environment and Society, McMaster University, 1280 Main Street West, Hamilton, ON L8S 4K1 Canada

This paper will be submitted to *Elsevier* and will included in its published form once accepted.

Abstract

μXRF analysis of mudstone samples from the Upper Cretaceous (Turonian) Ferron-Notom delta in Central Utah, USA were used to examine elemental proxies for paleo-salinity (Sr/Ba), organic matter (K/S), redox (V/Ni), and sediment sources (Zr/Rb, Ti/Fe, Ti/Ca). Twenty-nine mudstone samples were analyzed from four lithofacies including the prodelta, delta front, fluvial valley fill and shelf and fourteen elements (Ti, Fe, Ca, Sr, Ba, Ni, Rb, Zr, S, V, Cu, Mn, Si, and K) provided proxy ratios to detect variations in terrigenous sediments, carbonate production, salinity, grain size, and fluvial inputs in Ferron-Notom delta. The overall μXRF analysis showed good correspondence between the elemental data and the lithofacies and microfossil indices. Sr/Ba and Ca/Fe showed relationships with carbonate content and proximity to the shoreline. Sr/Ba was not a good indicator for paleo-salinity, but it was more responsive to lithological change of carbonate content. The previously derived microfossil salinity index seems to be a more accurate paleo-salinity indicator. Zr/Rb and Ti/Fe showed fluvial input of sediment, and it fit the lithofacies. Zr/Rb and Ti/Fe showed highest values within the fluvial valley fill facies relative to the other lithofacies (prodelta, delta front, and shelf) showing a response to the proximity of fluvial sediment source. V/Ni was used as an indicator for redox, and it matched the previously derived microfossil OM index ("bolivind-type" taxa) showing a strong relationship between eutrophication and redox trends. The study aims to establish important baseline geochemical compositions of sediment sources to establish patterns and trends with sediment succession in the deeper basin (offshore; i.e. Mancos Shale). Potentially, these patterns and trends from the nearshore and fluvial environments will provide important geochemical data to assess paleoclimate, and sea-level in the offshore sediment successions.

Keywords: Ferron-Notom delta, Upper Cretaceous, μXRF data, sequence stratigraphy, geochemical, Itrax-μXRF core scanner

4.1 Introduction

Micro X-ray fluorescence (μXRF) core scanning is newly developed instrumentation that allows high-resolution analyses of sediment cores (100-200μm). It is a non-destructive analytical method that is automated, providing great efficiency for analyzing long stratigraphic sequences (Turner et al., 2010; Giralt et al., 2011; Gregory et al., 2015; Profe et al., 2016; Peros et al., 2017; Gregory et al., 2019). The instrument has been widely applied to soft sediment cores, but less, so to rock cores. Numerous studies have investigated different elemental proxies and their

relationship with environmental changes (e.g. weathering) over geological time scales. Croudace and Rothwell (2015) have highlighted common elements that have been used as proxies, such as iron (Fe), titanium (Ti), potassium (K), silicon (Si), sulfur (S), calcium (Ca), zirconium (Zr), strontium (Sr), rubidium (Rb), manganese (Mn), copper (Cu), and barium (Ba). These elements and others have been used to detect changes in a variety of environmental variables including trends with dry/wet seasons, and biological productivity. Sediments can be analyzed as bulk samples from sediment traps or surface samples (Gregory et al., 2019) or split cores (Croudace and Rothwell, 2015).

In the present research, we analyze hand samples from the Upper Cretaceous (Turonian) Ferron-Notom delta using an ITRAX-μXRF core scanner, which will be compared with previously documented palynologic (Akyuz et al., 2015), foraminiferal and testate amoebae data (Turkistani et al., submitted, Chapter 2), along with lithofacies records (e.g. Zhu et al., 2012; Wu and Bhattacharya, 2015; Bhattacharyya et al., 2015b). The mudstone samples were obtained from the Caineville North outcrop on the western side of Ferron-Notom delta and represent six sequences (Zhu et al., 2012; Wu et al., 2012) from various lithofacies, such as the pro-delta, delta front, fluvial channels.

4.1.1 Elemental Proxies

There are many applications of μXRF analysis on lake and marine cores for detecting flood events, grain-size variations, and sediment provenance, but there are fewer studies that have examined coastal to shallow shelf depositional systems (e.g. deltaic facies). However, these environments are important for understanding long shale sequences further offshore (e.g. Mancos Shale) because they provide data on the geochemical make-up of the riverine and shallow shoreface sediment. This may allow separation of marine vs terrestrial sediment provenance and depositional processes using μXRF analysis and understanding of sea-level and climate forcing of the Cretaceous Western Interior Seaway (Croudace and Rothwell, 2015). Ti and Fe are considered good proxies for terrigenous sediment (fine-grained) input from rainfall, and discharge from rivers (Floods; Jansen et al., 1998). Ti is also used as a proxy for aeolian dust input (Itambi et al., 2009; Itambi et al., 2010; Croudace and Rothwell, 2015). Ti is resistant to diagensis and is immobile in sediment (redox-insensitive), while Fe can readily move within the sediment column (redox-sensitive). Ti is more resistant to weathering in terrestrial areas versus Fe (Marsh et al., 2007; Ben-Awuah et al., 2017). Therefore, Ti/Fe has been used as a proxy for precipitation and runoff, where high values indicate wetter (e.g. summer) periods with greater weathering and runoff, and lower values indicate drier (e.g. winter) periods (Itambi et al., 2010; Aufgebauer et al., 2012; Croudace and Rothwell, 2015). In the Cariaco basin in Venezuela, high values of Ti and Fe were

used to indicate wetter conditions, with more frequent rainfall and weathering (Calvert and Pedersen, 2007).

Ca is mainly used to indicate carbonate content in marine sediment (Croudace and Rothwell, 2015). The source of Ca in sediments is largely derived from fragments of shells, calcareous tests and small biogenic particulates (Silva et al., 2014). Therefore, ratios of Ca/Fe and Ti/Ca are often used for a variety of applications but reflect the proportion of biogenic carbonate to detrital clay content (Rothwell et al., 2006; Piva et al., 2008; Croudace and Rothwell, 2015). For example, turbidite beds (sand, silt, muds) often show enrichment in Fe, which is found in shallow sediments, while marine muds in the deeper part of the basin have higher Ca, and thus Ca/Fe can be used to distinguish turbidite versus marine beds (Rothwell et al., 2006). Generally, high Ca/Fe values and correspondingly low values of Ti/Ca indicate increasing marine influence and vice versa terrigenous and fluvial sediments transport to the basin, but can also be due to dissolution of carbonates (Rothwell et al., 2006; Gebhardt et al., 2008; Croudace and Rothwell, 2015). In the Late Holocene Tatos basin, in the Mauritius Islands, SW Indian ocean, a progression from wetland to shallow lake to wetland again showed low (Ca/Ti) values concurrent with increased freshwater input (rainfall/runoff), and high (Ca/Ti) values with increased marine influence (De Boer et al., 2014).

Zr/Rb has been used as a grain-size proxy in marine, lacustrine, and deltaic sediments (Turner et al., 2015), and is often used as a proxy for flood events, because Zr is abundant in coarser sediments as a heavy mineral (e.g. zircon), while Rb is abundant in clays (Dypvik and Harris, 2001; Wang et al., 2011; Croudace and Rothwell, 2015). During river floods, coarser sediments are transported basinwards, so higher values of Zr/Rb can be used for flood frequency, and magnitude (Wang et al., 2011; Turner et al., 2015). In the Yangtze River Delta plain, China, Wang et al. (2011) were able to reconstruct a 600-yr flood record from Zr/Rb. In another example, from the Upper Severn River Floodplain, (UK) flood events were recorded using Zr/Rb and Zr/Ti proxies (Jones et al., 2012).

Sr/Ba has been used as a proxy for salinity (Yandoka et al., 2015; Ben-Awuah et al., 2017), because Ba is less mobile and easily adsorbed by clay minerals and OM resulting in higher Ba concentrations in organic rich terrestrial sediment (Wang et al., 2020). Sr is not adsorbed by clay minerals and organic matter and thus is more mobile, so Sr is easily transported into marine environments, but Sr is also included in marine carbonates (aragonite; Wang et al., 2020). Relative, salinity can be determined using Sr/Ba ratios, where a low Sr/Ba value implies lower salinity, and a high Sr/Ba value implies a more "marine" environment (Deng and Qian, 1993; Ben-Awuah et al., 2017). For example, this trend was observed in the West Baram Delta, Sarawak Basin, Malaysia, South China Sea, where Sr/Ba values

show freshwater to marine influenced environments (Ben-Awuah et al., 2017).

K/S has been used as a proxy for organic matter (OM), because it relates to nutrient-rich organic particulates (Croudace and Rothwell, 2015). K is similar to Ba and is associated with clay minerals and OM and is less mobile, while S is associated with organic rich muds, and is found in oxidizing conditions, thus high values of K/S can indicate increased OM (Croudace and Rothwell, 2015; Ben-Awuah et al., 2017). Ni is a mobile element, which is high in clay and organic matter and less so in coarser sediments (Antić-Mladenović et al., 2011; Costa et al., 2018). Ni becomes soluble in oxic condition, and under dysoxic to anoxic conditions Ni is removed from the sediment into the water (Baioumy and Lehmann, 2017). V is also a mobile element, but it becomes immobilized and thus enriched in anoxic marine environments because of the increased activity of sulfate reducing bacteria (Baioumy and Lehmann, 2017; Costa et al., 2018). V/Ni is therefore often used as redox indicator to evaluate the bottom conditions (Zhang et al., 2011). For example, the West Baram Delta, Sarawak Basin, Malaysia, South China Sea, shows a range of V/Ni values indicative of reducing environments with variable marine and terrestrial OM input (Ben-Awuah et al., 2017; Baioumy and Lehmann, 2017).

4.1.2 Study Area

The Ferron sandstone is a member of the Mancos Shale Formation deposited during a wet climate in the Upper Cretaceous (Turonian) in the Western Interior Seaway (KWIS; Fig. 4.1; Wu et al., 2012; Zhu et al., 2012; Akyuz et al., 2015; Famubode and Bhattacharya, 2016). Three clastic deltas (Notom, Vernal, and Last Chance respectively) formed the Ferron Sandstone Member. The Notom delta, which is the area of interest, comprises six sequences, eighteen parasequences sets, which are well exposed in the Caineville North outcrop and represents the western side of the delta (Wu et al., 2012; Zhu et al., 2012; Akyuz et al., 2015). The area is well documented in the literature, and Zhu et al. (2012) and other studies have been carried out on other exposures of the Ferron-Notom delta in its eastern part (Wu and Bhattacharya, 2015; Wu et al., 2016b). Turkistani et al. (submitted, Chapter 2) analyzed the foraminifera and testate amoebae from the outcrops using morphogroups analysis (from Jones and Charnock, 1985), and performed biofacies analysis on samples collected from the same three outcrops within the Ferron-Notom delta. Akyuz et al. (2015) investigated the Ferron-Notom delta for its palynology and determined that the climate during which the Ferron-Notom delta was deposited was ever wet. Also, they found four intervals of marine dinoflagellates interbedded within fluvial channel deposits, which implied marine incursions to inland areas, which was confirmed later by Turkistani et al. (forthcoming, Chapter 3). Two main lithologies are found within the Caineville North

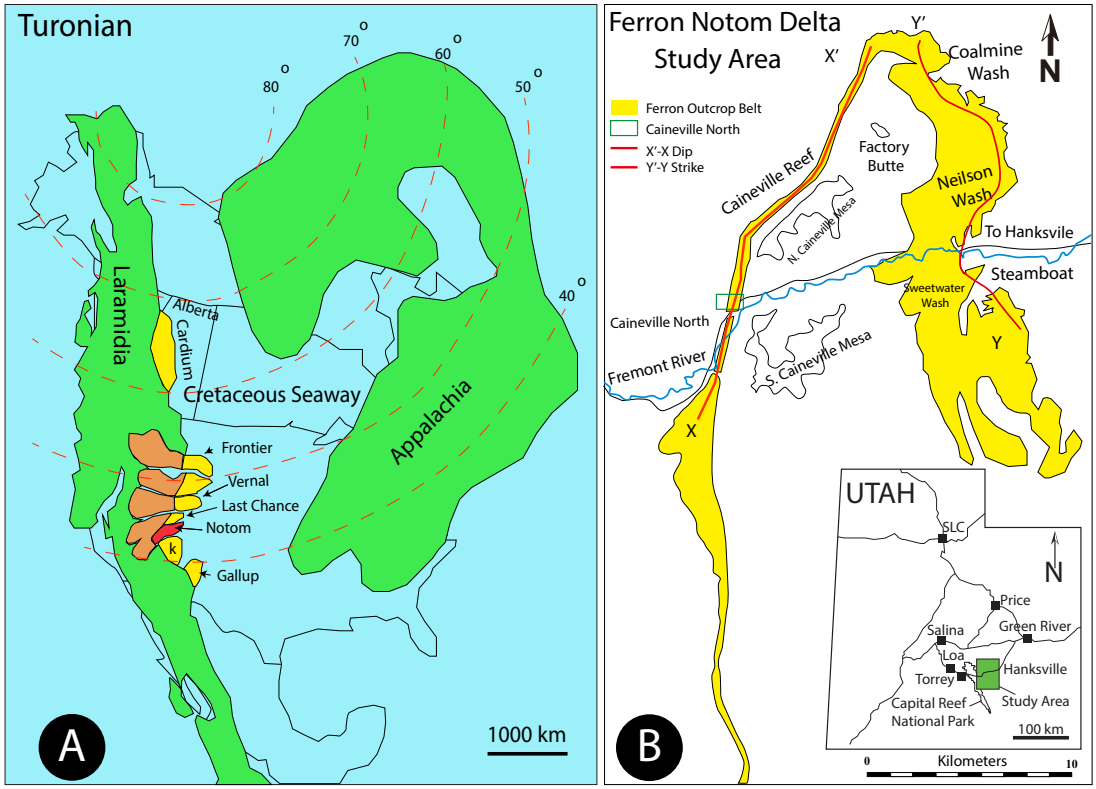

FIGURE 4.1: (A) North America continent during the Upper Cretaceous (Turonian), where the Western Interior Seaway split the continent into two subcontinents (Akyuz et al., 2015). (B) The Ferron-Notom delta showing the Caineville North outcrop on the western part of the delta (Li et al., 2010; Zhu et al., 2012).

outcrop, namely sandstone and mudstone that form the different lithofacies, such as prodelta, delta front and fluvial deposits (Li and Bhattacharya, 2013) as well as coal. Generally, sandstone elemental compositions vary based on the different proportions of quartz, feldspars and other rock fragments, but generally consist of Na, K, Mg, Al, Si, Fe, Ba, P, S, Mm, Ti, C, and Zr (Pettijohn, 1963). Similarly, mudstones share similar compositions, although the proportion of elements vary (Caracciolo et al., 2011).

Detrital-zircon U-Pb analysis by Kynaston (2019) shows that the bentonite beds within the Ferron-Notom delta originate from the volcanically active margin to the west, where volcanic ash may have traveled by airfall or transverse drainage. The other two sources of sediment in the Ferron-Notom delta are a result of the erosion of the Sevier Thrust Front and Mogollon highland batholiths that formed

by continental magmatism and drainage input from the mid-continental granite-rhyolite province (Kynaston, 2019).

4.1.3 Previous Biofacies Results

The Caineville North section consists of four lithofacies: the pro-delta of the Tununk Shale, the delta front, tidally-influenced tributary fluvial channels within the Ferron Sandstone, and the Bluegate Shale (shelf). Turkistani et al. (submitted) conducted morphogroup analysis on foraminifera and testate amoebae on the five outcrops of the Ferron-Notom delta. There were four morphogroups and eleven morphotypes, which were assigned to a potential environment. Agglutinated foraminifera morphogroup include: trochospiral to nearly planispiral (PS), initially planispiral to uniserial (PS/UnS), trochospiral (TS), miliolid (Mi), elongated uniserial (UnSE), uniocular-tubular (UnLT), biserial (BiS), and triserial(TrS) (2; Turkistani et al., submitted). Agglutinated testate amoebae morphotypes are flask-shaped (Ta-F), donut-shaped (Ta-D), and sack-shaped (Ta-S; Chapter 2 Turkistani et al., submitted). Overall, the most dominant species in the Caineville North samples are *Gavelinella spp.*, *Trochammina spp.*, *Reophax spp.*, *Bathysiphone spp.*, *Textularia spp.* *Neobulimina albertensis*, and *Difflugia spp.* (Testate amoebae).

Four biofacies were established based on the foraminiferal and testate amoebae morphotypes, and based on this analysis, a salinity index, and OM index were derived for the outcrops (Turkistani et al., forthcoming). Biofacies I was described as lowest salinity biofacies of tidally brackish water influenced, and Biofacies II is characterized as low salinity and brackish lagoon/estuary. Biofacies III has low to medium salinity lagoon/estuary, and Biofacies IV has medium to normal marine salinity of the shallow shelf/prodelta. The salinity index in the Caineville North outcrop showed an overall decreasing trend moving from the shallow shelf/prodelta facies to the delta front and into the fluvial valley fill facies. The salinity index then increases into the Bluegate Shale/shallow shelf facies. The OM index shows higher values in the prodelta facies, which decreases in the delta front and fluvial valley fill facies, but in the fluvial valley facies the OM index is highly variable. The OM index then increases with the shallow shelf facies of the Bluegate Shale. Both indices show trends with sequence boundaries and correlate with other analysed outcrops of Steamboat and Blue Hills (Turkistani et al., forthcoming).

4.2 Methodology

4.2.1 *Sample collection and preparation*

Twenty-nine mudstone samples ($\approx$ 10 cm^3) were collected from the Caineville North outcrop within the Ferron-Notom delta, central Utah, USA (Chapter 2-3; Turkistani et al., submitted; Turkistani et al., forthcoming). The outcrop located on the west of Ferron-Notom delta, Central Utah (Fig. 4.1 A and B). The Caineville North outcrop samples were used because it contains six sequences in the Notom delta, and a wide range of lithofacies (e.g. pro delta, delta front, fluvial-channels, and shelf; Zhu et al., 2012; Turkistani et al., forthcoming, Chapter 2).

4.2.2 *Sample preparation for μXRF analysis*

Sub-samples were disaggregated by soaking in distilled water overnight, and loaded in a Sequential Sample Reservoir (SSR) as described by Gregory et al. (2017). The SSR is comprised of acrylic cuvettes (1.5 x 1 x 1 cm) along a center line on an acrylic base. Sediment samples were loaded into each cuvette ensuring that samples were evenly packed with a spatula (Gregory et al., 2017).

A Cox ITRAX μXRF-CS was used to analyze samples using a Molybdenum (Mo) heavy element (Mo-HE) X-ray source at the McMaster University Core Scanning Facility (MUCS), at 40kV (e.g. voltage), 50 mA (current), and an exposure time of 15s. Step-size was 0.2 mm, down the central portion of each sample. The resultant elemental data was then averaged over the length of the cuvette and the data used for PCA analysis, and plotting of the data. A subset of the data (Cu, Mn, Fe, Ti, Ca, Sr, S, Zr, K, Si, Rb, Ni, V, Mn, and Ba) was used for PCA analysis using the (PCA function), which is included in the "FactoMineR" package in R (Sebastien Le, 2008), which uses a common scaling factor to normalize the data.

4.3 Results

4.3.1 Overall Elemental Composition

ITRAX-μXRF analysis detected forty-nine elements with fourteen elements used for analysis. These elements had relatively high values (cps) and were elements of interest for paleoenvironmental analysis. The boxplots (Fig. 4.2) show three different ranges of mean values and variability (InterQuartileRange-IQR) in the elemental data. The most abundant element is Fe (mean = 22479 cps, IQR = 5146 cps), but it had high variability, likewise Ca was also high (3285 cps) and variable (IQR = 5425 cps). Elements with moderately high values and low variability consists of: Si, Sr, Ni, Ti, Mn, Zr, Rb, and K (e.g. Mn = 171 cps to Ti = 1101

cps; IQR (Mn) = 114 cps to IQR (Ti) = 259 cps). Low value elements include Cu, S, Ba, and V, which range from ≈ 24 (S) to 37 (Ba) cps.

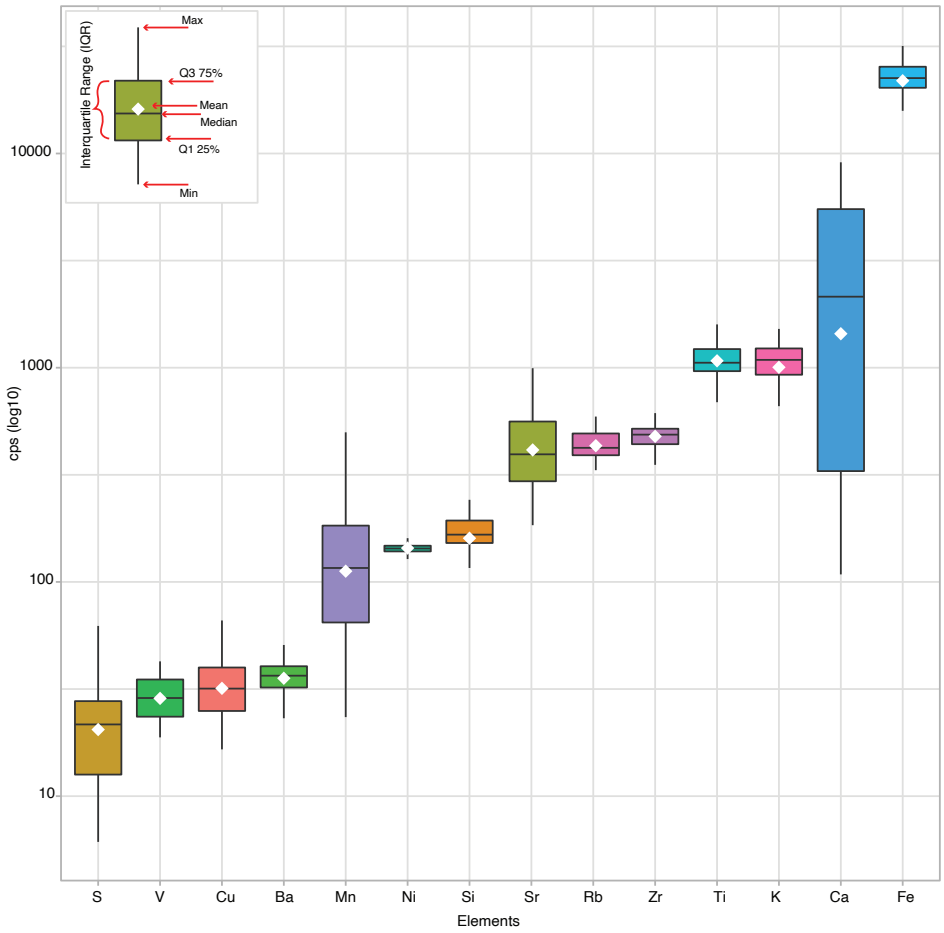

Figure 4.2: Box plots showing the average counts and variability of abundant elements in samples from the Caineville North.

4.3.2 PCA Analysis of Elemental Data

The PCA (Fig. 4.2) shows that Fe, Mn, Rb and V are strongly positively correlated, but negatively correlated with Ni and Zr. Ca, Sr, S, Si, Ba, and K are strongly correlated, and are inversely correlated with Ti, and Cu. The relationship between Ca, Sr and Mn, Fe, Rb and V could reflect a dysoxic to anoxic fine grained mud, where Ca and Sr increases in more oxygenated environments (Croudace and Rothwell, 2015). In addition, Ca and Sr are more commonly found in marine sediments (carbonates, aragonite), and their relationship with Fe, and Ti could reflect the relative proportions of terrigenous vs marine sediment. Ti and Fe amounts

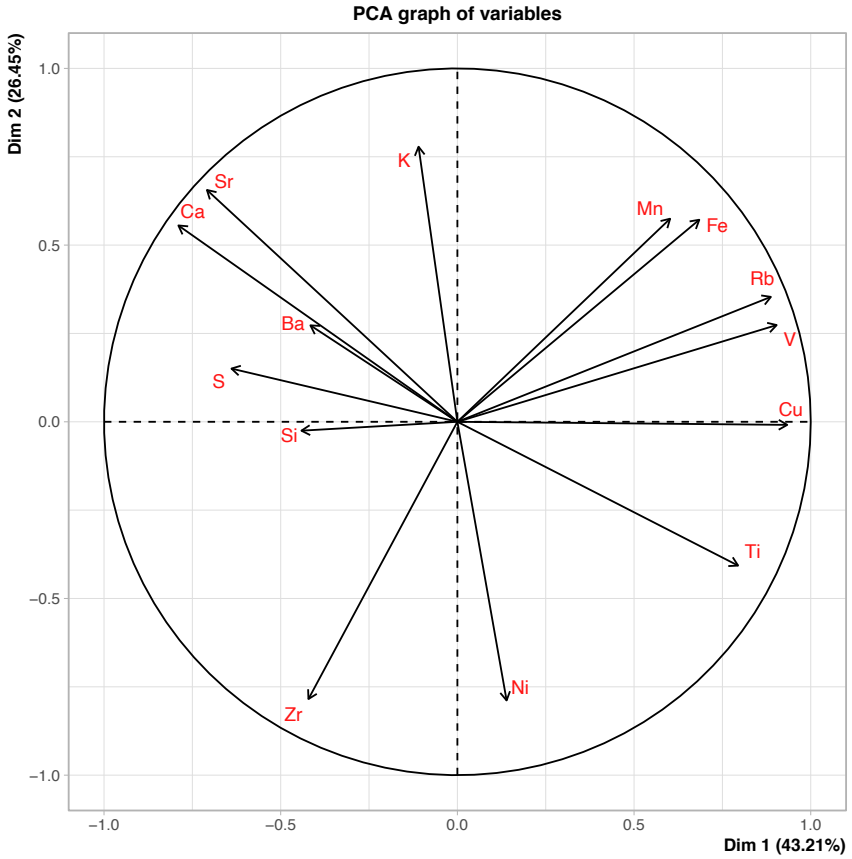

FIGURE 4.3: Principle components analysis (PCA) of most common elements ≈70%.

typically increase as a result of terrigenous sediment input with rainfall, runoff and floods (Croudace and Rothwell, 2015). Ca and V shows a strong relationship, and commonly when Ca increases, V also increases, because they both tend to vary with pH. In low pH conditions, Ca decreases, reflecting reducing conditions (Martins et al., 2018). K, Fe, Rb, Mn, Zr, Si, and Ni, are commonly used as indicators for terrigenous sediment transport, rainfall, runoff, grain-size variation, and sediment provenances and typically show good correlations (Croudace and Rothwell, 2015; McNeill-Jewer et al., 2019). In addition, Si, K, Rb, Mn, and Fe, are often sensitive to grain-size variation, as increases in grain-size lead to increased in Si, while K, Rb, and Fe predominate in finer sediment (Ben-Awuah et al., 2017). In the PCA (Fig. 4.3), Si is low compared to K and Rb because the samples are mostly mudstones. The relationship between K and Si can also be used as an indicator of weathering, with increases in K and decreases in Si indicative of wetter conditions (Ben-Awuah et al., 2017).

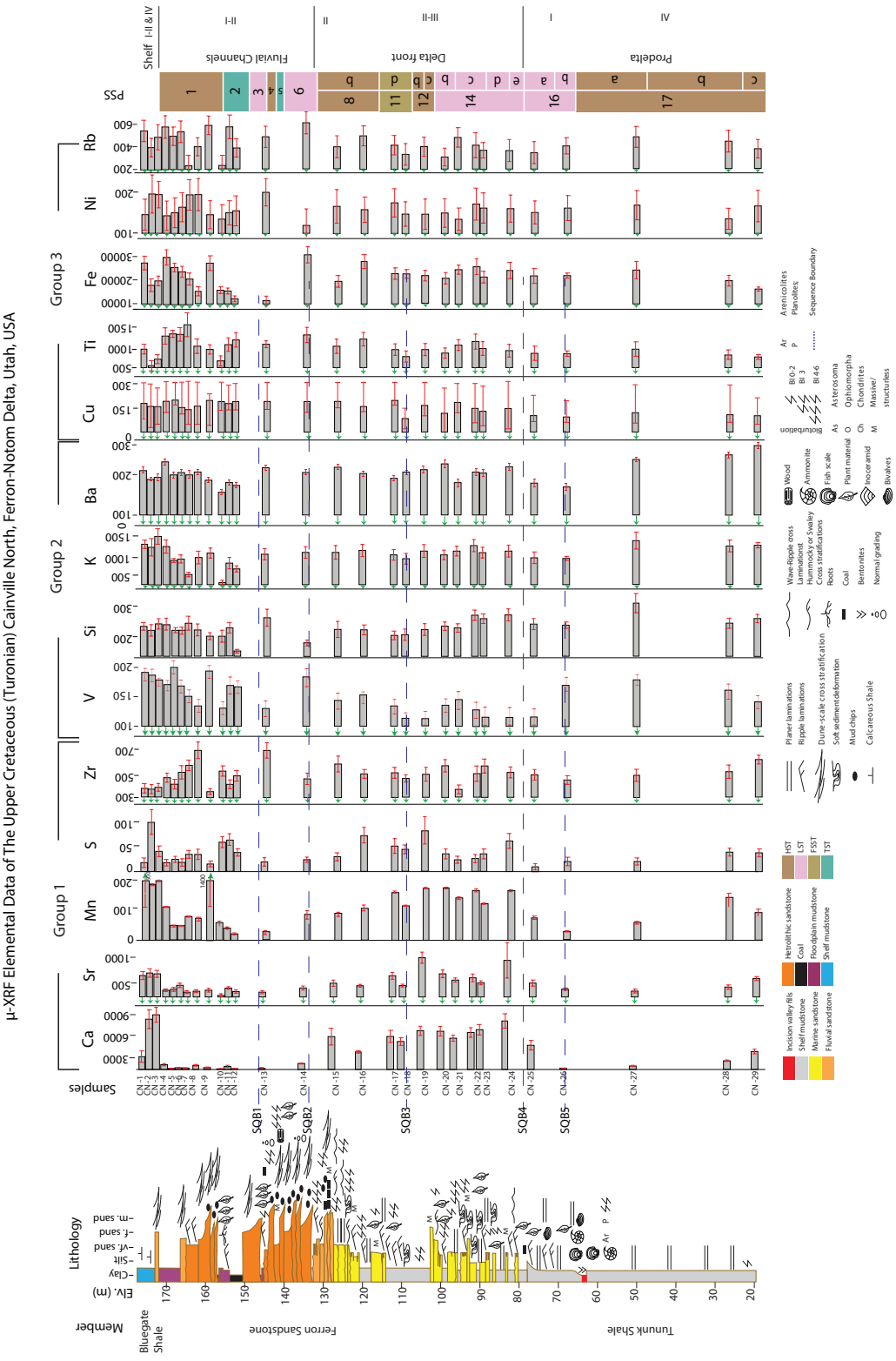

FIGURE 4.4: Lithological section of Caineville North, parasequences sets, system tracks and the average μXRF counts of elemental data.

4.3.3 Elemental Trends

Group 1 Elements

The elements are grouped based on their overall variability in the Caineville North outcrop. (Figs. 4.2, 4.4). Group 1 elements include Ca, Sr, S, Mn, and Zr, and they have the most variability in the outcrop and thus are the most sensitive to environmental change. In general, Group 1 elements were high in the delta front (SQB 2-4) and then increased between the fluvial channel and shelf facies (Bluegate Shale). However, Zr did not show this increase at the transition to the Bluegate Shale. Group 1 elements also showed higher values at the base relative to the upper portion in the prodelta facies of the Tununk Shale.

Group 2 Elements

Group 2 elements include V, Si, K and Ba which are moderately variable throughout the outcrop and show less consistent variation in comparison to the Group 1 elements (Figs. 4.2, 4.4). Group 2 elements generally show increased values below SQB5 in the prodelta (Tununk Shale) and then also in the shelf facies of the Bluegate Shale, although this is the most pronounced with V and to some degree K. Overall, Ba and Si show the least amount of variability throughout the outcrop.

Group 3 Elements

The third group of elements includes Cu, Ti, Fe, Ni, and Rb, which show a slight overall increase upward through the outcrop, and is the most pronounced with Ti (Figs. 4.2, 4.4). However, there is very little consistency amongst the elements, although Ti and Cu do show some similarity.

4.4 Discussion

4.4.1 Paleo Salinity: Sr/Ba and Microfossil Salinity Index

Sr/Ba has been used as a proxy for salinity in several studies (Deng and Qian, 1993; Ben-Awuah et al., 2017), where high values of Sr/Ba are indicative of increased salinity. However, in the Caineville North outcrop, Sr/Ba seems to be more responsive to changes in sediment type (Fig. 4.5). Sr/Ba increases in the top most part of the Tununk Shale (CN 25, 26 $>$ 10; i.e. prodelta), in the delta front (CN 16 to 24, $>$ 10), and the very top shelf lithofacies (Bluegate Shale; CN 1-4, $\approx$ 15.0 - 20.0). The lowest Sr/Ba values are in the fluvial valley fill lithofacies (CN 5 - 15, $<$ 10.0; Table 4.1; Fig. 4.5), and show higher values in the mudstone associated with the sandstones and a shallow marine environment (shallow shoreface).

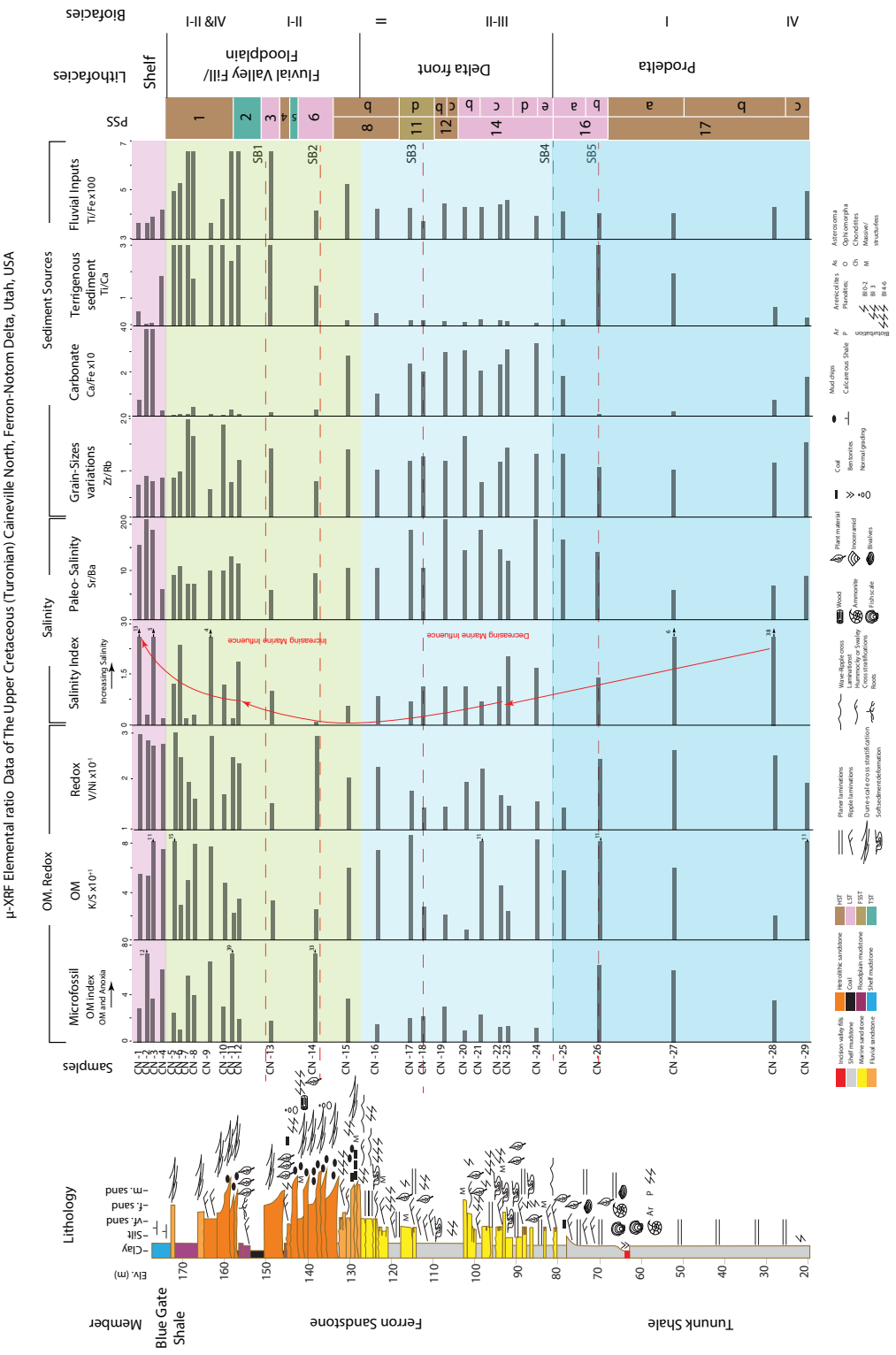

FIGURE 4.5: Lithological section of Caineville North, showing biofacies and elemental ratios used in paleoenvironmental analysis.

Table 4.1: Elemental ratios used in Caineville North to interpret paleoenvironment conditions.

Ratio	Value	Interpretation	References
Sr/Ba	↑	Salinity	Deng and Qian (1993) Yandoka et al. (2015) Ben-Awuah et al. (2017)
V/Ni	↑	Dysoxic/Anoxic	Lewan (1984) Galarraga et al. (2008) Ben-Awuah et al. (2017)
Zr/Rb	↑	Grain size/Flood event	Dypvik and Harris (2001) Wang et al. (2011) Jones et al. (2012) Turner et al. (2015)
Ca/Fe	↑	Biogenic Carbonate	Rothwell et al. (2006) Gebhardt et al. (2008) Piva et al. (2008) De Boer et al. (2014) Silva et al. (2014)
Ti/Fe	↑	Fluvial input	Jansen et al. (1998) Calvert and Pedersen (2007) Marsh et al. (2007) Itambi et al. (2009) Itambi et al. (2010) Aufgebauer et al. (2012) Ben-Awuah et al. (2017)
Ti/Ca	↑	Terrigenous input	Rothwell et al. (2006) Gebhardt et al. (2008) Piva et al. (2008) De Boer et al. (2014) Silva et al. (2014)
K/S	↑	Organic Matter (OM)	Croudace and Rothwell (2015)

Sr is abundant in shells (i.e. aragonite; Markulin et al., 2019), and the high Sr/Ba values within the sandier intervals are likely due to the break down of shell material in the shallow marine environment with waves and currents. The Sr/Ba ratio seems to be largely a response to changing Sr because Ba does not vary much in the outcrop. The Ba maybe associated with the mudstone lithology, which was analyzed throughout the outcrop and not the sandy beds. The microfossil salinity index (Chapter 3; Turkistani et al., forthcoming) seems to be more representative of salinity change in the Caineville North rather than Sr/Ba, which appears to be more lithologically controlled. The microfossil salinity index shows higher values in the prodelta (Tununk Shale) and the shallow shelf lithofacies of the Bluegate Shale, and lower salinity in the delta front and fluvial valley fill facies. In contrast, the Sr/Ba ratio generally shows the inverse of this relationship. Therefore, the Sr/Ba ratio seems to be more a reflection of proximity to the shoreline, and a shallow marine environment. The high Sr/Ba values that were recorded at the base of the Bluegate Shale represents the marine transition with sea-level rise.

4.4.2 Organic Matter (OM) and Redox: K/S, V/Ni and Microfossil OM Index

Several studies have used K/S as a proxy for organic matter (OM) in sediment (Croudace and Rothwell, 2015), and V/Ni has been used as a proxy for reducing environments (Adams and Weaver, 1958; Lewan, 1984; Lerman, 1989; Jones et al., 1994; Dypvik and Harris, 2001; Roy and Roser, 2013; Ben-Awuah et al., 2017). High values of K/S are indicative of increases in OM in sediment (Croudace and Rothwell, 2015), and high values of V/Ni are indicative of reducing environments (dysoxic/anoxic), while V/Ni low values are indicative of suboxic environments (Aufgebauer et al., 2012). In Caineville North, the K/S values are generally high and variable, but there are decreases in the delta front (CN 18 - 20) and the fluvial valley fill facies (CN 11 - 14; Fig. 4.5). The K/S values being high in the prodelta fits with the lithofacies, because there is an abundance of plant fossils in the interval, but the K/S does not appear to be very reflective of OM content overall throughout the Caineville North outcrop and does not match the lithofacies very well. V/Ni values generally vary between 0.1 and 0.3 throughout the outcrop. The higher values in the prodelta (below SQB 5) and flood plain (CN 5 - 7) sandstone and shelf shales (Bluegate) is a good match with lithofacies, and the shallow near shore of the delta front is more oxygenated because of increased currents (hence the sandy facies). The microfossil OM index (Chapter 3; Turkistani et al., forthcoming) does not fit well with the K/S (OM), but fits very well the V/Ni (redox). "Bolivind-type" taxa have been used to identify eutrophic and low oxygen conditions in deltaic settings, which is used to calculate the OM microfossil

index (Huerta-Diaz, Morse, et al., 1992; Andersson et al., 1994; Turkistani et al., forthcoming, Chapter 3).

4.4.3 Sediment Sources: Zr/Rb, Ti/Fe, Ca/Fe, Ti/Ca

Zr/Rb is a commonly used ratio as a proxy for grain-size variations as well as flood events (Fig. 4.5 - Fig. 4.5; Sudom and St. Arnaud, 1971; Milne and Fitzpatrick, 1977; Schneider et al., 1997; Calvert and Pedersen, 2007; Moreno et al., 2007; Cuven and Francus, 2010; Burnett et al., 2007; Wang et al., 2011; Chawachai et al., 2013). In the Caineville North outcrop, the Zr/Rb (Fig. 4.5) values only show a subtle change in grain-size, because all the analyzed samples were mudstones, but there is a slight increase in Zr/Rb with the delta front, where it is shallow and undergoes more reworking of sediment (sandier). There are also higher values in the fluvial valley fill, which is also sandier, and closest to the probable input of zircons from fluvial sources. Zr/Rb has been shown to depend on river flow and climatic changes, such as frequency of rainfall and runoff, along with river floods (Pastouret et al., 1978; Calvert and Pedersen, 2007).

Ti/Fe, Ti/Ca, Ca/Fe are common proxies for fluvial input (terrigenous sediment), and carbonate production, respectively (Aufgebauer et al., 2012; Croudace and Rothwell, 2015). In the Caineville North outcrop, Ti/Fe, Ca/Fe, Ti/Ca all share similar trends or inverse trends to each other, which follows carbonate content (Ca/Fe) or fluvial input sources. The Ca/Fe shows an inverse relationship with Ti/Fe, where carbonate increases and terrigenous sediment decreases, and vice versa, where there is a decline in carbonate content, there are increases in terrigenous sediment. The relationship between Ca/Fe and Ti/Ca also shows relationships with Sr/Ba because Ca is also a reflection of carbonate content. The Ti/Fe values show similarity with Zr/Rb values because Ti is at least partially associated with titanomagnetite, which like zircon (Zr) is a heavy mineral, and would be expected to be concentrated in fluvial sediments. However, compared to Zr/Rb the degree of variability with Ti/Fe is greater throughout the outcrop.

4.5 Applications of Microfossils and Elemental Ratios to Shale Facies in The Deep Basin

4.5.1 Sediment Sources and Transport

In the Caineville North outcrop, Sr/Ba seems to be more responsive to the changes in sediment type, where high values are associated with the delta front facies, and at the base of the shelf facies (Bluegate Shale). These higher Sr/Ba values in the Bluegate Shale may represent the shallow marine transition to the relatively deep

shelf but above storm wave base (Fig. 4.4 - Fig. 4.5). Ca/Fe shows similar trends as Sr/Ba in the delta front and fluvial valley fill. As discussed, the increase of Sr/Ba and Ca/Fe in the delta front is likely due to the breakdown of shell material and an indicator for a shallow marine environment. Further offshore, Sr/Ba in shale sequences may show increases due to storm transport of nearshore sediments to the deep basin. The Ca/Fe ratio may show similar trends, but could also be responsive to phytoplankton or zooplankton productivity in the upper water column.

Zr/Rb and Ti/Fe show potential to identify the frequency of river flood events associated with hyperpycnal or hypopycnal flow out into the basin. Zr/Rb and Ti/Fe could increase offshore due to sediment transported via storms, or hypo and hyperpycnal flows with river flood events (Schieber, 2016). The frequency of these events could be related to climate variability with rainfall and weathering patterns as well as sea-level and proximity to the riverine sediment source. Hyperpycnal flows have been shown to reach up to 250km offshore in the Late Cenomanian-Turonian Kaskapau Formation of the Western Canadian foreland basin(Varban and Plint, 2008).

4.5.2 Redox Indicator

The V/Ni redox ratio shows a good match with the Caineville North outcrop lithofacies, and fits the microfossil OM index, which reflects relative anoxia and eutrophication (Fig. 4.5 - Fig. 4.5). Generally, in the deep basin, OM relates to productivity of phytoplankton, and also OM export through hyper and hypopycnal flows from riverine sources in the form of fine particulate matter (Engel et al., 2011). Ocean circulation also affect phytoplankton production as result of mixing between cold and warm water masses (i.e. Cretaceous Western Interior Seaway), and development of extreme low oxygen conditions (Hay et al., 1993). V and Ni are also mobile elements that can be attached to OM and fine grain sediments (Baioumy and Lehmann, 2017; Costa et al., 2018), which may transported offshore by storms, hyperpycnal flow or hypopycnal plums during river flood events that extend offshore depending on size of the river (Bhattacharya and MacEachern, 2009; Plint, 2014). Therefore, V/Ni could show increases offshore low oxygen conditions, but may also be responding to sediment inputs from riverine sources.

4.6 Conclusion

Overall, the μXRF analysis of mudstone samples from the Caineville North outcrop showed good correspondence between the elemental data and the lithofacies and microfossil indices. Sr/Ba and Ca/Fe showed relationships with carbonate content and proximity to the shoreline, where biogenic shell production would be

the highest relative to the other facies. It does not appear that Sr/Ba is a good indicator of paleo-salinity, because it did not match the salinity microfossil index, but was responding to lithology, and biogenic carbonate production.

Zr/Rb and Ti/Fe showed good correspondence with facies indicating fluvial inputs of sediment. The fluvial valley fill facies had the highest Zr/Rb and Ti/Fe values, with Ti/Fe showing the greatest variability relative to the other lithofacies (prodelta, delta front, and shelf). This variability in Ti/Fe responded well to distance from the fluvial sediment source, decreasing into the prodelta and shelf facies.

V/Ni had a very good correspondence with the OM microfossil index indicating a strong relationship between eutrophication and redox trends. The "bolivind-type" taxa used in the microfossil index have been shown to indicate low oxygen conditions (anoxia) in modern deltaic sediments (e.g. Mississippi; Rabalais and Turner, 2006) associated with anthropogenic eutrophication impacts. This study established important end-member geochemical compositions of sediment sources (i.e. fluvial and shallow marine) that will be important for establishing patterns and trends with sediment successions in the offshore basin (e.g. Mancos Shale). These long depositional sequences (+80m) can potentially provide important paleoclimate and sea-level records that have yet to be fully explored, and this work will be seminal for establishing trends and casual mechanisms for these records. μXRF core scanning of these long succession at very high resolution (e.g. 0.1mm) may provide important paleoenvironmental information that has yet to be explored.

4.7 Acknowledgment

This work was made possible through Natural Sciences and Engineering Research Council (NSERC) Discovery Grants (EGR — 2015-057250) and the Canada Foundation for Innovation John R. Evans Leaders Fund (CFI-JELF grant 105-04523). CRD to Dr. Bhattacharya, as well as BP Canada, and the Susan Cunningham Research Chair in Geology. King Abdulaziz University funded a scholarship through the Kingdom of Saudi Arabia Embassy, and the Kingdom of Saudi Arabia Cultural Bureau, Ottawa, ON, Canada. Canadian Center for Electron Microscopy (CCEM), McMaster University, Hamilton, ON, Canada, provided SEM training. Saudi Digital Library (SDL) for using their database.

Chapter 5

Conclusions

This research has successfully demonstrated that microfossil assemblages of foraminifera, and testate amoebae provide useful paleoenvironmental information in Cretaceous deltaic successions. Five outcrops within the Upper Cretaceous (Turonian) Ferron-Notom Delta (Caineville North, Steamboat, Blue Hills, Coalmine Wash and Neilson Wash) were examined with various lithofacies encompassing the prodelta, delta front, and tidally-influenced tributary valley fill. This microfossil analysis shows relationships between bio and lithofacies that demonstrates their utility.

Overall, the foraminifera ("bolivind-type" taxa and trochospiral) and testate amoebae morphotypes can provide a good salinity estimation and a relative measure of the OM of the sediment. Both indices follow lithofacies trends in the three outcrops and have good potential for further application in other studies of the Ferron to establish the extent of marine incursion into the backwater environments and sea-level. The salinity index using the morphotypes can be easily measured and applied to other studies. Furthermore, this index could be applied to coastal succession in various geological contexts.

The investigation of the Caineville North outcrop showed good correspondence between the elemental data and the lithofacies and microfossil indices. Sr/Ba and Ca/Fe showed relationships with carbonate content and proximity to the shoreline, where biogenic shell production would be the highest relative to the other facies. It does not appear that Sr/Ba is a good indicator of paleo-salinity, because it did not match the salinity microfossil index, but was responding to lithology, and biogenic carbonate production. V/Ni had a very good correspondence with the OM microfossil index indicating a strong relationship between eutrophication and redox trends. The "bolivind-type" taxa used in the microfossil index have been shown to indicate low oxygen conditions (anoxia) in modern deltaic sediments (e.g., Mississippi) associated with anthropogenic eutrophication impacts.

This dissertation established important end-member geochemical compositions of sediment sources (i.e. fluvial and shallow marine) that will be important for establishing patterns and trends with sediment successions in the offshore basin (e.g., Mancos Shale). These long depositional sequences (+80m) can potentially provide important paleoclimate and sea-level records that have yet to be fully explored, and this research will be seminal for establishing trends and casual mechanisms for these records. μXRF core scanning of these long succession at very high resolution (e.g., 200mm) may provide important paleoenvironmental information that has yet to be explored.

5.0.1 Future Work

1. Using transported testate amoebae into basin to reconstruct river flood events.
2. Using geochemical composition of sediment sources will be important for investigated patterns and tends in the offshore basin, where long deposition sequences can provide important information on paleoclimate and sea-level records that have yet to be fully explored.

References

Adams, J. and Weaver, C. (1958). Th-to-u ratios as indicators of sedimentary process - an example of geochemistary facies. *American Associations of Petroleum Geology Bullitin* 42, 387–430.

Akyuz, I., Warny, S., Famubode, O., and Bhattacharya, J. (2015). Palynology of the Upper Cretaceous (Turonian) Ferron Sandstone Member, Utah, USA: identification of marine flooding surfaces and Milankovitch cycles in subtropical, ever-wet, paralic to non-marine palaeoenvironments. *Palynology* 0(0), 1–15.

Alday, M., Cearreta, A., Freitas, M., and Andrade, C. (2013). Modern and late Holocene foraminiferal record of restricted environmental conditions in the Albufeira Lagoon, SW Portugal. *Geologica acta* 11(1), 0075–84.

Alperin, M. I., Cusminsky, G. C., and Bernasconi, E. (2011). Benthic foraminiferal morphogroups on the Argentine continental shelf. *The Journal of Foraminiferal Research* 41(2), 155–166.

Altenbach, A. V. (1988). Deep-sea benthic foraminifera and flux rates of organic carbon. *Rev. Paleobiol* 2, 719–720.

Alve, E. and Nagy, J. (1986). Estuarine foraminiferal distribution in Sandebukta, a branch of the Oslo Fjord. *The Journal of Foraminiferal Research* 16(4), 261–284.

Alve, E. (1990). Variations in estuarine foraminiferal biofacies with diminishing oxygen conditions in Drammensfjord, SE Norway. In: *Paleoecology, biostratigraphy, paleoceanography and taxonomy of agglutinated foraminifera.* Springer, 661–694.

Anbuselvan, N. et al. (2018). Benthic Foraminifera from Shelf Sediments of the Bay of Bengal, Central East Coast, India. *Thalassas: An International Journal of Marine Sciences* 34(1), 13–52.

Andersson, P. S., Wasserburg, G., Ingri, J., and Stordal, M. C. (1994). Strontium, dissolved and particulate loads in fresh and brackish waters: the Baltic Sea and Mississippi Delta. *Earth and Planetary Science Letters* 124(1-4), 195–210.

Antić-Mladenović, S., Rinklebe, J., Frohne, T., Stärk, H.-J., Wennrich, R., Tomić, Z., and Ličina, V. (2011). Impact of controlled redox conditions on nickel in a serpentine soil. *Journal of Soils and Sediments* 11(3), 406–415.

Armstrong, H. and Brasier, M. (2013). *Microfossils (2nd ed.)* John and Sons: Wiley.

Ashckenazi-Polivoda, S., Edelman-Furstenberg, Y., Almogi-Labin, A., and Benjamini, C. (2010). Characterization of lowest oxygen environments within ancient upwelling environments: Benthic foraminifera assemblages. *Palaeogeography, Palaeoclimatology, Palaeoecology* 289(1-4), 134–144.

Asioli, A., Medioli, F. S., and Patterson, R. T. (1996). Thecamoebians as a tool for reconstruction of paleoenvironments in some Italian lakes in the foothills of the southern Alps (Orta, Varese and Candia). *Journal of Foraminiferal Research* 26(3), 248–61.

Atwater, B. T. (1987). Evidence for great Holocene earthquakes along the outer coast of Washington State. *Science* 236, 942–946.

Atwater, B. T. (1992). Geologic evidence for earthquakes during the past 2000 years along the Copalis River, southern coastal Washington. *Journal of Geophysical Research*. v. 97(B2), 1901–1920.

Aufgebauer, A., Panagiatopoulos, K., Wagner, B., Schaebitz, F., Viehberg, F., Vogel, H., Zanchetta, G., Sulpizio, R., Leng, M., and Damaschke, M. (2012). Climate and environmental change over the last 17 ka recorded in sediments from Lake Prespa (Albania/F.Y.R. of Macedonia/Greece). *Quat Int* 274, 122–135.

Babalola, L. O. (2009). Late holocene paleoclimatic and paleoceanographic records in anoxic basins, Seymour-Belize Inlet Complex, British Columbia. PhD thesis. Carleton University.

Baioumy, H. and Lehmann, B. (2017). Anomalous enrichment of redox-sensitive trace elements in the marine black shales from the Duwi Formation, Egypt: evidence for the late Cretaceous Tethys anoxia. *Journal of African Earth Sciences* 133, 7–14.

Bapst, D. W. (2012). *paleotree: Paleontological and Phylogenetic Analyses of Evolution*.

Bartlett, G. A. (1966). Distribution and abundance of foraminifera and thecamoebian in Miramichi River and Bay. Report no. 66-2, 104 p.

Bassi, D., Fugagnoli, A., Posenato, R., and Scott, D. B. (2008). Testate amoebae from the Early Jurassic of the Western Tethys, north-east Italy. *Palaeontology* 51(6), 1335–1339.

Ben-Awuah, J., Padmanabhan, E., and Sokkalingam, R. (2017). Geochemistry of mioscene sedimentary rocks from offshore west baram delta, Sarawak basin, malaysia, south china sea: implications for weathering, provenance, tectonic setting, paleoclimate and paleoenvironment of deposition. *Geosccience Journal* 21, 167–185.

Berger, W. H. (1971). Planktonic foraminifera; sediment production in an oceanic front. *The Journal of Foraminiferal Research* 1(3), 95–118.

Berkeley, A., Perry, C. T., and Smithers, S. G. (2009). Taphonomic signatures and patterns of test degradation on tropical, intertidal benthic foraminifera. *Marine Micropaleontology* 73(3-4), 148–163.

Berkeley, A., Perry, C. T., Smithers, S. G., Horton, B., and Taylor, K. G. (2007). A review of the ecological and taphonomic controls on foraminiferal assemblage development in intertidal environments. *Earth-Science Reviews* 83(3-4), 205–230.

Bernhard, J. M. (1986). Characteristic assemblages and morphologies of benthic foraminifera from anoxic, organic-rich deposits; Jurassic through Holocene. *Journal of Foraminiferal Research* 16(3), 207–215.

Bernier, P. (1984). Les formations carbonatées du Kimméridgien et du Portlandien dans le Jura méridional Stratigraphie, micropaléontologie, sédimentologie. *Doc. Lab. Géol. Lyon pp* 92, 803.

Bhalla, S. N. and Talib, A. (1991). Callovian–Oxfordian foraminifera from Jhurio Hill, Kutch, Western India. *Rev. Paléobiol.* 10, 85–114.

Bhattacharya, J. P. and Tye, R. S. (2004). Searching for modern Ferron analogs and application to subsurface interpretation. *Regional to Wellbore Analog for Fluvial–Deltaic Reservoir Modeling: The Ferron Sandstone of Utah: American Association of Petroleum Geologists, AAPG Studies in Geology* 50, 39–57.

Bhattacharya, J. and MacEachern, J. (2009). Hyperpycnal Rivers and Prodeltaic Shelves in The Cretaceous Seaway of North America. *Journal of Sedimentary Reseach* 79, 184–209.

Bhattacharyya, P., Bhattacharya, J., and Khan, S. (2015a). Paleo-Channel Reconstruction and Grain Size Variability in Fluvial Deposits, Ferron Sandstone, Notom Delta, Hanksville, Utah. *Sedimentary Geology* 325, 17–25.

Bhattacharyya, P., Bhattacharya, J. P., and Khan, S. D. (July 2015b). Paleochannel reconstruction and grain size variability in fluvial deposits, Ferron Sandstone, Notom Delta, Hanksville, Utah. *Sedimentary Geology* 325, 17–25. ISSN: 0037-0738.

Brotzen, F. (1942). Die Foraminiferengattung Gavelinella nov. gen. und die Systematik der Rotaliformes. *Arsbok Sveriges Geologiska Undersokning* 36(8), 1–60.

Bąk, K. (2004). Deep-water agglutinated foraminiferal changes across the Cretaceous/Tertiary and Paleocene/Eocene boundaries in the deep flysch environment; eastern Outer Carpathians (Bieszczady Mts Poland). *In Grzybowski Foundation Special Publication* 8, 1–56.

Burnett, A., Soregham, M., Scholz, C., and Brown, E. (2007). Tropical eas african climate change and its relation to global climate: a record from lake Tanganyika, tropical east africa, over the past 90kyr. *Paleogeography Paleoclimatology palaeoecology* 303, 155–167.

Calvert, S. and Pedersen, T. (Jan. 2007). Chapter Fourteen Elemental Proxies for Palaeoclimatic and Palaeoceanographic Variability in Marine Sediments: Interpretation and Application. *Developments in Marine Geology* 1, 567–644. ISSN: 1572-5480.

Caracciolo, L., Le Pera, E., Muto, F., and Perri, F. (2011). Sandstone petrology and mudstone geochemistry of the Peruc–Korycany Formation (Bohemian Cretaceous Basin, Czech Republic). *International Geology Review* 53(9), 1003–1031.

Cearreta, A., Benito, X., Ibáñez, C., Trobajo, R., and Giosan, L. (2016). Holocene palaeoenvironmental evolution of the Ebro Delta (Western Mediterranean Sea): Evidence for an early construction based on the benthic foraminiferal record. *The Holocene* 26(9), 1438–1456.

Cetean, C. G., Blc, R., Kaminski, M. A., and Filipescu, S. (2011). Integrated biostratigraphy and palaeoenvironments of an upper Santonian - upper Campanian succession from the southern part of the Eastern Carpathians. *Romania. Cretaceous Research* 32(5), 575–590.

Charman, D. J., Gehrels, W. R., Manning, C., and Sharma, C. (2010). Reconstruction of recent sea-level change using testate amoebae. *Quaternary Research* 73(2), 208–219.

Châtelet, E. A. du, Francescangeli, F., Bouchet, V., and Frontalini, F. (2018). Benthic foraminifera in transitional environments in the English Channel and the southern North Sea: A proxy for regional-scale environmental and paleoenvironmental characterisations. *Marine environmental research* 137, 37–48.

Chawachai, S., Chabangborn, A., Kylander, M., Lowemark, L., Morth, C., Blaauw, M., Klubseang, W., Reimer, P., and Fritz S.and Wohlfarth, B. (2013). Lake kumphawapi an archive of holocene paleoenvironmental and palaeoclimatic changes in the northeast thiland. *Quaternary Science Review* 68, 59–75.

Chen, H., Shaw, T. A., Wang, J., Engelhart, S., Nikitina, D., Pilarczyk, J. E., Walker, J., Garcıéa-Artola, A., and Horton, B. P. (2020). Salt-marsh foraminiferal distributions from mainland northern Georgia, USA: an assessment of their viability for sea-level studies. *Open quaternary.* 6(1), 1–19.

Cobban, W. A., Walaszczyk, I., Obradovich, J. D., and McKinney, K. C. (2006). *A USGS Zonal Table for the Upper Cretaceous Middle Cenomanian–Maastrichtian of the Western Interior of the United States Based on Ammonites, Inoceramids, and Radiometric Ages*. Tech. rep.

Coleman, J. (1982). Deltaic Environments of Deposition. *Sandstone Depositional Environments: AAPG Memoir 31* (31), 139.

Collins, E. S. (1996). *Marsh-estuarine benthic foraminiferal distributions and Holocene sea-level reconstructions along the South Carolina coastline*. Tech. rep. Ph.D. diss., Dalhousie University, Halifax, Canada (unpublished manuscript), 240 p.

Colpaert, C., Nikitenko, B., and Khafaeva, S. (2017). Stratigraphy and ecostratigraphic distribution of foraminiferal morphogroups from the Upper Jurassic of the Makar'yev section (Unzha River, Volga River basin). *Russian Geology and Geophysics* 58(1), 70–86.

Coogan, J. C. and Decelles, P. G. (2007). Regional structure and kinematic history of the Sevier fold-and-thrust belt. *Reply. Bulletin of the Geological Society of America* 119(3-4), 508–512.

Corbeanu, R. M., Wizevich, M. C., Bhattacharya, J. P., Zeng, X., and Mcmechan, G. A. (2004). Three-dimensional architecture of ancient lower delta-plain point bars using ground-penetrating radar. *AAPG Studies in Geology* 50, 427–449.

Corliss, B. H. (1985). Microhabitats of benthic foraminifera within deep-sea sediments. *Nature* 314(6010), 435–438.

Corliss, B. H. (1991). Morphology and microhabitat preferences of benthic foraminifera from the northwest Atlantic Ocean. *Marine Micropaleontology* 17(3-4), 195–236.

Corliss, B. H. and Chen, C. (1988). Morphotype patterns of Norwegian Sea deep-sea benthic foraminifera and ecological implications. *Geology* 16(8), 716–719.

Corner, G. D., Steinsund, P. I., and Aspeli, R. (1996). Distribution of recent benthic foraminifera in a subarctic fjord-delta: Tana, Norway. *Marine Geology* 134(1-2), 113–125.

Costa, K. M., Anderson, R. F., McManus, J. F., Winckler, G., Middleton, J. L., and Langmuir, C. H. (2018). Trace element (Mn, Zn, Ni, V) and authigenic uranium (aU) geochemistry reveal sedimentary redox history on the Juan de Fuca Ridge, North Pacific Ocean. *Geochimica et Cosmochimica Acta* 236, 79–98.

Croudace, I. and Rothwell, R., eds. (2015). *Micro-XRF Studies of Sediment Cores: Applications of a Non-Destructive Tool for Environmental Sciences*. Dordrecht, NL: Springer.

Culver, S. J., Mallinson, D. J., Corbett, D. R., Leorri, E., Rouf, A. A., Shazili, N. A. M., Yaacob, R., Whittaker, J. E., Buzas, M. A., and Parham, P. R. (2012). Distribution of foraminifera in the Setiu estuary and lagoon, Terengganu, Malaysia. *The Journal of Foraminiferal Research* 42(2), 109–133.

Culver, S. J. (2019). *Interpreting Paleoenvironments with Microfossils*.

Cushman, J. A. and Cole, W. S. (1930). *Pleistocene foraminifera from Maryland*.

Cushmann, J. A. (1917). A Monograph of the Foraminifera od the North Pacific Ocean Part VI. *Miliolidae. MILIOLIDAE. Smithsonian Institution Bulletin* 161. US Government Printing Office.

Cuven, S. and Francus P.and Lamoureux, S. (2010). Estimation of grain size variability with micro x-ray fluorescence in laminated lacustrine sediments, cape bounty, canadian high arctic. *Journal of Paleolimnology* 44, 803–817.

De Boer, E. J., Tjallingii, R., Vélez, M. I., Rijsdijk, K. F., Vlug, A., Reichart, G.-J., Prendergast, A. L., Louw, P. G. de, Florens, F. V., Baider, C., et al. (2014). Climate variability in the SW Indian Ocean from an 8000-yr long multi-proxy record in the Mauritian lowlands shows a middle to late Holocene shift from negative IOD-state to ENSO-state. *Quaternary Science Reviews* 86, 175–189.

Decelles, P. G., Lawton, T. F., and Mitra, G. (1995). Thrust timing, growth of structural culminations, and synorogenic sedimentation in the type Sevier orogenic belt, western United States. *Geology* 23(8), 699–702.

Deng, H. and Qian, K. (1993). Sedimentary geochemistry and environmental analysis. *Gansu science and technology press, Lanzhou*, 18–31.

Dubicka, Z. and Peryt, D. (2014). Classification and evolutionary interpretation of late Turonian-early Campanian Gavelinella and Stensioeina (Gavelinellidae, benthic foraminifera) from western Ukraine. *The Journal of Foraminiferal Research* 44(2), 151–176.

Dypvik, H. and Harris, N. (2001). Geochemical facies analysis of fine-grained siliciclastics using th/u, zr/rb and (zr+ rb)/sr ratios. *Chemical Geology* 181, 131–146.

Eduardo, K., Paul, A. M. L., Malcolm, N. H., and ., B. (1990). Latest Cenomanian-earliest Turonian low-oxygen tolerant benthonic foraminifera; a case-study from the Sergipe Basin (N.E. Brazil) and the western Anglo-Paris Basin (southern England). *Palaeogeography, Palaeoclimatology, Palaeoecology* 77(2), 145–177.

Elliott, T. (1989). Deltaic systems and their contribution to an understanding of basin-fill successions. *Geological Society, London, Special Publications* 41(1), 3–10.

Ellison, R. L. (1995). Paleolimnological analysis of Ullswater using testate amoebae. *Journal of Paleolimnology* 13(1), 51–63.

Ellison, R. L. and Nichols, M. M. (1976). Modern and Holocene foraminifera in the Chesapeake Bay region. In: *First International Symposium on Benthonic Foraminifera of the Continental Margins. Part A*, 131–51.

Engel, A., Händel, N., Wohlers, J., Lunau, M., Grossart, H.-P., Sommer, U., and Riebesell, U. (2011). Effects of sea surface warming on the production and composition of dissolved organic matter during phytoplankton blooms: results from a mesocosm study. *Journal of Plankton Research* 33(3), 357–372.

Famubode, O. and Bhattacharya, J. (2016). Sequence Stratigraphic Analysis of the Youngest Nonmarine Sequence In the Cretaceous Ferron Notom Delta, South Central Utah, U.S.A. *Journal of Sedimentary Research* 86(3), 168–198. ISSN: 1527-1404.

Farooqui, A., Kumar, A., Jha, N., Pande, A., and Bhattacharya, D. (2010). A thecamoebian assemblage from the Manjir formation (early Permian) of northwest Himalaya, India. *E-Journal Earth Science India* 3, 146–153.

Farr, R. H., Clapham, A., Reinhardt, E. G., Boyce, J., Collins, S., and John, R. (2020). Using marine deposits to understand terrestrial human environments: 6000-year old hyperpycnal flash-flood events and their implications. *Journal of Archaeological Science: Reports* 30(102176).

Fatela, F., Moreno, J., Moreno, F., Araujo, M. F., Valente, T., Antunes, C., Taborda, R., Andrade, C., and Drago, T. (2009). Environmental constraints of foraminiferal assemblages distribution across a brackish tidal marsh (Caminha, NW Portugal). *Marine Micropaleontology* 70(1-2), 70–88.

Fernandes, É., Teixeira, C., and Bordalo, A. A. (2019). Coupling between Hydrodynamics and Chlorophyll a and Bacteria in a Temperate Estuary: A Box Model Approach. *Water* 11(3), 588.

Fielding, C. R. (2011). Foreland basin structural growth recorded in the Turonian Ferron Sandstone of the Western Interior Seaway Basin. *USA. Geology* 39(12), 1107–1110.

Fishbein, E. and Patterson, R. T. (1993). Error-weighted maximum likelihood (EWML): a new statistically based method to cluster quantitative micropaleontological data. *Journal of Paleontology* 67(3), 475–486.

Foissner, W. and Schiller, W. (2001). Stable for 15 million years: scanning electron microscope investigation of Miocene euglyphid thecamoebians from Germany, with description of the new genus Scutiglypha. *European Journal of Protistology* 37(2), 167–180.

Franks, P. C., Coleman, G. L., Plummer, N., and Hamblin, W. K. (1959). Cross-stratification, Dakota Sandstone (Cretaceous), Ottawa County, Kansas. *Kansas Geol. Survey Bull* 134(6), 223–238.

Galarraga, F., Reategui, K., Martinez, A., Llamas, J., and Marquez, G. (2008). V/Ni Ratio as a parameter in paleoenvironment characterization of non-mature-Crude Oils from several Latin American Basins. *Journal of Petroleum Science and Engineering* 61, 9–14.

Gayes, P. T., Scott, D. B., Collins, E. S., and Nelson, D. D. (1992). A late Holocene sea-level irregularity in South Carolina. *Society of Economic Paleontologist and Mineralists* (48). Special Publication, 154–60.

Gebhardt, H., Sarnthein, M., Grootes, P. M., Kiefer, T., Kuehn, H., Schmieder, F., and Röhl, U. (2008). Paleonutrient and productivity records from the subarctic North Pacific for Pleistocene glacial terminations I to V. *Paleoceanography* 23(4).

Gehrels, W. R., Roe, H. M., and Charman, D. J. (2001). Foraminifera, testate amoebae and diatoms as sea-level indicators in UK saltmarshes: a quantitative multiproxy approach. *Journal of Quaternary Science: Published for the Quaternary Research Association* 16(3), 201–220.

Ghosh, A. and Filipsson, H. L. (2017). Applications of Foraminifera, Testate Amoebae and Tintinnids in Estuarine Palaeoecology. In: *Applications of Paleoenvironmental Techniques in Estuarine Studies*. Springer, 313–337.

Giralt, S., Rico-Herrero, M. T., Vega, J. C., and Valero-Garc.s, B. L. (2011). Quantitative climate reconstruction linking meteorological, limnological and XRF core scanner datasets: the Lake Sanabria case study, NW Spain. *J. Paleolimnol.* 46, 487–502.

Goldstein, S. T. (1988). Foraminifera of relict salt marsh deposits, St. Catherines Island, Georgia; taphonomic implications. *Palaios* 3(3), 327–334.

Gooday, A. J. (1993). Deep-sea benthic foraminiferal species which exploit phytodetritus: characteristic features and controls on distribution. *Marine Micropaleontology* 22(3), 187–205.

Gorbarenko, S., Psheneva, O., Aeremova, A., Matul, A., Tiedemann, R., and Nürnberg, D. (2010). Paleoenvironment changes in the NW Okhotsk Sea for the last 18 kyr determined with micropaleontological, geochemical and lithological data. *Deep-Sea Research I* 57, 797–811.

Gregory, B. R., Patterson, R. T., Reinhardt, E. G., Galloway, J. M., and Roe, H. M. (Sept. 2019). An evaluation of methodologies for calibrating Itrax X-ray fluorescence counts with ICP-MS concentration data for discrete sediment samples. *Chemical Geology* 521, 12–27. ISSN: 0009-2541.

Gregory, B. R., Peros, M., Reinhardt, E. G., and Donnelly, J. P. (May 2015). Middle–late Holocene Caribbean aridity inferred from foraminifera and elemental data in sediment cores from two Cuban lagoons. *Palaeogeography, Palaeoclimatology, Palaeoecology* 426, 229–241. ISSN: 0031-0182.

Gregory, B. R., Reinhardt, E. G., Macumber, A. L., Nasser, N. A., Patterson, R. T., Kovacs, S. E., and Galloway, J. M. (2017). Sequential sample reservoirs for Itrax-XRF analysis of discrete samples. *Journal of paleolimnology* 57(3), 287–293.

Gupta, B. K. S. (2003). Foraminifera in marginal marine environments. In: *Modern foraminifera*. Springer, 141–159.

Haman, D. (1990). Living thecamoebid distribution, biotopes and biofacies in an upper deltaic plain lacustrine subenvironment, Lac des Allemands, Louisiana. *Revista Española de Micropaleontologica* 22, 47–60.

Hammer, Ø., Harper, D., and Ryan, P. D. (2001). PAST: Paleontological Statistics Software Package for Education and Data Analysis. *Palaeontologia Electronica* 4(1), 1–9.

Hay, W. W., Eicher, D., and Diner, R. (1993). Physical oceanography and water masses in the Cretaceous Western Interior Seaway. In: *Evolution of the western interior basin*. Vol. 39. Geological Association of Canada St. John's, 297–318.

Haynes, J. R. (1973). Foraminifera. *Nature* 246(5434), 541–541.

Hayward, B. W., Grenfell, H. R., Sabaa, A. T., Kay, J., and Clark, K. (2011). Ecological distribution of the foraminifera in a tidal lagoon–brackish lake, New Zealand, and its Holocene origins. *Journal of Foraminiferal Research* 41(2), 124–137.

Hayward, B. W., Grenfell, H. R., and Scott, D. B. (1999). Tidal range of marsh foraminifera for determining former sea-level heights in New Zealand. *New Zealand Journal of Geology and Geophysics* 42(3), 395–413.

Hayward, B. W. and Hollis, C. J. (1994). Brackish foraminifera in New Zealand; a taxonomic and ecologic review. *Micropaleontology* 40(3), 185–222.

Heron-Allen, E. and Earland, A. (1930a). Some new foraminifera from the S Atlantic; III Miliammina, a new siliceous genus. *Journal of the Royal Microscopical Society London* 50(1), 38–45.

Heron-Allen, E. and Earland, A. (1930b). Some new foraminifera from the S Atlantic; III Miliammina, a new siliceous genus. *Journal of the Royal Microscopical Society London* 50(1), 38–45.

Hill, R. B. (1982). Depositional Environments of the Upper Cretaceous Ferron Sandstone south of Notom. *Geology Studies* 29, 59–83.

Hintz, C., Chandler, G., Bernhard, J., McCrokle, D., Havach, S., Blanks, J., and Shaw, T. (2004). A phyiscochemically constrained seawater culturing system for production of benthic foraminifera. *Limnology and Oceanography: methods* 2, 160–170.

Houghton, J. T., Jenkins, G. J., and Ephraums, J. J. (1990). Climate change: the IPCC scientific assessment. *American Scientist;(United States)* 80(6).

Hudackova, N., Sotak, J., Ruman, A., Rybar, S., and Milovsky, R. (2018). Marsh-type agglutinated foraminifera from Upper Miocene sediments of the Danube Basin. *MICROPALEONTOLOGY* 64(5-6), 481–492.

Huerta-Diaz, M. A., Morse, J. W., et al. (1992). Pyritization of trace metals in anoxic marine sediments. *Geochim. Cosmochim. Acta* 56(7), 2681–2702.

Hughes, G. (2004). Middle to late Jurassic biofacies of Saudi Arabia. *Rivista Italiana di Paleontologia e Stratigrafia (Research In Paleontology and Stratigraphy)*, 110–110.

Itambi, A. C., Dobeneck, T. V., Mulitza, S., Bickert, T., and Heslop, D. (Mar. 2009). Millennial-scale northwest African droughts related to Heinrich events and Dansgaard-Oeschger cycles: Evidence in marine sediments from offshore Senegal. *Paleoceanography* 24 (1). ISSN: 08838305.

Itambi, A. C., Dobeneck, T. von, and Adegbie, A. T. (Mar. 2010). Millennial-scale precipitation changes over Central Africa during the late Quaternary and Holocene: evidence in sediments from the Gulf of Guinea. *Journal of Quaternary Science* 25(3), 267–279. ISSN: 0267-8179.

Jain, S. and Farouk, S. (2017). Shallow water agglutinated foraminiferal response to Late Cretaceous–Early Paleocene sea-level changes in the Dakhla Oasis, Western Desert, Egypt. *Cretaceous Research* 78, 240–257.

Jansen, J., Van der Gaast, S., Koster, B., and Vaars, A. (1998). CORTEX, a shipboard XRF-scanner for element analyses in split sediment cores. *Mar Geol* 151, 143–153.

Jenkins, C. D. (2000). The ecological significance of foraminifera in the Kimmeridgian of Southern England. *Grzybowski Foundation Special Publication* 7, 167–178.

Jones, A. F., Macklin, M. G., and Brewer, P. A. (2012). A geochemical record of flooding on the upper River Severn, UK, during the last 3750 years. *Geomorphology* 179, 89–105.

Jones, R. and Charnock, M. (1985). Morphogroups of agglutinating foraminifera. Their life positions and feeding habits and potential applicability in (paleo) ecological studies. *Revue de paléobiologie* 4(2), 311–320.

Jones, W. M., Scaloni, A., and Manning, J. M. (1994). [17] Acylaminoacyl-peptidase. In: *Methods in enzymology*. Vol. 244. Elsevier, 227–231.

Kaminski, M. A., Boersma, A., Tyszka, J., and Holbourn, A. E. L. (1995). Response of deep-water agglutinated foraminifera to dysoxic conditions in the California Borderland Basins. *Grzybowski Found. Spec. Publ* 3, 131–140.

Karl, H. (1976). Depositional history of Dakota Formation (Cretaceous) sandstones, southeastern Nebraska. *Journal of Sedimentary Research* 46(1), 124–131.

Kliza, D. A. (1994). Distribution of Arcellacea in freshwater lakes of Pond Inlet and Bylot Island. *Unpublished honours thesis, Carleton University, Ottawa, Ontario.* 52. Northwest Territories. Honours thesis, p–p.

Koutsoukos, E. A., Leary, P. N., and Hart, M. B. (1990). Latest Cenomanian—earliest Turonian low-oxygen tolerant benthonic foraminifera: a case-study from the Sergipe basin (NE Brazil) and the western Anglo-Paris basin (southern England). *Palaeogeography, Palaeoclimatology, Palaeoecology* 77(2), 145–177.

Kumar, A., Farooqui, A., and Jha, N. (2011). Early Permian glacio-marine thecamoebian assemblages from the northwest Himalayas, India. *Journal of Micropalaeontology* 30(1), 75–89.

Kumar, A. and Patterson, R. T. (2002). Dinoflagellate cyst assemblages from Effingham Inlet, Vancouver Island, British Columbia, Canada. *Palaeogeography, Palaeoclimatology, Palaeoecology* 180(1-3), 187–206.

Kynaston, D. and Bhattacharya, J. P. (2019). Facies Architecture and Time Stratigraphic Relationships of Confined Tributary Valley Fills and Unconfined Fluvial Systems within the Backwater, Ferron-Notom Delta, Utah. *Journal of Sedimentary Research*.

Kynaston, D. A. (2019). STRATIGRAPHY, PROVENANCE, TIMING AND CONTROL OF INCISED VALLEYS IN THE FERRON SANDSTONE. PhD thesis. McMaster University.

Laut, L., Clemente, I., Martins, V., Frontalini, F., Raposo, D., Belart, P., Habib, R., Fortes, R., and Lorini, M. (2017). Benthic Foraminifera and Thecamoebians of Godineau River Estuary, Gulf of Paria, Trinidad Island. *Anuário do Instituto de Geociências.* 4(2), 118–143.

Leckie, R. M. (1985). Foraninifera of the Cenomanian-Turonian Boundary Interval, Greenhorn Formation, Rock Canyon Anticline, Pueblo, Colorado. *Special Publications of SEPM.*

Leckie, R. M. and Olson, H. C. (2003). Foraminifera as proxies for sea-level change on siliciclastic margins. *Special Publications of SEPM.*

Leidy, J. (1874). Notice of some new fresh-water rhizopods. *Proceedings of the Academy of Natural Sciences of Philadelphia, Series* 3(83), 77–79.

Lemaska, A. (2005). Comparison of deep-water agglutinated foraminifera from the hemipelagic variegated shales (Lower Turonian-Lower Santonian) and the turbiditic Godula beds (Upper Santonian-Campanian) in the Lanckorona-Wadowice area. *Studia Geologica Polonica* 124, 259–272.

Leorri, E., Gehrels, W. R., Horton, B. P., Fatela, F., and Cearreta, A. (2010). Distribution of foraminifera in salt marshes along the Atlantic coast of SW Europe: tools to reconstruct past sea-level variations. *Quaternary International* 221(1-2), 104–115.

Lerman, A. (1989). lakes: chemistry, Geology and Physics. *Geological Press Beijing.*

Lewan, M. D. (1984). Factors controlling the proportionality of vanadium to nickel in crude oils. *Geochimica et Cosmochimica Acta* 48(11), 2231–2238.

Li, W., Bhattacharya, J., and Zhu, Y. (2011a). Architecture of a forced regressive systems tract in the Turonian Ferron "Notom Delta", southern Utah, U.S.A. *Marine and Petroleum Geology* 28(8), 1517–1529. ISSN: 02648172.

Li, W., Bhattacharya, J. P., and Campbell, C. (2010). Temporal Evolution of Fluvial Style in a Compound Incised-Valley Fill, Ferron "Notom Delta", Henry Mountains Region, Utah (U.S.A.) *Journal of Sedimentary Research* 80(6), 529–549. ISSN: 1527-1404.

Li, W., Bhattacharya, J. P., Zhu, Y., Garza, D., and Blankenship, E. (2011b). Evaluating delta asymmetry using three-dimensional facies architecture and ichnological analysis, Ferron 'Notom Delta', Capital Reef, Utah, USA. *Sedimentology* 58(2), 478–507. ISSN: 00370746.

Li, W. and Zhu, Y. (2014). High-frequency and low-amplitude relative sea-level changes in the Turonian Ferron Notom Delta, Henry Mountains region Utah, USA: implications for sequence stratigraphy and hydrocarbon exploration. *Petroleum Science* 11(1), 14–27.

Li, Y. and Bhattacharya, J. P. (2013). Facies-Architecture Study of A Stepped, Forced Regressvie Compound Incised Valley In the Ferron Notom Delta, Southern Central Utah, U.S.A. *Journal of Sedimentary Research* 83(3), 206–225. ISSN: 1527-1404.

Li, Y., Bhattacharya, J. P., Ahmed, S., and Garza, D. (2018). Re-evaluating the Paleogeography of the River-dominated and Wave-influenced Ferron Notom Delta, Southern Central Utah: an Integration of Detailed Facies-architecture and Paleocurrent Analysis. *Journal of Sedimentary Research* 88(2), 214–240.

Li, Z. and Schieber, J. (2018). Detailed facies analysis of the Upper Cretaceous Tununk Shale Member, Henry Mountains Region, Utah: Implications for mudstone depositional models in epicontinental seas. *Sedimentary Geology* 364, 141–159.

Li, Z., Bhattacharya, J., and Schieber, J. (2015). Evaluating along-strike variation using thin-bedded facies analysis, Upper Cretaceous Ferron Notom Delta, Utah. *Sedimentology* 62(7), 2060–2089.

Lipps, J. H. (1981). What, if anything, is micropaleontology? *Paleobiology* 7(2), 167–199.

Lloyd, J. (2000). Combined Foraminiferal and Thecamoebian Environmental Reconstruction from an Isolation Basin in NW Scotland: Implications for Sea-Level Studies. *The Journal of Foraminiferal Research* 30(4), 294–305.

Marins, M., Pinto, A., Frontalini, F., Fonseca, M. da, Terroso, D., Laut, L., Zaaboub, N., Rodrigues, M., and Rocha, F. (2016). Can benthic foraminifera be used as bio-indicators of pollution in areas with a wide range of physicochemical variability. *Estuarine, Coastal and Shelf Sceince* 182, 211–225.

Markulin, K., Peharda, M., Mertz-Kraus, R., Schöne, B. R., Uvanović, H., Kovač, Ž., and Janeković, I. (2019). Trace and minor element records in aragonitic bivalve shells as environmental proxies. *Chemical Geology* 507, 120–133.

Marsh, R., Mills, R. A., Green, D. R., Salter, I., and Taylor, S. (Sept. 2007). Controls on sediment geochemistry in the Crozet region. *Deep-Sea Research Part II: Topical Studies in Oceanography* 54 (18-20), 2260–2274. ISSN: 09670645.

Martins, M., Yamashita, C., eSousa, S., Koutsoukos, E., Disaro, S., Debenay, J., and Duleba, W. (2018). Response of benthic foraminifera to environmental variability: Importance of benthic foraminifera in Monitoring studies. *IntechOpen*, 1–27.

Matyszkiewicz, J. and Felisiak, I. (1992). Microfacies and diagenesis of an Upper Oxfordian carbonate buildup in Mydlniki (Cracow area, Southern Poland). *Facies* 27(1), 179–189.

McCarthy, F. M., Collins, E. S., McAndrews, J. H., Kerr, H. A., Scott, D. B., and Medioli, F. S. (1995). A comparison of postglacial arcellacean ("thecamoebian")

and pollen succession in Atlantic Canada, illustrating the potential of arcellaceans for paleoclimatic reconstruction. *Journal of Paleontology* 69(5), 980–993.

McNeil, D. H. and Caldwell, W. G. E. (1981). Cretaceous rocks and their foraminifera in the Manitoba escarpment. *Cretaceous rocks and their foraminifera in the Manitoba escarpment*.

McNeill-Jewer, C. A., Reinhardt, G., E., Collins, S., Kovacs, S., May-Chan, W., Devos, F., and LeMaillot, C. (2019). The effect of seasonal rainfall on nutrient input and biological productivity in the Yax Chen cave system (Ox Bel Ha), Mexico, and implications for XRF core studies of paleohydrology. *Palaeogeography, Palaeoclimatology, Palaeoecology.* 534, 109–289.

Medioli, F. S., Scott, D. B., and Abbott, B. H. (1987). a Case-Study of Protozoan Intraclonal Variability - Taxonomic Implications. *Journal of Foraminiferal Research* 17(1), 28–47.

Medioli, F. and Barbara, E. (1995). Marginal marine foraminifera and thecamoebians in the Upper Cretaceous to Eocene deposits of the south-central Pyrenees, Spain.

Medioli, F., Scott, D., Collins, E., and McCarthy, F. (1990a). Thecamoebians from the early Cretaceous deposits of Ruby Creek, Alberta (Canada). 793–812. *Paleoecology, biostratigraphy, paleopceanography and taxonomy of agglutinated foraminifera. Proceedings of the NATO Advanced Study Institute, Kluwer, NATO ASI Series C* 327, 1–1017.

Medioli, F. S., Scott, D. B., Collins, E. S., and McCarthy, F. M. (1990b). Fossil thecamoebians: present status and prospects for the future. In: *Paleoecology, biostratigraphy, paleoceanography and taxonomy of agglutinated Foraminifera.* Springer, 813–839.

Milne, A. R. and Fitzpatrick, R. W. (1977). Minerals in soil environments. In: Madison, WI: Soil Science Society of America. Chap. Titanium and zirconium minerals, 1131–1205.

Moreno, F., Giralt, A., Valero-Garces, S., Saez, B., Bao, A., Pergo, R., Pueyo, R., Gonzalez-Samperiz, J., and Taberner, P. (2007). a 14kyr record of the tropical Andes: the Lago Chungara sequence (18os, northern Chilean Altiplano). *Quat Int* 161, 4–21.

Müller-Navarra, K. (2018). Salt-marsh foraminifera and their potential for sea-level studies in the North Sea region. PhD thesis. University of Hamburg.

Mullineaux, L. S. (1987). Organisms living on manganese nodules and crusts: distribution and abundance at three North Pacific sites. *Deep Sea Research Part A. Oceanographic Research Papers* 34, 165–184.

Murray, J. W., Alve, E., and Jones, B. W. (2011). A new look at modern agglutinated benthic foraminiferal morphogroups: Their value in palaeoecological interpretation. *Palaeogeography, Palaeoclimatology, Palaeoecology* 309(3-4), 229–241.

Murray, J. W. (2006). *Ecology and applications of benthic foraminifera*. Cambridge University Press.

Murray, J. W. and Alve, E. (1999a). Natural dissolution of modern shallow water benthic foraminifera: taphonomic effects on the palaeoecological record. *Palaeogeography, Palaeoclimatology, Palaeoecology* 146(1-4), 195–209.

Murray, J. W. and Alve, E. (1999b). Taphonomic experiments on marginal marine foraminiferal assemblages: how much ecological information is preserved? *Palaeogeography, Palaeoclimatology, Palaeoecology* 149(1-4), 183–197.

Murray, J. W. (1973). Distribution and ecology of living benthic foraminiferids. *Heinemann Educational Books*.

Mutti, E., Seguret, M., and Sgavetti, M. (1988). Sedimentation and deformation in the Tertiary Sequences of the Pyrenees. *American Association of Petroleum Geologists* 7. Field Trip 7, 153 p, 169.

Nagy, J., Reolid, M., and Rodrguez-Tovar, F. J. (2009). Foraminiferal morphogroups in dysoxic shelf deposits from the Jurassic of Spitsbergen. *Polar Research* 28(2), 214–221.

Nagy, J. (1992). Environmental significance of foraminiferal morphogroups in Jurassic North Sea deltas. *Palaeogeography, Palaeoclimatology, Palaeoecology* 95(1-2), 111–134.

Nagy, J., Gradstein, F. M., Gibling, M. R., and Thomas, F. C. (1995). Foraminiferal stratigraphy and paleoenvironments of Late Jurassic to Early Cretaceous deposits in Thakkhola, Nepal. *Micropaleontology* 41(2), 143–170.

Nagy, J., Hess, S., Dypvik, H., and Bjaerke, T. (2011). Marine Shelf to paralic biofacies of Upper Triassic to Lower Jurassic deposits in Spitsbergen. *Palaeogeography, Palaeoclimatology, Palaeoecology* 300, 138–151.

Nagy, J. and Johansen, H. O. (1989). Preservation and distribution pattern of Reophax metensis (foraminifera) in the Jurassic of the North Sea. *The Journal of Foraminiferal Research* 19(4), 337–348.

Nagy, J. (2016). A sequence stratigraphic model of benthic foraminiferal facies trends with Triassic and Jurassic examples. *Marine Micropaleontology* 122, 99–114.

Nichols, M. M. (1977). Response and recovery of an estuary following a river flood. *Journal of Sedimentary Research* 47(3), 1171–1186.

Nielsen, K. S., Schroder-Adams, C., Leckie, D. A., Haggart, J. W., and Elderbak, K. (2008). Turonian to Santonian paleoenvironmental changes in the Cretaceous Western Interior Sea: The Carlile and Niobrara formations in southern

Alberta and southwestern Saskatchewan. *Canada. Palaeogeography, Palaeoclimatology, Palaeoecology* 270, 64–91.

Nigam, R., Khare, N., and Borole, D. (1992). Can benthic foraminiferal morphogroups be used as indicators of paleomonsoonal precipitation? *Estuarine, Coastal and Shelf Science* 34(6), 533–542.

Ogden, C. G. and Hedley, R. H. (1980). *An atlas of freshwater testate amoebae– British Museum (Natural History) and*. London and Oxford: Oxford University Press.

Oksanen, J., Blanchet, F. G., Friendly, M., Kindt, R., Legendre, P., McGlinn, D., Minchin, P. R., O'Hara, R. B., Simpson, G. L., Solymos, P., Stevens, M. H. H., Szoecs, E., and Wagner, H. (2019). *vegan: Community Ecology Package*. R package version 2.5-6.

Oliver, W. (1971). Depositional Systems in Woodbine Formation (Upper Cretaceous), Northeast Texas. *AAPG Bulletin* 55(1), 156–156.

Ozarko, D., Patterson, R., and Williams, H. (1997). Marsh Foraminifera from Nanaimo, British Columbia (Canada); implications of infaunal habitat and taphonomic biasing. *The Journal of Foraminiferal Research* 27(1), 51–68.

Pastouret, L., Chamley, H., Delibrias, G., Duplessy, J. C., and Thiede, J. (1978). Late Quaternary climatic changes in western tropical Africa deduced from deep-sea sedimentation off the Niger delta. *Oceanologica Acta* 1, 217–232.

Patterson, R. T. (1990). Intertidal benthic foraminiferal biofacies on the Fraser River Delta, British Columbia: modern distribution and paleoecological importance. *Micropaleontology*, 229–244.

Patterson, R. T. and Kumar, A. (2002). A review of current testate rhizopod (thecamoebian) research in Canada. *Palaeogeography, Palaeoclimatology, Palaeoecology* 180(1–3), 225–251.

Patterson, R., Hutchinson, I., Guilbault, J., and Clague, J. (2000). A comparison of the vertical zonation of diatom, Foraminifera, and macrophyte assemblages in a coastal marsh; implications for greater paleo-sea level resolution. *Micropaleontology* 46(3), 229–244.

Peros, M., Collins, S., G'Meiner, A. A., Reinhardt, E. G., and Pupo, F. M. (2017). Multistage 8.2 kyr event revealed through high-resolution XRF core scanning of Cuban sinkhole sediments. *Geophys. Res*, 7374–7381.

Peterson, F. and Ryder, R. T. (1975). Cretaceous rocks in the Henry Mountains region, Utah and their relation to neighboring regions.

Pettijohn, F. J. (1963). *Chemical composition of sandstones, excluding carbonate and volcanic sands: Representative analyses*. 440. US Government Printing Office.

Phleger, F. B. and Bradshaw, J. S. (1966). Sedimentary environments in a marine marsh. *Science* 154(3756), 1551–1553.

Piva, A., Asioli, A., Schneider, R. R., Trincardi, F., Andersen, N., Colmenero-Hidalgo, E., Dennielou, B., Flores, J. A., and Vigliotti, L. (Jan. 2008). Climatic cycles as expressed in sediments of the PROMESSI borehole PRAD1-2, central Adriatic, for the last 370 ka: 1. Integrated stratigraphy. *Geochemistry, Geophysics, Geosystems* 9 (1). ISSN: 15252027.

Plint, G. (2014). Mud dispersal across a Cretaceous prodelta: storm-generated, wave-enhanced sediment gravity flows inferred from mudstone microtexture and microfacies. *Sedimentology* 61(3), 609–647.

Porter, S. A. and Knoll, A. H. (2000). Testate amoeba in the Neoproterozoic Era: evidence from vase-shaped microfossils in the Chutar Group, Grand Canyon. *Paleobiology* 26(3), 360–385.

Profe, J., Zolitschka, B., Schirmer, W., Frechen, M., and Ohlendorf, C. (2016). Geochemistry unravels MIS 3/2 paleoenvironmental dynamics at the loess–paleosol sequence Schwalbenberg II, Germany. *Palaeogeogr. Palaeoclimatol. Palaeoecol* 459, 537–551.

Rabalais, N. N. and Turner, R. E. (2006). Oxygen depletion in the Gulf of Mexico adjacent to the Mississippi River. In: *Past and present water column anoxia*. Springer, 225–245.

Rebolledo, L., Sepúlveda, J., Lange, C., Pantoja, S., Bertrand, S., Hughen, K., and Figueroa, D. (2008). Late Holocene marine productivity changes in Northern Patagonia-Chile inferred from a multi-proxy analysis of Jacaf Channel sediments. Estuarine Coastal Shelf. *Science* 80, 314–322.

Reinhardt, E., Patterson, R., Blenkinsop, J., and Raban, A. (1998). Paleoenvironmental evolution of the inner basin of the ancient harbor at Caesarea Maritima, Israel; foraminiferal and Sr isotopic evidence. *Revue de Paleobiologie* 17(1), 1–21.

Reolid, M., Duarte, L. V., and Rita, P. (Oct. 2018). Changes in foraminiferal assemblages and environmental conditions during the T-OAE (Early Jurassic) in the northern Lusitanian Basin, Portugal. *Palaeogeography, Palaeoclimatology, Palaeoecology* 520, 30–43.

Reolid, M. and Nagy, J. (2005). Jurassic transgressive–regressive cycles in carbonate and siliciclastic shelf facies: comparison of foraminiferal assemblages. *Abstracts. 7th Int. Workshop Agglutinated Foraminifera, Urbino, Italy, pp. 63–65*, 63–65.

Reolid, M., Rodrıéguez-Tovar, F. J., Nagy, J., and Olóriz, F. (2008). Benthic foraminiferal morphogroups of mid to outer shelf environments of the Late Jurassic (Prebetic Zone, southern Spain): characterization of biofacies and environmental significance. *Palaeogeography, Palaeoclimatology, Palaeoecology* 261(3-4), 280–299.

Retallack, G. and Dilcher, D. L. (1981). Early angiosperm reproduction: Prisca reynoldsii, gen. et sp. nov. from mid-Cretaceous coastal deposits in Kansas, USA. *Palaeontographica B* 179(5-6), 103–137.

Richards, B. H. and Bhattacharya, J. P. (2018). Stratigraphy of the Fluvial-To-Marine Transition Zone Associated with A Forced-Regressive Compound Incised-Valley System In the Turonian Ferron Notom Delta, Utah, U. *S.A. Journal of Sedimentary Research* 88(3), 311–326.

Riveiros, N. V. and Patterson, R. T. (2009). Late Holocene paleoceanographic evidence of the influence of the Aleutian Low and North Pacific High on circulation in the Seymour-Belize inlet complex, British Columbia, Canada. *Quaternary Science Reviews* 28(25-26), 2833–2850.

Rothwell, R. G., Hoogakker, B., Thomson, J., Croudace, I. W., and Frenz, M. (2006). Turbidite emplacement on the southern Balearic Abyssal Plain (western Mediterranean Sea) during Marine Isotope Stages 1–3: an application of ITRAX XRF scanning of sediment cores to lithostratigraphic analysis. *Geological Society, London, Special Publications* 267(1), 79–98.

Roy, D. K. and Roser, B. P. (2013). Climatic control on the composition of Carboniferous–Permian Gondwana sediments, Khalaspir basin, Bangladesh. *Gondwana Research* 23(3), 1163–1171.

Saraswati, P. K. and Srinivasan, M. (2015). *Micropaleontology: Principles and applications*. Springer.

Sars, G. O. (1872). *Undersogelser over Hardangerfjordens fauna. Fordhandlunger i Videnskabsselsk.] i Kristiana*.

Schafer, C. (1974). Distribution of benthic foraminifera: Their use in delimiting local nearshore environments. *Offshore Geology of Canada, Eastern Canada, Geological Survey of Canada* 1, 103–108.

Schieber, J. (2016). Mud re-distribution in epicontinental basins–Exploring likely processes. *Marine and Petroleum Geology* 71, 119–133.

Schneider, R. R., Price, B., Muller, P. J., Kroon, D., and Alexander, I. (1997). Monsoon related variations in Zaire (Congo) sediment load and influence of fluvial silicate supply on marine productivity in the east equatorial Atlantic during the last 200,000 years. *Paleoceanography* 12, 463–481.

Scott, D. B. and Medioli, F. S. (1983). Agglutinated rhizopods in Lake Erie: modern distribution and stratigraphic implications. *Journal of Paleontology*, 809–820.

Scott, D. B., Brown, K., Collins, E. S., and Medioli, F. S. (1995a). A new sea-level curve from Nova Scotia: evidence for a rapid acceleration of sea-level rise in the late mid- Holocene. *Canadian Journal of Earth Sciences, v.* 32, 2071–80.

Scott, D. B., Gayes, P. T., and Collins, E. S. (1995b). Mid- Holocene precedent for a future rise in sea-level along the Atlantic coast of North America. *Journal of Coastal Research, v.* 11, 615–22.

Scott, D. B. and Medioli, F. S. (1980a). Living vs. total foraminiferal populations: their relative usefulness in paleoecology. *Journal of Paleontology* 54, 814–34.

Scott, D. B., Medioli, F. S., and Schafer, C. T. (1977). Temporal changes in foraminiferal distribution in Miramichi River Estuary, New Brunswick. *Canadian Journal of Earth Sciences* 14, 1566–87.

Scott, D. B., Schafer, C. T., and Medioli, F. S. (1980). Eastern Canadian estuarine foraminifera; a framework for comparison. *The Journal of Foraminiferal Research* 10(3), 205–234.

Scott, D. B., Medioli, F. S., and Schafer, C. T. (2005). *Monitoring in coastal environments using foraminifera and thecamoebian indicators*. Cambridge University Press.

Scott, D. B., Mudie, P. J., and Bradshaw, J. S. (1976). Benthonic foraminifera of three southern Californian lagoons; ecology and Recent stratigraphy. *The Journal of Foraminiferal Research* 6(1), 59–75.

Scott, D. B., Suter, J. R., and Kosters, E. C. (1991). Marsh foraminifera and arcellaceans of the lower Mississippi Delta; controls on spatial distributions. *Micropaleontology* 37(4), 373–392.

Scott, D. and Medioli, F. (1980b). Post-glacial emergence curves in the Maritimes determined from marine sediments in raised basins. *Proceedings of coastlines* 80, 428–446.

Scott, D. and Medioli, F. (1980c). Quantitative studies of marsh foraminiferal distributions in Nova Scotia: Their implications for the study of sea-level changes. *Cushman Foundation for Foraminiferal Research, Special Publication* 17, 58.

Scott, D. and Medioli, F. (1978). Vertical zonations of marsh foraminifera as accurate indicators of former sea-levels. *Nature* 272(5653), 528–531.

Sebastien Le Julie Josse, F. H. (2008). FactoMineR: An R Package for Multivariate Analysis. *Journal of Statistical Software* 25(1), 1–18.

Severin, K. P. (1983). Test morphology of benthic foraminifera as a discriminator of biofacies. *Marine Micropaleontology* 8(1), 65–76.

Shaw, T. (Nov. 2013). Reconstructing historical sea-level trends for the Croatian coast of the Adriatic Sea using salt-marsh foraminifera. PhD thesis. University of Liverpool.

Siemers, C. T. (1976). Sedimentology of the Rocktown channel sandstone, upper part of the Dakota Formation (Cretaceous), central Kansas. *Journal of Sedimentary Research* 46(1), 97–123.

Silva, J., Srinivasalu, S., Roy, P., and Jonathan, M. (2014). Environmental conditions inferred from multi-element Environmental conditions inferred from multi-element concentrations in sediments off Cauvery delta, Southeast India. *Environ Earth Sci* 71, 2043–2058.

Singh, V., Pandita, S. K., Tewari, R., Hengstum, P. J. van, Pillai, S. S., Agnihotri, D., Kumar, K., and Bhat, G. (2015). Thecamoebians (testate amoebae)

straddling the Permian-Triassic boundary in the Guryul Ravine section, India: evolutionary and palaeoecological implications. *PloS one* 10(8), e0135593.

Smart, C., King, S., Gooday, A., Murray, J., and Thomas, E. (1994). A benthic foraminifera proxy of pulsed organic matter paleofluxes. *Marine Micropaleontology* 23, 89–99.

Sudom, M. D. and St. Arnaud, R. J. (1971). Use of quartz, zirconium and titanium as indices in pedological studies. *Canadian Journal of Soil Science* 51, 385–396.

Szydo, A. (2004). The distribution of agglutinated foraminifera in the Cieszyn Basin. *Polish Outer Carpathians. Grzybowski Foundation Special Publication* 8, 461–470.

Teal, J. (2001). Salt marshes and mud flats. *Encyclopedia of ocean sciences*, 2490–2495.

Tesi, T., Miserocchi, S., Goñi, M., Turchetto, M., Langone, L., De Lazzari, A., Albertazzi, S., and Correggiari, A. (2011). Influence of distributary channels on sediment and organic matter supply in event-dominated coastal margins: the Po prodelta as a study case. *Biogeosciences* 8(2), 365.

Tibert, N. E. and Scott, D. B. (1999). Ostracodes and Agglutinated Foraminifera as Indicators of Paleoenvironmental Change inan Early Carboniferous Brackish Bay. *Atlantic Canada. Palaios* 14(3), 246–260.

Turkistani, M. N., Reinhardt, E., Kynaston, D., and Bhattacharya, J. (forthcoming). Foraminifera and Thecamoebian Morphogroups and Biofacies of the Upper Cretaceous (Turonian) Ferron-Notom Delta, Utah, USA. *Cretaceous*.

Turkistani, M. N., Reinhardt, E., Kynaston, D., and Bhattacharya, J. (submitted). Foraminifera and thecamoebians morphogroup analysis of the Upper Cretaceous (Turonian) Ferron-Notom Delta, Central Utah, USA. *Journal of Foraminiferal Research*.

Turner, J., Davis, S., Langdon, C., Scaife, R., Holmes, N., Leng, M., Mulrooney, G., and Cummins, T. (2010). A multiproxy (pollen, stable isotope, chironomid and μXRF) record for the Late Glacial to Holocene transition from Thomastown Bog, Ireland. *J. Quat. Sci* 6, 514–528.

Turner, J. N., Jones, A. F., Brewer, P. A., Macklin, M. G., and Rassner, S. M. (2015). Micro-XRF applications in fluvial sedimentary environments of Britain and Ireland: progress and prospects. In: *Micro-XRF Studies of Sediment Cores*. Springer, 227–265.

Tyszka, J. (1994). Response of middle Jurassic benthic foraminiferal morphogroups to dysoxic/anoxic conditions in the Pieniny Klippen Basin, Polish Carpathians. *Palaeogeography, Palaeoclimatology, Palaeoecology* 110(1), 1.

Ullah, M. S., Bhattacharya, J. P., and Dupre, W. R. (2015). Confluence Scours Versus Incised Valleys: Examples from the Cretaceous Ferron Notom Delta, Southeastern Utah, US a confluence scours versus incised valleys: examole from the Ferron-Notom Delta. *Journal of Sedimentary Research* 85(5), 445–458.

Uresk, J. (1979). Sedimentary environment of the Cretaceous Ferron Sandstone near Caineville. *Geology Studies* 26, 81–100.

van Hengstum, P., Reinhardt, E., Medioli, F., and Grocke, D. (2007). Exceptionally preserved late Albian (cretaceous) Arcellaceans (thecamoebians) from the Dakota formation near Lincoln, Nebraska, USA. *The Journal of Foraminiferal Research* 37(4), 300–308.

Varban, B. L. and Plint, G. A. (2008). Palaeoenvironments, palaeogeography, and physiography of a large, shallow, muddy ramp: Late Cenomanian-Turonian Kaskapau Formation, Western Canada foreland basin. *Sedimentology* 55(1), 201–233.

Vernal, A. de and Pedersen, T. F. (1997). Micropaleontology and palynology of core PAR87A-10: A 23,000 year record of paleoenvironmental changes in the Gulf of Alaska, northeast North Pacific. *Paleoceanography* 12(6), 821–830.

Wang, A., Wang, Z., Liu, J., Xu, N., and Li, H. (2020). The Sr/Ba ratio response to salinity in clastic sediments of the Yangtze River Delta. *Chemical Geology*, 119923.

Wang, M. J., Zheng, H. B., Xie, X., Fan, D. D., Yang, S. Y., Zhao, Q. H., and Wang, K. (2011). A 600-year flood history in the Yangtze River drainage: Comparison between a subaqueous delta and historical records. *Chinese Science Bulletin* 56 (2), 188–195. ISSN: 10016538.

Wightman, W. G. (1990). Estuarine and marsh foraminifera from the Lower cretaceous of the Lusitanian Basin, West Portugal. In: *Paleoecology, biostratigraphy, paleoceanography and taxonomy of agglutinated foraminifera.* Springer, 739–764.

Willis, G. C. (1999). The Utah thrust system-an overview. *Geology of Northern Utah and Vicinity* 1, 1–10.

Witzke, B. J., Ludvigson, G. A., Poppe, J. R., and Ravn, R. L. (1983). Cretaceous Paleogeography along the Eastern Margin of the Western Interior Seaway, Iowa Southern Minnesota, and Eastern Nebraska and South Dakota. In: Rocky Mountain Section (SEPM).

Wu, C. and Bhattacharya, J. (Mar. 2015). Paleohydrology and 3D Facies Architecture of Ancient Point Bars , Ferron Sandstone, Notom Delta, South-central Utah. *Journal of Sedimentary Research*, 399–418.

Wu, C., Ullah, M. S., Lu, J., and Bhattacharya, J. P. (2016a). Formation of point bars through rising and falling flood stages: Evidence from bar morphology. *sediment transport and bed shear stress: Sedimentology, v.* 63, 1458–1473.

Wu, C., Ullah, M., Lu, J., and Bhattacharya, J. (2016b). Formation of point bars through rising and falling flood stages: Evidence from bar morphology, sediment transport and bed shear stress. *Sedimentology* 63, 1458–1473.

Wu, C. (2013). Heterogeneity, paleohydrology, and 3D facies architecture of ancient point bars, Ferron Sandstone, Notom Delta, South-central Utah. PhD thesis. University of Houston.

Wu, H. L., Wang, M. C., Wu, A. B., Hsu, W. Y., Kao, S. O., and Tseng, C. C. (2012). Subjective global assessment is a nutritional status marker for chronic peritoneal dialysis patients. *Nutritional Sciences Journal* 37(3), 110–118.

Yandoka, B. M. S., Abdullah, W. H., Abubakar, M., Hakimi, M. H., and Adegoke, A. K. (2015). Geochemical characterisation of Early Cretaceous lacustrine sediments of Bima Formation, Yola Sub-basin, Northern Benue Trough, NE Nigeria: Organic matter input, preservation, paleoenvironment and palaeoclimatic conditions. *Marine and Petroleum Geology* 61, 82–94.

Zhang, T., Trela, W., Jiang, S.-Y., Nielsen, J. K., and Shen, Y. (2011). Major oceanic redox condition change correlated with the rebound of marine animal diversity during the Late Ordovician. *Geology* 39(7), 675–678.

Zhu, Y., Bhattacharya, J., Li, W., Lapen, T., Jicha, B., and Singer, B. (2012). Milankovitch-scale sequence stratigraphy and stepped forced regressions of the Turonian Ferron Notom Deltaic Complex, south-central Utah, U.S.A. *Journal of Sedimentary Research* 82(9), 723–746.

Zhu, Y. (2010). *Sequence Stratigraphy and facies architecture of the Cretateous Ferron Notom Delta Complex, South-Central Utah, USA*. University of Houston.